EXPLICIT MODELS FOR FLEXURAL EDGE AND INTERFACIAL WAVES IN THIN ELASTIC PLATES

A thesis submitted for the degree of

Doctor of Philosophy

by

Elena Kossovich

School of Information Systems, Computing and Mathematics

Brunel University

October 2011

Abstract

In the thesis explicit dual parabolic-elliptic models are constructed for the Konenkov flexural edge wave and the Stoneley-type flexural interfacial wave in case of thin linearly elastic plates. These waves do not appear in an explicit form in the original equations of motion within the framework of the classical Kirchhoff plate theory. The thesis is aimed to highlight the contribution of the edge and interfacial waves into the overall displacement field by deriving specialised equations oriented to aforementioned waves only. The proposed models consist of a parabolic equation governing the wave propagation along a plate edge or plate junction along with an elliptic equation over the interior describing decay in depth. In this case the parabolicity of the one-dimensional edge and interfacial equations supports flexural wave dispersion. The methodology presented in the thesis reveals a dual nature of edge and interfacial plate waves contrasting them to bulk-type wave propagating in thin elastic structures. The thesis tackles a number of important examples of the edge and interfacial wave propagation. First, it addresses the propagation of Konenkov flexural wave in an elastic isotropic plate under prescribed edge loading. For the latter, parabolic-elliptic explicit models were constructed and thoroughly investigated. A similar problem for a semi-infinite orthotropic plate resulted in a more general dual parabolic-elliptic model. Finally, an analogous model was derived and analysed for two isotropic semi-infinite Kirchhoff plates under perfect contact conditions.

Contents

List of Figures

Chapter 1

Introduction

1.1 Introduction to work

1.1.1 Localised wave phenomena, state of art

The history of localised waves in elasticity theory began with the famous paper by Rayleigh (1885) where he described the so-called Rayleigh wave propagating along the surface of an elastic half-space and decaying away from the surface. For many years the Rayleigh wave speed has been one of the properties that attracted significant interest of the scientists. It is well-known that the secular equation for this wave speed, derived by Rayleigh (1885), has an unexplicit form which makes it hard to solve. The most common approach is to find solutions using numerical methods, although there are many attempts to find them analytically. Several approximate formulae are well-known (e.g., see Achenbach (1973)). The exact solution has been found much later and was presented in papers by Rahman and Barber (1995) and then by Nkemzi (1997). The latter was simplified by Malischevsky (2000). Another exact formula was derived by Rahman and Michelitsch (2006).

Although the Rayleigh surface wave was discovered in an elastic isotropic half-space, there exist a lot of analogous waves that occur in the bodies of different shapes and made of anisotropic materials. For example, surface waves propagate in the circular discs which was described experimentally in Oliver et al. (1954). However, for the aforementioned problem solution was valid only for the low frequency limit. For the cases of higher frequencies several theories were developed (e.g see McCoy and Mindlin (1963), Sinclair and Stephens (1971), Cerv (1988)). Nowadays it is accepted that the three-dimensional theory of elasticity is

mandatory to explain the propagation of such waves (e.g. see Lawrie and Kaplunov (2011)). When the considered bodies are made of anisotropic materials, these cases involve much more complex formulation. A detailed review on localised waves in anisotropic bodies was given in the work by Chadwick and Smith (1977). Equations for surface wave speed in bodies made of orthotropic materials were presented in Ogden and Vinh (2004) and in Pham and Ogden (2004). The exact solution for the aforementioned equations was demonstrated in Vinh and Ogden (2005). The proofs of uniqueness of the surface wave speed were suggested in many works, one of the most significant being that by Mielke and Fu (2004). The effect of pre-stress on the Rayleigh wave propagation is described in the works by Dowaikh and Ogden (1990) and Chadwick (1995). Localised waves also propagate on the interface between two elastic materials (both solid, or fluid and solid). Such a wave was discovered by Stoneley (1924) and named after the author. The equations for these wave speeds are relatively more involved as compared to the ones described above. In Barnett et al. (1985) theory concerning wave uniqueness and existence in anisotropic materials is explained. Fundamental ideas are also found in Chadwick and Borejko (1994). The effect of pre-stress on the Stoneley interfacial wave propagation was described by Dowaikh and Ogden (1991). Also, the interfacial waves on the boundary between elastic and acoustic media were studied by Scholte (see Scholte (1947)) and independently by Gogoladse (1948). These waves are now usually referred to as Scholte-Gogoladse waves.

Many years after the discovery of the Rayleigh wave its flexural analog for the Kirchhoff plate theory was found (see Timoshenko and Woinowsky-Krieger (1987) and section 1.3 for more details). The equation for its wavenumber $p = p_k$ is the famous Konenkov dispersion equation in the form

$$\sqrt{p^2 - 1}((1 - \nu)p^2 + 1)^2 - \sqrt{p^2 + 1}((1 - \nu)p^2 - 1)^2 = 0. \tag{1.1}$$

The method of its obtaining is presented in section 2.1.1 of the thesis.

The history of Konenkov flexural edge wave discovery is quite complicated and interesting (see Norris et al. (2000)). The flexural edge wave was first found by Konenkov (1960) and later by Sinha (1974), Thurston and McKenna (1974). Also, the paper by Ishlinskii (1954) precedes the one of Konenkov and describes a similar problem which originates from the theory of plate stability. The most interesting property of Konenkov flexural edge wave is its dispersion (i.e. its speed depends on the frequency of the applied force or the plate material

eigenfrequency). It is also worth mentioning that this wave is sensitive to the plate thickness (see Lawrie and Kaplunov (2011)). The development of the flexural edge waves theory is similar to the one for Rayleigh waves. They can be found in the cases of plate anisotropy (see Norris (1994), Thompson et al. (2002), Zakharov and Becker (2003), Piliposian et al. (2010), also Fu (2003), Fu and Brookes (2006), Lu et al. (2007)) as well as in the layered plates (see Zakharov (2002), Zakharov (2004)) and in the plates with cracks (see Norris and Wang (1994), Thompson and Abrahams (2005), Thompson and Abrahams (2007)). Furthermore, the effects of fluid loading were considered by Norris and Abrahams (2000). In the cases of circular plates the exact dispersion relation expressed in terms of Bessel functions was derived by Destrade and Fu (2008). The Stoneley-type flexural interfacial wave propagation at the junction of two plates was investigated by Zilbergleit and Suslova (1983).

Localised edge waves may also occur in thin semi-infinite cylindrical shells governed by the Kirchhoff-Love theory (see Kaplunov et al. (2000)). Both Rayleigh and Konenkov flexural edge waves may appear, coinciding with the short-wave limit of the circumferential waves localized near the traction-free shell edge. Unfortunately, the shell curvature is not always negligible in the asymptotic analysis mentioned above, therefore we need to take into account its effect because of the coupling between the bending and extensional displacements. This effect results in the low-level radiation damping of the extensional shell edge wave (Kaplunov et al. (2000)). Furthermore, there exists a curvature super-low frequency edge wave which has no analogue among the plate edge waves and is governed by the so-called "semi-membrane" shell theory (Goldenveizer (1961)). The recent works on edge waves propagation in thin elastic shells are Gulgazaryan et al. (2008), Kaplunov and Wilde (2000), Kaplunov and Wilde (2002) and Fu and Kaplunov (2011).

The aforementioned edge waves also appear in the theory of three-dimensional plates. It is natural to assume that all the aforementioned localised waves are incorporated into the full edge wave solutions as special cases (Lawrie and Kaplunov (2011)). For example, according to the finite-element and experimental study of Lagasse and Oliner (1976), the fundamental three-dimensional antisymmetric edge wave in the low-frequency limit becomes the Konenkov one. The following works demonstrate interesting and useful approaches to finding the flexural and surface waves in the three-dimensional plates: Kaplunov et al. (2005), Zernov and Kaplunov (2008), Lagasse and Oliner (1976) and Krushynska (2011).

The edge resonance phenomena in the most elementary cases is connected with the afore-mentioned wave propagation (e.g. see Wilde et al. (2010)). This fact was mentioned in the works Kaplunov et al. (2004b), Prikazchikov et al. (2007) and, for interface resonance, Rogerson and Krynkin (2007).

Our approach to flexural edge and interfacial waves relies on a recently developed one for surface and interfacial waves. It is obvious that both surface and edge waves seem to be hidden in mathematical formulations of the original problems (Kaplunov et al. (2006)). Useful approach to express them is to construct the explicit models that describe the surface waves and extract their contribution from the general formulations. These models, highlighting the dual hyperbolic-elliptic nature of surface waves, have recently been created by Kaplunov et al. (2006) for elastic and piezoelastic surface waves (namely, Rayleigh and Bleustein-Gulyaev surface waves). They contain elliptic equations describing the decay in the interior away from the surface, and a hyperbolic equation at the surface corresponding to wave propagation. The models provide significant simplifications of the problems formulation. They also prove to be an efficient tool in capturing the transient dynamic behavior associated with the Rayleigh wave, for example, in the case of a moving load problem (see Kaplunov et al. (2010)). The aforementioned models were also presented in the papers Kaplunov et al. (2004a), Kaplunov and Kossovich (2004) and Dai et al. (2010).

Development of similar models for flexural edge and interfacial waves seems not a trivial extension of the approach for surface waves, especially taking into account the dispersive nature of Konenkov and Konenkov-type waves. Therefore the main goal of this thesis is to derive explicit approximate models to describe the flexural edge and interfacial waves. We consider various cases of isotropic and anisotropic plates as well as the case of interfacial waves for two perfectly bonded plates. The resulting models include elliptic equations characterising the decay of the wave away from the edge into the interior domain, and a parabolic equation at the edge. Thus, the constructed asymptotic models reveal the dual parabolic-elliptic nature of the flexural edge and interfacial waves.

1.1.2 Work summary

Chapter 1 of the thesis is the introductory chapter containing all the preliminary knowledge which is mandatory for understanding the main results and derived models of localised flex-

ural waves. In Section 1.2 we introduce all the methods that have been used in the thesis. Section 1.3 contains a brief description of the Kirchhoff plate theory equations and boundary conditions. This theory forms the basis of our work.

The main results are presented in Chapters 2-4. The classical problem of vibrations of an isotropic semi-infinite plate is considered in Section 2.1 of Chapter 2. The edge wave propagation under homogeneous boundary conditions is investigated in Section 2.1.1. We follow the steps described by Konenkov (1960) and derive the dispersion equation for the so-called Konenkov flexural edge wave coefficient. The problem of applied bending moment is considered in the next Section 2.1.2. The solution in terms of integral transforms and the explicit dual parabolic-elliptic model of the Konenkov flexural edge wave are constructed. The latter contains a one-dimensional parabolic equation for the plate edge and an elliptic equation characterising the wave decay into the interior domain. The results for the exact solution and approximate solutions corresponding to the classical Konenkov flexural edge wave are compared graphically. A similar problem of applied shear force is reviewed in Section 2.1.3. The exact solution and an approximate model are now derived for the rotation angle instead of the deflection as in the previous section. In Section 2.2 we consider the flexural edge wave if an isotropic circular plate. The first-order approximation is found taking into account the curvature correction. The results for the leading and first-order solutions are compared with the exact solution found by Destrade and Fu (2008).

Chapter 3 deals with the edge vibrations of an orthotropic semi-infinite plate. The first Section 3.1 contains the analysis of the homogeneous edge wave. The derived dispersion equation has an explicit solution which can be reduced to the isotropic case. The Konenkov flexural edge wave coefficient is now shown to depend on 4 parameters. The next two Sections, 3.2 and 3.3, contain exact solutions for an applied bending moment and shear force, respectively. They are also dedicated to deriving more general approximate dual parabolic-elliptic models of the Konenkov flexural edge wave. The results are again compared graphically.

Finally, Chapter 4 contains some problems of vibrations in two joined isotropic semi-infinite plates. In Section 4.1 the homogeneous Stoneley-type flexural interfacial wave is considered, the dispersion equation for the interfacial wave coefficient is derived and numerical solutions of this equation are computed. Section 4.2 contains the derivation of an exact solution and a dual parabolic-elliptic model of plate's vibration near the junction under the

loading by a bending moment. The results are presented graphically for the case of a specific bending moment. In Section 4.3 we proceed with the same scheme of solution and model derivation as concerns the problem of applied shear force.

Conclusion summarises all the results thus obtained including the constructed explicit dual parabolic-elliptic models.

1.2 Methods

In this section we describe methods to be used while finding solutions for the problems considered in the thesis.

1.2.1 Laplace operators in different coordinate systems

The Laplace operator Δ_L is very important in many problems of physics and applied mathematics. In the two-dimensional Cartesian coordinates it is defined by

$$\Delta_L = \frac{\partial^2}{\partial x^2} + \frac{\partial^2}{\partial y^2}. \tag{1.2}$$

For the polar coordinate system, which is connected with the Cartesian one by the equalities

$$r^2 = x^2 + y^2, \quad \phi = \tan^{-1}\left(\frac{y}{x}\right), \tag{1.3}$$

we will denote the Laplace operator as $\Delta_{L,r,\phi}$ to distinguish it from the Cartesian operator. It is given by

$$\Delta_{L,r,\phi} = \frac{\partial^2}{\partial r^2} + \frac{1}{r}\frac{\partial}{\partial r} + \frac{1}{r^2}\frac{\partial^2}{\partial \phi^2} \tag{1.4}$$

1.2.2 Integral transforms

Many of the problems in mechanics and applied mathematics are connected with the partial differential equations. When analysing them, it is very convenient to use the so-called integral transforms which allow us to reduce the number of the variables in the equations and therefore reduce their complexity. In the thesis we use Laplace and Fourier integral transforms whose descriptions are presented below.

1.2.2.1 Laplace integral transform

The Laplace integral transform is the function $\mathcal{L}\left[f(t)\right]$ defined by

$$\mathcal{L}\left[f(t)\right] = F^{\mathcal{L}}(s) = \int\limits_{0}^{\infty} e^{-st} f(t) dt \tag{1.5}$$

One of the most important properties of the Laplace transform is the derivative property, which is

$$\mathcal{L}\left[f^{(n)}(t)\right] = s^n F^{\mathcal{L}}(s) - s^{n-1} f(0) - s^{n-2} f'(0) - \ldots - f^{(n-1)}(0). \tag{1.6}$$

Here, $f^{(n)}$ denotes the n-th derivative of the function f with respect to the variable t.

In the thesis we consider only the homogeneous initial data, therefore we can use the reduced derivative property of Laplace transform which is

$$\mathcal{L}\left[f^{(n)}(t)\right] = s^n F^{\mathcal{L}}(s). \tag{1.7}$$

The inverse Laplace transform is

$$f(t) = \int\limits_{0}^{\infty} F^{\mathcal{L}}(s) e^{st} ds.$$

In the thesis we apply the Laplace transform to the time-coordinate t or its dimensionless analogue τ (see below in the text).

1.2.2.2 Fourier integral transform

The Fourier integral transform $F^{\mathcal{F}}(p)$ of a function $f(x)$ is defined by

$$F^{\mathcal{F}}(p) = \mathcal{F}\left[f(x)\right] = \frac{1}{\sqrt{2\pi}} \int\limits_{-\infty}^{\infty} e^{-ixp} f(x) dx, \tag{1.8}$$

and the inverse Fourier transform is

$$f(x) = \frac{1}{\sqrt{2\pi}} \int\limits_{-\infty}^{\infty} e^{ixp} F^{\mathcal{F}}(p) dp. \tag{1.9}$$

The Fourier integral transform, as well as that of Laplace, has the derivative property given by the following expression

$$\mathcal{F}\left[f^{(n)}(x)\right] = (ip)^n F^{\mathcal{F}}(p). \tag{1.10}$$

In the thesis we apply the Fourier integral transform to the x-coordinate (or its dimensionless analogue ξ).

1.2.3   Contour Integration

As it was mentioned above in Section 1.2.2, here we use integral transforms and, therefore, the related integrals. For example, the inverse Fourier transform requires taking the integral in form (1.9). Sometimes the integrand has singularities located on the real axis. In the thesis, we deal with the integrands having several singularities on the real line, namely two poles symmetrical around the origin. For this reason, here and below we take into consideration the integrand function $f(x)$, which has two poles, $x = \pm x_k$. Finding the result of integration of

$$\int_{-\infty}^{\infty} f(x)dx \tag{1.11}$$

becomes possible if we use the path of integrating which avoids these poles. The method used here is the contour integration avoiding these poles around the semi-circles with a small radius r, which is suggested by the Cauchy Principle Value theorem (e.g. see Henrici (1988)). For this reason we split the interval of integration into 5 segments, as shown in Figure 1.1.
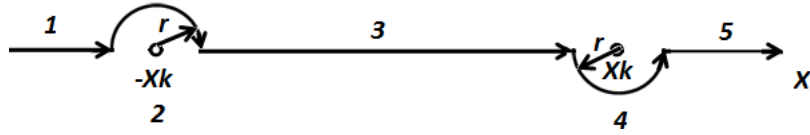
Figure 1.1: Intervals of integration splitting of the original interval

The segments 1 $(-\infty < x < -x_k - r)$, 3 $(-x_k + r < x < x_k - r)$ and 5 $(x_k + r < x < \infty)$ do not contain any singularities, and within the 2 and 4 we use the contour integration. Additive property of integration allows us to rewrite (1.11) as follows

$$\int_{-\infty}^{\infty} f(x)dx = \int_{-\infty}^{-x_k-r} f(x)dx + \int_{2} f(z)dz + \int_{-x_k+r}^{x_k-r} f(x)dx$$
$$+ \int_{4} f(z)dz + \int_{x_k+r}^{\infty} f(x)dx. \tag{1.12}$$

Hereafter, $f(z)$ is the function of the real argument $f(x)$, extended to the complex plane.

Now we study the contour integrals on intervals 2 and 4. We remark that the way around the poles is chosen in order to satisfy the Sommerfeld radiation conditions (see below in the text). We parametrise the variable z in the first integral to specify the contour 2 by setting $z = -x_k - re^{i\phi}$, where $\pi \leq \phi \leq 0$. Note that this parametrization defines the direction of the integration. For contour 4, we set $z = x_k - re^{i\pi}$ with $\pi \leq \phi \leq 2\pi$, and finally integral (1.11)

can be defined in the following form

$$\int_{-\infty}^{\infty} f(x)dx = \int_{-\infty}^{-x_k-r} f(x)dx + \int_{\pi}^{0} ire^{i\phi} f_1(\phi)d\phi + \int_{-x_k+r}^{x_k-r} f(x)dx$$
$$+ \int_{\pi}^{2\pi} ire^{i\phi} f_2(\phi)d\phi + \int_{x_k+r}^{\infty} f(x)dx, \qquad (1.13)$$

where $f_1(\phi) = f(-x_k - re^{i\phi})$ whereas $f_2(\phi) = f(x_k - re^{i\phi})$.

It should be mentioned that the values of the contour integrals around the poles $x = \pm x_k$ define the contribution of these singularity points into the overall result of the integration (1.13).

1.2.4 Residue Theory

We consider the Laurent series

$$f(z) = \sum_{n=-\infty}^{\infty} a_n(z - z_0)^n \qquad (1.14)$$

of the complex variable function $f(z)$ around point z_0. The constant a_{-1} of these series is called the residue of $f(z)$. An important property of the residues is that if $f(z)$ is analytic at z_0, its residue at this point is zero. Unfortunately, the converse is not always true (e.g, if $f(z) = \frac{1}{z}$, for which it is well-known that the residue at point $z = 0$ of this function is 0.). We denote the residue of a function $f(z)$ at z_0 point as $Res_{z=z_0}(f(z))$.

Residues of $f(z)$ function may be found without explicitly expanding it into the Laurent series. If $f(z)$ has a pole of order m at the point $z = z_0$, then the residue can be found by the formula

$$Res_{z=z_0}(f(z)) = \frac{1}{(m-1)!} \frac{d^{m-1}}{dz^{m-1}} [(z - z_0)^m f(z)]_{z=z_0}. \qquad (1.15)$$

The Cauchy integral theorem says that the value of a contour integral of any contour in the complex plane depends only on the properties of a few special points inside the contour, and therefore

$$\oint_{\gamma} f(z)dz = 2\pi i \sum_{a \in A} Res_{z=a}(f(z)), \qquad (1.16)$$

where A is the set of all poles of the function $f(z)$ inside the closed contour γ. Here and below, we used the material from the book by Henrici (1988).

One of the most useful theorems of the residue theory application is the Jourdan's lemma. Its statement is:

Consider a complex-valued, continuous function $f(z)$, defined on a semicircular contour $C_R = \{z : z = Re^{i\theta}, \theta \in [0, \pi]\}$ of radius $R > 0$ lying in the upper half-plane, centred at the origin. If the function $f(z)$ is of the form $f(z) = e^{ipz}g(z)$, $z \in C_R$ with a parameter $p > 0$, then Jordan's lemma states the following upper bound for the contour integral

$$\left| \int_{C_R} f(z)\, dz \right| \leq \frac{\pi}{p} \max_{\theta \in [0,\pi]} \left| g\left(Re^{i\theta}\right) \right|. \tag{1.17}$$

An analogous statement for a semicircular contour in the lower half-plane holds when $p < 0$.

If $f(z)$ is defined and continuous on the semicircular contour C_R for all large R and $M_R := \max_{\theta \in [0,\pi]} \left| g\left(Re^{i\theta}\right) \right| \to 0$ as $R \to \infty$, then by Jordan's lemma

$$\lim_{R \to \infty} \int_{C_R} f(z)\, dz = 0. \tag{1.18}$$

Application of the Jourdan's lemma allows to find the improper integral of the above function $f(z)$ as follows

$$\int_{-\infty}^{\infty} f(x)\, dx = 2\pi i \sum_{a \in A} Res_{z=a}(f(z)), \tag{1.19}$$

where A is a finite set of non-real points of singularity of $g(z)$.
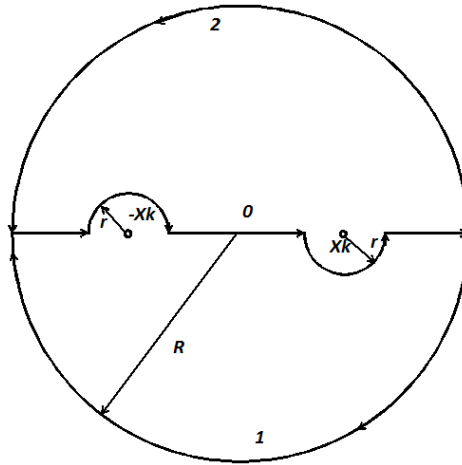
Figure 1.2: Contours of integration. Separation of the poles

Now let the function $f(z) = e^{\pm ipz}g(z)$ satisfy all the conditions of Jourdan's lemma except for the function $g(z)$ to have two real points of singularity $z = \pm p_k$. It is obvious that we cannot apply the lemma directly for finding the integral (1.19). To avoid this complexity, we introduce two following closed contours of integration as shown in Figure 1.2. Here, $r << R$

and $r << 1$. As it can be seen, contour 1 has $z = -p_k$ and contour 2 contains $z = p_k$ inside. Then, we can apply the Jourdan's lemma and state that

$$\int_{-\infty}^{\infty} f(x)\, dx = 2\pi i Res_{z=\pm p_k}\left(f(z)\right), \tag{1.20}$$

where for the negative value of p we choose contour 1 and for positive p we take contour 2.

1.3 Governing equations

1.3.1 Equations of motion for Kirchhoff theory of thin elastic plate bending

In their renowned book Timoshenko and Woinowsky-Krieger (1987), the authors derive an equation for the mid-plane small deflection w in the Kirchhoff classical theory of plate bending. It is applicable for various types of materials. Onwards we study two different shapes of plates, namely semi-infinite and circular ones.

1.3.1.1 Equations of motion in Cartesian coordinate system
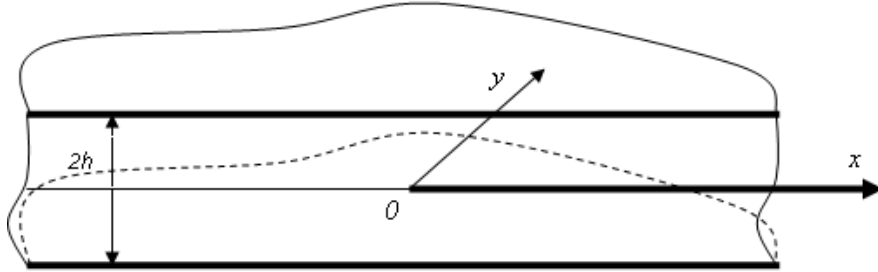
Figure 1.3: Semi-infinite plate. Cartesian coordinate system

In the case of a semi-infinite plate, it is natural to use the Cartesian coordinate system. We specify the directions of the x and y coordinate axes as shown in Figure 1.3. We assume that a plate occupies the space $-\infty < x < \infty$ and $0 \leq y < \infty$ with $-h \leq z \leq h$. In the Kirchhoff plate theory, the equilibrium equation in the Cartesian coordinate system is formulated in the two-dimensional space and takes the following form (here and below see Timoshenko and Woinowsky-Krieger (1987) for more details)

$$\frac{\partial^2 M_x}{\partial x^2} + \frac{\partial^2 M_y}{\partial y^2} - 2\frac{\partial^2 M_{xy}}{\partial x \partial y} = -q, \tag{1.21}$$

where M_x, M_y, M_{xy} are bending moments, q is the intensity of a transverse load.

In the dynamics of plates with traction-free faces, considered below, q is

$$q = -2\rho h \frac{\partial^2 w}{\partial t^2}, \tag{1.22}$$

where h is the half-thickness of the plate, ρ - the density of plate material and w is the plate deflection.

We assume that the material properties of the plate are constant along all directions. Such a material is called isotropic (e.g. see Courtney (1990)). This assumption is justified for many metals, including steel, ets. Such materials are characterised by two constants, namely the Young's modulus E and the Poisson's ratio ν.

To present equation (1.21) in terms of the deflection w of the plate, we express the moments M_x, M_y and M_{xy} as

$$\begin{aligned}
M_x &= -D\left(\frac{\partial^2 w}{\partial x^2} + \nu \frac{\partial^2 w}{\partial y^2}\right), \\
M_y &= -D\left(\frac{\partial^2 w}{\partial y^2} + \nu \frac{\partial^2 w}{\partial x^2}\right), \\
M_{xy} &= D(1-\nu)\frac{\partial^2 w}{\partial x \partial y}.
\end{aligned} \tag{1.23}$$

where D is the flexural rigidity of the plate specified by

$$D = \frac{2Eh^3}{3(1-\nu^2)}. \tag{1.24}$$

Now, substituting (1.24) into (1.21), we obtain the equation of motion in terms of the deflection w as

$$\frac{\partial^4 w}{\partial x^4} + 2\frac{\partial^4 w}{\partial x^2 \partial y^2} + \frac{\partial^4 w}{\partial y^4} + \frac{2\rho h}{D}\frac{\partial^2 w}{\partial t^2} = 0, \tag{1.25}$$

or, in a symbolic form,

$$\Delta_L^2 w + \frac{2\rho h}{D}\frac{\partial^2 w}{\partial t^2} = 0, \tag{1.26}$$

where the differential Laplace operator Δ_L was introduced in Section 1.2.

As it has been mentioned, the material properties of the plate are assumed to be the same along all directions. However, there are cases when this assumption is violated. Let us assume that there exist three planes of material symmetry with respect to its elastic properties. A material with these properties is called orthotropic (e.g. see Courtney (1990)). In the Kirchhoff plate theory the elastic relations are reduced to the 2-dimensional formulae. For the latter case, the four constants, E_x', E_y', E'' and G are used to characterise the elastic

properties of the plate. Taking the aforementioned directions of symmetry as coordinate axes, we may start from the same equation (1.21). In doing so, the bending moments M_x, M_y and M_{xy} are now expressed in terms of the deflection w by the following equalities

$$
\begin{aligned}
M_x &= -\left(D_x \frac{\partial^2 w}{\partial x^2} + D_1 \frac{\partial^2 w}{\partial y^2}\right), \\
M_y &= -\left(D_y \frac{\partial^2 w}{\partial y^2} + D_1 \frac{\partial^2 w}{\partial x^2}\right), \\
M_{xy} &= 2D_{xy} \frac{\partial^2 w}{\partial x \partial y}.
\end{aligned}
\tag{1.27}
$$

Here

$$
\begin{aligned}
D_x &= \frac{E'_x h^3}{3}, \quad D_y = \frac{E'_y h^3}{3}, \\
D_1 &= \frac{E'' h^3}{3}, \quad D_{xy} = \frac{G h^3}{3}.
\end{aligned}
\tag{1.28}
$$

Also, note that the bending stiffnesses D_x, D_y, D_1, and D_{xy} must satisfy the foundational inequalities

$$
D_{xy} > 0, \quad D_x + D_y > 0, \quad D_x D_y - D_1^2 > 0,
\tag{1.29}
$$

which arise from the condition of the positive definiteness of the strain energy density $dV = M_{xy} \frac{\partial^2 w}{\partial x \partial y} - \frac{1}{2}\left(M_x \frac{\partial^2 w}{\partial x^2} + M_y \frac{\partial^2 w}{\partial y^2}\right)$.

On substituting (1.27) into equation (1.21) we get the sought for equation of motion. It is

$$
D_x \frac{\partial^4 w}{\partial x^4} + 2\left(D_1 + 2D_{xy}\right) \frac{\partial^4 w}{\partial x^2 \partial y^2} + D_y \frac{\partial^4 w}{\partial y^4} + 2\rho h \frac{\partial^2 w}{\partial t^2} = 0.
\tag{1.30}
$$

In fact, isotropy is a particular case of orthotropy, in which the material parameters E'_x, E'_y, E'', and G are expressed through E and ν as

$$
E'_x = E'_y = \frac{E}{1 - \nu^2}, \quad E'' = \frac{\nu E}{1 - \nu^2}, \quad G = \frac{E}{2(1 + \nu)},
\tag{1.31}
$$

while the bending stiffnesses D_x, D_y, D_1 and D_{xy} are connected with the flexural rigidity D by

$$
D_x = D_y = D, \quad D_1 = \nu D, \quad D_{xy} = 2(1 - \nu)D.
\tag{1.32}
$$

1.3.1.2   Equation of motion in polar coordinate system

The polar coordinate system becomes optimal when dealing with bending of a circular plate. We return to the case when the plate is an isotropic one. The equation of motion is

$$
\Delta_{L,r,\phi}^2 w + \frac{2\rho h}{D} \frac{\partial^2 w}{\partial t^2} = 0,
\tag{1.33}
$$
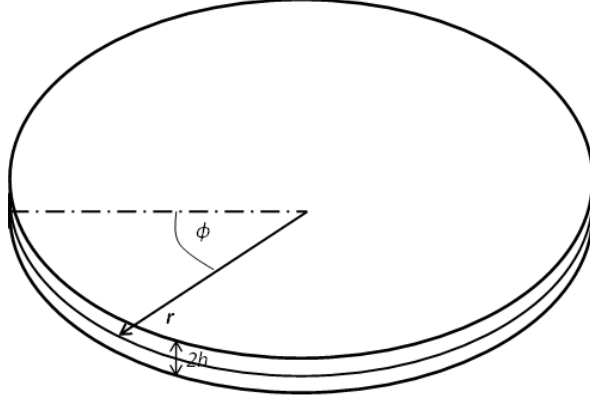
Figure 1.4: Circular plate. Polar coordinate system

where $\Delta_{L,r,\phi}$ is the differential operator presented above in Section 1.2. This equation can be directly obtained by using the relations between Polar and Cartesian coordinates (1.3).

1.3.2 Boundary conditions

1.3.2.1 Cartesian coordinates

We begin with a semi-infinite plate. Assuming that x and y coordinates are taken as shown in Figure 1.3, we consider three types of boundary conditions, including a traction-free edge and also one loaded by external bending moment or shear forces.

If the plate edge is entirely free, it is reasonable to assume that there are no bending and twisting moments, and also no vertical shear forces being indicative, therefore the boundary conditions at $y = 0$ are

$$M_y \;=\; 0, \quad M_{xy} \;=\; 0, \quad S_y \;=\; 0. \tag{1.34}$$

However, it is obvious that only two boundary conditions are sufficient for finding the deflection w. To get rid of this contradiction we have to introduce the so-called Kirchhoff shear force (see Kirchhoff (1850) for more information).

$$V_y = \left(S_y - \frac{\partial M_{xy}}{\partial y} \right). \tag{1.35}$$

In fact, the latter can be justified as a pretty delicate asymptotic analysis of the original 3D problem of elasticity, taking into account boundary layers (e.g. see Friedrichs (1955)).

In terms of deflection w (1.35) can be rewritten as: for an isotropic material

$$V_y = -D \left(\frac{\partial^3 w}{\partial y^3} + (2 - \nu) \frac{\partial^3 w}{\partial x^2 \partial y} \right),$$

for an orthotropic material

$$V_y = -\left(D_y \frac{\partial^3 w}{\partial y^3} + (D_1 + 4D_{xy}) \frac{\partial^3 w}{\partial x^2 \partial y} \right).$$

Thus, the boundary conditions at $y = 0$ are

$$M_y \quad = \quad 0, \quad V_y \quad = \quad 0, \qquad (1.36)$$

or, in terms of the deflection w: for an isotropic plate

$$\begin{aligned}
\frac{\partial^2 w}{\partial y^2} + \nu \frac{\partial^2 w}{\partial x^2} &= 0, \\
\frac{\partial^3 w}{\partial y^3} + (2 - \nu) \frac{\partial^3 w}{\partial x^2 \partial y} &= 0,
\end{aligned} \qquad (1.37)$$

and for an orthotropic material

$$\begin{aligned}
D_y \frac{\partial^2 w}{\partial y^2} + D_1 \frac{\partial^2 w}{\partial x^2} &= 0, \\
D_y \frac{\partial^3 w}{\partial y^3} + (D_1 + 4D_{xy}) \frac{\partial^3 w}{\partial x^2 \partial y} &= 0.
\end{aligned} \qquad (1.38)$$

If the plate edge is loaded, we consider the combination of the bending moments and shear forces. Due to the linear nature of the problem, we can separate the original problem into two; in doing so, the first problem corresponds to the loading in the form of a bending moment, whereas the second one deals with a shear force prescribed at the edge. In this thesis, the problems for the deflection caused by moments and shear forces are studied separately.
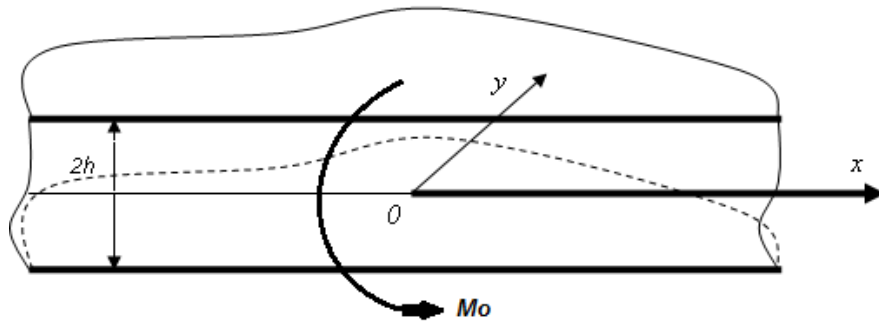
Figure 1.5: Bending moment at the plate edge. Loading scheme

For a bending moment $M_y = M_0(x, t)$ applied at the plate edge $y = 0$ as shown in Figure 1.5, the boundary conditions become

$$M_y \quad = \quad M_0(x, t), \quad V_y \quad = \quad 0. \qquad (1.39)$$

In terms of w they can be rewritten as: for an isotropic plate

$$\frac{\partial^2 w}{\partial y^2} + \nu \frac{\partial^2 w}{\partial x^2} = -\frac{M_0(x,t)}{D},$$

$$\frac{\partial^3 w}{\partial y^3} + (2 - \nu) \frac{\partial^3 w}{\partial x^2 \partial y} = 0; \tag{1.40}$$

and for an orthotropic plate

$$D_y \frac{\partial^2 w}{\partial y^2} + D_1 \frac{\partial^2 w}{\partial x^2} = -M_0(x,t),$$

$$D_y \frac{\partial^3 w}{\partial y^3} + (D_1 + 4D_{xy}) \frac{\partial^3 w}{\partial x^2 \partial y} = 0. \tag{1.41}$$

Figure 1.6: Transverse shear force at the plate edge. Scheme of loading

For a shear force $N_y = N_0(x,t)$ applied at the plate edge $y = 0$ as shown in Figure 1.6, the boundary conditions become

$$M_y = 0, \quad V_y = N_0(x,t). \tag{1.42}$$

In terms of w they are: for an isotropic plate

$$\frac{\partial^2 w}{\partial y^2} + \nu \frac{\partial^2 w}{\partial x^2} = 0,$$

$$\frac{\partial^3 w}{\partial y^3} + (2 - \nu) \frac{\partial^3 w}{\partial x^2 \partial y} = -\frac{N_0}{D}; \tag{1.43}$$

and for an orthotropic plate

$$D_y \frac{\partial^2 w}{\partial y^2} + D_1 \frac{\partial^2 w}{\partial x^2} = 0,$$

$$D_y \frac{\partial^3 w}{\partial y^3} + (D_1 + 4D_{xy}) \frac{\partial^3 w}{\partial x^2 \partial y} = -N_0. \tag{1.44}$$

1.3.2.2   Boundary conditions in polar coordinates

Considering an isotropic plate, the bending moments M_r, M_ϕ and $M_{r,\phi}$ and shear forces S_r and S_ϕ are expressed in terms of the deflection w as follows

$$
\begin{aligned}
M_r &= -D\left[\frac{\partial^2 w}{\partial r^2} + \nu\left(\frac{1}{r}\frac{\partial w}{\partial r} + \frac{1}{r^2}\frac{\partial^2 w}{\partial \phi^2}\right)\right], \\
M_\phi &= -D\left[\frac{1}{r}\frac{\partial w}{\partial r} + \frac{1}{r^2}\frac{\partial^2 w}{\partial \phi^2} + \nu\frac{\partial^2 w}{\partial r^2}\right], \\
M_{r,\phi} &= (1-\nu)D\left(\frac{1}{r}\frac{\partial^2 w}{\partial r\partial \phi} - \frac{1}{r^2}\frac{\partial w}{\partial \phi}\right),
\end{aligned}
\tag{1.45}
$$

and

$$
\begin{aligned}
S_r &= -D\frac{\partial}{\partial r}\left(\Delta_{L,r,\phi}w\right), \\
S_\phi &= -D\frac{1}{r}\frac{\partial}{\partial \phi}\left(\Delta_{L,r,\phi}w\right).
\end{aligned}
\tag{1.46}
$$

For a traction-free plate edge, boundary conditions have the same form as in Cartesian coordinates, i.e. at $r = R$ (where R is the outer radius of a circular plate), we get

$$
M_r = 0, \quad V_r = 0,
\tag{1.47}
$$

where M_r is specified by the first formula in (1.45), and

$$
V_r = \left(S_r - \frac{1}{r}\frac{\partial M_{r,\phi}}{\partial \phi}\right).
$$

In terms of the deflection w, boundary conditions finally become

$$
\begin{aligned}
\frac{\partial^2 w}{\partial r^2} + \nu\left(\frac{1}{r}\frac{\partial w}{\partial r} + \frac{1}{r^2}\frac{\partial^2 w}{\partial \phi^2}\right) &= 0, \\
\frac{\partial}{\partial r}\left(\Delta_{L,r,\phi}w\right) + (1-\nu)\frac{1}{r}\frac{\partial}{\partial \phi}\left(\frac{1}{r}\frac{\partial^2 w}{\partial r\partial \phi} - \frac{1}{r^2}\frac{\partial w}{\partial \phi}\right) &= 0.
\end{aligned}
\tag{1.48}
$$

Chapter 2

Konenkov flexural edge wave in isotropic plate

2.1 Konenkov flexural edge wave in semi-infinite plate

In this section we consider flexural edge waves appearing in a semi-infinite isotropic plate. Various boundary conditions are considered. An approximate parabolic-elliptic explicit model is formulated.

2.1.1 Homogeneous edge wave

2.1.1.1 Basic equations

We consider elastic bending of an isotropic semi-infinite plate. The equation of motion was formulated in Section 1.3.1 (see (1.25) or (1.26)). First, we study the homogeneous boundary conditions along the plate edge, written in form (1.37).

After introducing new dimensionless quantities by the formulae

$$\xi = \frac{x}{h}, \quad \eta = \frac{y}{h}, \quad W^* = \frac{w}{h}, \quad \tau = \frac{t}{T}, \tag{2.1}$$

where h is the half-thickness of the plate, T is a typical time scale, and applying the Fourier and Laplace integral transforms[1] with respect to ξ-coordinate ($\xi \to ip$) and τ-coordinate

---

[1] Fourier and Laplace transforms will be used further for solving non-homogeneous problems.

$(\tau \to s)$, equation of motion (1.25) and the boundary conditions (1.37) become

$$\frac{d^4\hat{W}}{d\eta^4} - 2p^2\frac{d^2\hat{W}}{d\eta^2} + (p^4 + \lambda_0^2 s^2)\hat{W} = 0, \tag{2.2}$$

where

$$\lambda_0^2 = \frac{2\rho h^5}{T^2 D} \tag{2.3}$$

is the dimensionless frequency parameter, and at $\eta = 0$

$$\begin{aligned}
\frac{d^2\hat{W}}{d\eta^2} - \nu p^2\hat{W} &= 0, \\
\frac{d^3\hat{W}}{d\eta^3} - (2-\nu)p^2\frac{d\hat{W}}{d\eta} &= 0.
\end{aligned} \tag{2.4}$$

Now, we need to find the solution of equation (2.2) with boundary conditions (2.4) which decays at the infinity.

2.1.1.2 Konenkov flexural edge wave speed in isotropic plate

The solution of problem (2.2)-(2.4) can be taken in the form

$$\hat{W}(\eta) = Ce^{-\gamma\eta}, \tag{2.5}$$

On substituting it into (2.2) we find the values of the parameter γ

$$\begin{aligned}
\gamma_{1,2} &= \pm\sqrt{p^2 + i\lambda_0 s}, \\
\gamma_{3,4} &= \pm\sqrt{p^2 - i\lambda_0 s}
\end{aligned}$$

According to the conditions at infinity (therefore, we need $Re(\gamma_i) > 0$, $i = 1, 2, 3, 4$) we write the sought for solution as follows

$$\hat{W}(\eta) = Ae^{-\alpha\eta} + Be^{-\beta\eta}, \tag{2.6}$$

where

$$\begin{aligned}
\alpha &= \sqrt{p^2 + i\lambda_0 s}, \\
\beta &= \sqrt{p^2 - i\lambda_0 s},
\end{aligned} \tag{2.7}$$

and A and B are arbitrary constants.

We substitute (2.6) into the boundary conditions (2.4). This leads to a system of two linear equations for the unknowns A and B. We write this system in matrix form. Thus,

$$\begin{bmatrix} \alpha^2 - \nu p^2 & \beta^2 - \nu p^2 \\ (\alpha^2 - (2-\nu)p^2)\alpha & (\beta^2 - (2-\nu)p^2)\beta \end{bmatrix} \begin{bmatrix} A \\ B \end{bmatrix} = \begin{bmatrix} 0 \\ 0 \end{bmatrix}. \tag{2.8}$$

System (2.8) has a non-zero solution only when the determinant of the matrix in the left-hand side equals to zero. As a result, we get

$$(\beta - \alpha)\left[\alpha^2\beta^2 - (\alpha^2 + \beta^2)\nu p^2 + 2(1 - \nu)\alpha\beta p^2 + \nu(2 - \nu)p^4\right] = 0, \tag{2.9}$$

or

$$s^2\lambda_0^2 + (1 - \nu^2)p^4 + 2(1 - \nu)\sqrt{p^4 + s^2\lambda_0^2}p^2 = 0. \tag{2.10}$$

Before proceeding to the analysis of this equation, let us introduce the parameter

$$c = \frac{\sqrt{-is\lambda_0}}{p} \tag{2.11}$$

In terms of c, equation (2.10) can be rewritten as

$$1 - \nu^2 - c^4 + 2(1 - \nu)\sqrt{1 - c^4} = 0. \tag{2.12}$$

Now, we multiply the above equation by

$$X(c) = 1 - \nu^2 - c^4 - 2(1 - \nu)\sqrt{1 - c^4}, \tag{2.13}$$

which never equals zero at the zeros of the denominator. This can be seen in Figure 2.1. We
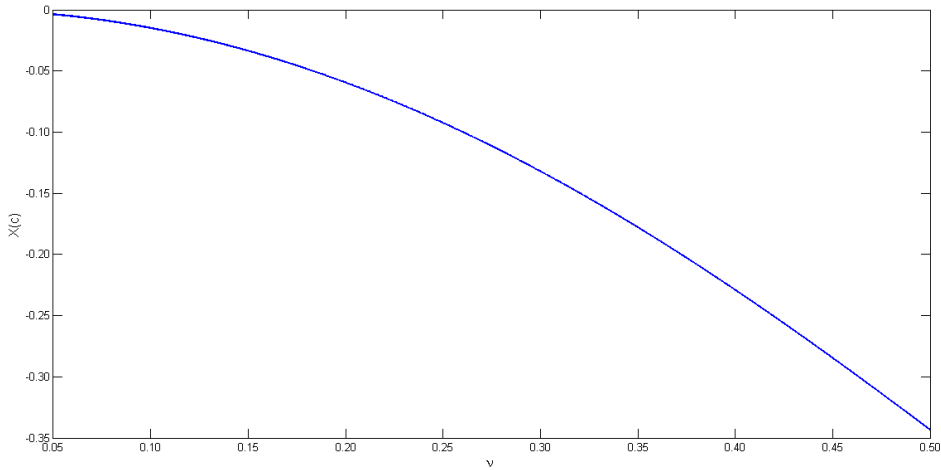
Figure 2.1: Function $X(c)$ at the first zero of denominator versus Poisson's ratio

use this function below when operating with the solutions of the related problems.

Then, it becomes straightforward to find the solutions of the amended equation in the following form

$$\begin{aligned}
c_k^4 &= (1 - \nu)\left[3\nu - 1 + 2\sqrt{2\nu^2 - 2\nu + 1}\right], \\
c_2^4 &= (1 - \nu)\left[3\nu - 1 - 2\sqrt{2\nu^2 - 2\nu + 1}\right].
\end{aligned} \tag{2.14}$$
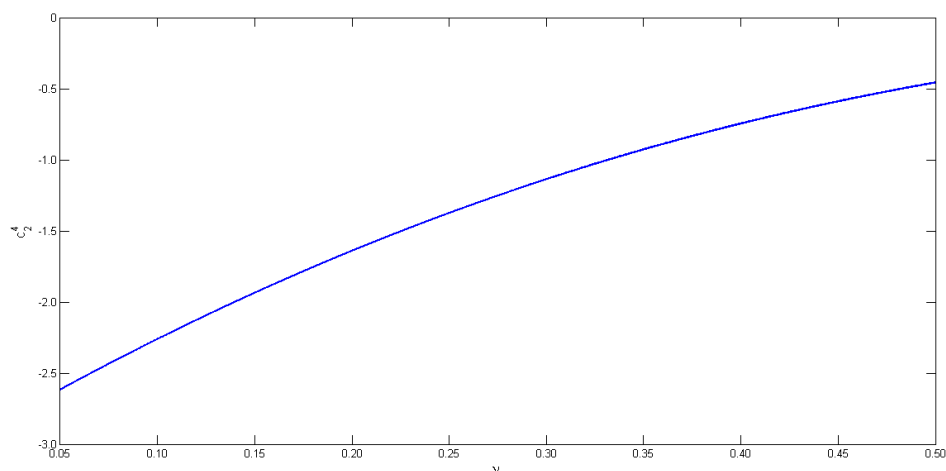
Figure 2.2: Second root c_2^4 versus Poisson's ratio

It can be seen in Figure 2.2 that c_2^4 has a negative value, and, therefore, it has no physical meaning. The only root of this equation, in which we are interested in, is the root c_k corresponding to the so-called Konenkov flexural edge wave speed (Konenkov (1960)). Note that Konenkov flexural edge wave speed depends on a number of parameters including the frequency parameter λ_0, therefore we treat c_k as a Konenkov flexural edge wave coefficient. Dependence of c_k on Poisson's ratio is shown in Figure 2.3.
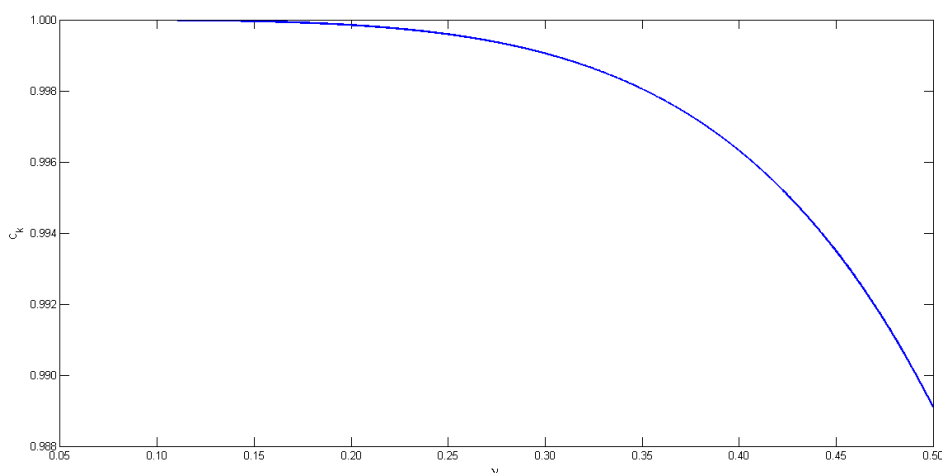
Figure 2.3: Konenkov flexural edge wave coefficient versus Poisson's ratio

2.1.2   Bending moment at plate edge

2.1.2.1   Basic equations

Now we assume that a bending moment is applied at the semi-infinite plate edge $y = 0$. In this case, the equation of motion can be taken in form (1.25) as before. The boundary conditions for this type of loading were considered in Section 1.3.2 (see formula (1.42)).

As in Section 2.1.1, we introduce dimensionless quantities (2.1) and after applying the integral transforms we arrive at equation of motion (2.2). Boundary conditions (1.43) transform to

$$
\begin{aligned}
\frac{d^2\hat{W}}{d\eta^2} - \nu p^2 \hat{W} &= -\hat{M}_0, \\
\frac{d^3\hat{W}}{d\eta^3} - (2-\nu)p^2 \frac{d\hat{W}}{d\eta} &= 0,
\end{aligned}
\tag{2.15}
$$

where $\hat{M}_0(p, s)$ is the transformed dimensionless bending moment applied at the plate edge

$$
\hat{M}_0(p, s) = \frac{h}{\sqrt{2\pi}D} \int_{-\infty}^{\infty} e^{-ip\xi} \left(\int_0^{\infty} M_0^*(\xi, \tau) e^{-s\tau} d\tau \right) dp.
\tag{2.16}
$$

2.1.2.2   Exact solution in terms of integral transforms

We further seek for the solution of problem (2.2), (2.15) in form (2.6), where α and β are the parameters from (2.7). The substitution of the solution into boundary conditions (2.15) results in a system of linear equations for the unknown constants A and B. It can be presented in a matrix form as

$$
\begin{bmatrix}
\alpha^2 - \nu p^2 & \beta^2 - \nu p^2 \\
(\alpha^2 + (2-\nu)p^2)\alpha & (\beta^2 + (2-\nu)p^2)\beta
\end{bmatrix}
\begin{bmatrix}
A \\
B
\end{bmatrix}
=
\begin{bmatrix}
-\hat{M}_0 \\
0
\end{bmatrix}.
\tag{2.17}
$$

In Section 2.1.1 we explored only the determinant of this system, whereas now we express its solution as

$$
A = \frac{\Delta_1}{\Delta}, \quad B = \frac{\Delta_2}{\Delta},
\tag{2.18}
$$

where

$$
\begin{aligned}
\Delta &=
\begin{vmatrix}
\alpha^2 - \nu p^2 & \beta^2 - \nu p^2 \\
(\alpha^2 - (2-\nu)p^2)\alpha & (\beta^2 - (2-\nu)p^2)\beta
\end{vmatrix} \\[2mm]
&= (\beta - \alpha)\left[\alpha^2\beta^2 - (\alpha^2 + \beta^2)\nu p^2 + 2(1-\nu)\alpha\beta p^2 + \nu(2-\nu)p^4 \right],
\end{aligned}
$$

and

$$\Delta_1 = \begin{vmatrix} -\hat{M}_0 & \beta^2 - \nu p^2 \\ 0 & (\beta^2 - (2-\nu)p^2)\beta \end{vmatrix} = -\hat{M}_0 \left[\beta^2 - (2-\nu)p^2\right]\beta,$$

$$\Delta_2 = \begin{vmatrix} \alpha^2 - \nu p^2 & -\hat{M}_0 \\ (\alpha^2 - (2-\nu)p^2)\alpha & 0 \end{vmatrix} = \hat{M}_0 \left[\alpha^2 - (2-\nu)p^2\right]\alpha.$$

Finally, the transformed solution for a semi-infinite plate deflection, expressed through parameter c (see (2.11)) appears as

$$\hat{W}(\eta) = \frac{\hat{M}_0}{-is\lambda_0}\frac{c^2}{c^4 - c_k^4}\frac{\Delta_1(c)e^{-\frac{\sqrt{-is\lambda_0}}{c}\alpha_c\eta} + \Delta_2(c)e^{-\frac{\sqrt{-is\lambda_0}}{c}\beta_c\eta}}{\Delta(c)}X(c), \tag{2.19}$$

with

$$\begin{aligned}
\Delta_1(c) &= \left[(1-\nu) - c^2\right]\sqrt{1+c^2}, \\
\Delta_2(c) &= -\left[(1-\nu) + c^2\right]\sqrt{1-c^2}, \\
\Delta(c) &= (\beta_c - \alpha_c)(c^4 - c_2^4),
\end{aligned} \tag{2.20}$$

and

$$\begin{aligned}
\alpha_c &= \sqrt{1-c^2}, \\
\beta_c &= \sqrt{1+c^2},
\end{aligned} \tag{2.21}$$

where $X(c)$ is given by (2.13).

2.1.2.3 Derivation of explicit dual parabolic-elliptic model for Konenkov flexural edge wave

Our goal now is to determine the Konenkov flexural edge wave contribution in exact solution (2.19). It is natural to assume that this contribution is dominated by the poles $c = \pm c_k$ of the denominator. For this reason, we expand the transformed solution around its zeros $c = \pm c_k$ to take into account only the contribution of the Konenkov flexural edge wave. Thus, we get in the leading order at the plate edge $\eta = 0$

$$\hat{W}_e = Q_e^{(1)}(c_k)\frac{\hat{M}_0}{-is\lambda_0}\frac{c^2}{c^4 - c_k^4}, \tag{2.22}$$

where

$$Q_e^{(1)} = \frac{\Delta_1(c_k) + \Delta_2(c_k)}{\Delta(c_k)}X(c_k), \tag{2.23}$$

or, in terms of the transform parameter p, we have

$$\hat{W}_e = -Q_e^{(1)}\hat{M}_0\frac{p^2}{p^4 c_k^4 + s^2\lambda_0^2}. \tag{2.24}$$

The last expression satisfies the following dimensionless equation

$$c_k^4 \frac{\partial^4 W_e^*}{\partial \xi^4} + \lambda_0^2 \frac{\partial^2 W_e^*}{\partial \tau^2} = Q_e^{(1)} \frac{h^2}{D} \frac{\partial^2 M_0^*(\xi, \tau)}{\partial \xi^2},$$

which corresponds to the equation in the original dimensional variables

$$c_k^4 \frac{\partial^4 w_e}{\partial x^4} + \frac{2\rho h}{D} \frac{\partial^2 w_e}{\partial t^2} = Q_e^{(1)} \frac{1}{D} \frac{\partial^2 M_0}{\partial x^2}, \qquad (2.25)$$

where $w_e(x, t)$ is the edge deflection associated with the Konenkov flexural edge wave.

To obtain an equation over the interior domain we substitute the expression for the Konenkov flexural edge wave poles $s^2 = -\frac{c_k^4}{\lambda_0^2} p^4$ into the transformed equation of motion (2.2), resulting in

$$\frac{d^4 \hat{W}_{in}}{d\eta^4} - 2p^2 \frac{d^2 \hat{W}_{in}}{d\eta^2} + (1 - c_k^4) p^4 \hat{W}_{in} = 0. \qquad (2.26)$$

In the original variables the latter becomes

$$\frac{\partial^4 w_{in}}{\partial y^4} + 2\frac{\partial^4 w_{in}}{\partial x^2 \partial y^2} + (1 - c_k^4)\frac{\partial^4 w_{in}}{\partial x^4} = 0, \qquad (2.27)$$

with $w_{in}(x, y)$ is the deflection within the interior domain, induced by the Konenkov flexural edge wave.

The first boundary condition for $w_{in}(x, y)$ may be taken as

$$w_{in}(x, 0) = w_e(x), \qquad (2.28)$$

while the second one may be implied in the form

$$\frac{\partial^2 w_{in}}{\partial y^2} = -\nu \frac{\partial^2 w_e}{\partial x^2}. \qquad (2.29)$$

Such a choice of the boundary conditions is specified by the idea of the model. Let us consider the case when the boundary conditions have more intuitive form

$$\begin{aligned} w_{in}(x, 0) &= w_e(x), \\ \frac{\partial^2 w_{in}}{\partial y^2} &= -\nu \frac{\partial^2 w_e}{\partial x^2} - \frac{M_0}{D}, \end{aligned}$$

where $w_e(x, t)$ is the edge deflection induced by the Konenkov wave only, therefore the solution into the interior, due to the elliptic nature of its equation (2.27), naturally should be a decay of w_e, and, therefore, should be some function of it. Now, due to the linear character of the problem, we may split the solution and the boundary conditions into

$$\begin{aligned} w_{in,1}(x, 0) &= w_e(x), \\ \frac{\partial^2 w_{in,1}}{\partial y^2} &= -\nu \frac{\partial^2 w_e}{\partial x^2}, \end{aligned}$$

and

$$
\begin{aligned}
w_{in,2}(x,0) &= 0, \\
\frac{\partial^2 w_{in,2}}{\partial y^2} &= -\frac{M_0}{D},
\end{aligned}
$$

Solution $w_{in,1}$ obviously gives the sought for wave decay within the interior, whereas $w_{in,2}$ is the deflection induced by the external bending moment excitation only and obviously is not a deformation from the flexural edge wave. Therefore it should be omitted due to the model nature and method of its construction.

The derived model clearly reveals a dual parabolic-elliptic nature of the Konenkov flexural edge wave. It consists of a parabolic equation (2.25) along the edge and elliptic equation (2.27) over the interior along with boundary conditions (2.28)-(2.29). It is in contrast to a hyperbolic-elliptic nature of the classical Rayleigh wave for which we get a hyperbolic equation instead of the parabolic one at the edge (see Rayleigh (1885) and Kaplunov et al. (2006)).

2.1.2.4   Comparison with exact solution

In the section above we obtained exact solution (2.19) in terms of integral transforms, and also derived explicit dual parabolic-elliptic model for Konenkov flexural edge wave (see (2.25), (2.27)-(2.29)). Next, we compare these solutions by applying the inverse Fourier transform and plotting the graphs for these solutions expressed through the dimensionless deflections. We consider a bending moment $M_0(x,t) = M_0\delta(x)e^{-i\omega t}$ applied at the plate edge $y = 0$. Here and below, Poisson's ratio is assumed to be $\nu = \frac{1}{3}$. In this case, the frequency parameter takes the form

$$
\lambda_0 = \sqrt{\frac{2\rho h^5 \omega^2}{D}}. \tag{2.30}
$$

Also, for the harmonic case under study, the deflection $w(x,y,t)$ may be found as $w(x,y,t) = W(x,y)e^{-i\omega t}$. Thus, we do not need to apply the Laplace integral transform. For the point-moment $\hat{M}_0$ we rewrite the exact solution in a more convenient form using the parameter p, i.e.

$$
\hat{W}(\eta) = \hat{M}_0 \frac{p^2}{p^4 - p_k^4} \frac{\Delta_1(p)e^{-\alpha\eta} + \Delta_2(p)e^{-\beta\eta}}{\Delta(p)} X(p). \tag{2.31}
$$

Here,

$$
\alpha = \sqrt{p^2 - \lambda_0}, \quad \beta = \sqrt{p^2 + \lambda_0}, \tag{2.32}
$$

$$
\begin{aligned}
\Delta_1(p) &= [(1-\nu)p^2 - \lambda_0]\sqrt{p^2 + \lambda_0}, \\
\Delta_2(p) &= -[(1-\nu)p^2 + \lambda_0]\sqrt{p^2 - \lambda_0}, \\
\Delta(p) &= c_k^4 c_2^4 (\beta - \alpha)(p^4 - p_2^4), \\
X(p) &= (1-\nu^2)p^4 - 2(1-\nu)\sqrt{p^4 - \lambda_0^2}p^2 - \lambda_0^2,
\end{aligned}
\tag{2.33}
$$

with

$$
p_k = \frac{\sqrt{\lambda_0}}{c_k}, \quad p_2 = \frac{\sqrt{\lambda_0}}{c_2}.
\tag{2.34}
$$

The deflection corresponding to the Konenkov flexural edge wave may be found from formula (2.31) by isolating the contribution of the poles $p = \pm p_k$ in the overall solution. This contribution follows from the contour integration (see Section 1.2.3). The result of integration W_e^* is

$$
W_e^* = \frac{1}{\sqrt{2\pi}} \left[\int_2 \hat{W}(\eta, z_1) e^{iz_1\xi} dz_1 + \int_4 \hat{W}(\eta, z_2) e^{iz_2\xi} dz_2 \right].
\tag{2.35}
$$

Here and below, the radius r of the semi-circles in Figure 1.1 is taken as

$$
r = \frac{|1 - c_k|}{10000},
\tag{2.36}
$$

due to the sensitivity of the calculations in Matlab. This is the lower limit of the universal expression for r in all problems solved in the thesis.

The solution of parabolic equation (2.25) follows immediately from the residue theory (see Section 1.2.4). It is given by

$$
W_e^* = \frac{1}{\sqrt{2\pi}} \int_{-\infty}^{\infty} \hat{W}_e(\eta, p) e^{ipx} dp = \frac{2\pi i}{\sqrt{2\pi}} Res_{z=p_k}(\hat{W}_e(\eta, z) e^{izx}),
\tag{2.37}
$$

where

$$
\hat{W}_e(\eta, p) = Q_e^{(1)} \hat{M}_0 \frac{p^2}{p^4 - p_k^4}
\tag{2.38}
$$

with

$$
Q_e^{(1)} = \frac{\Delta_1(p_k) + \Delta_2(p_k)}{\Delta(p_k)} X(p_k).
\tag{2.39}
$$

Therefore, the explicit solution for the dimensionless plate edge deflection W_e^* corresponding to the Konenkov flexural edge wave is given by

$$
W_e^*(\xi) = \sqrt{2\pi} i Q_e^{(1)} \hat{M}_0 \frac{1}{2p_k} e^{ip_k\xi}.
\tag{2.40}
$$

The graph of the deflection at the plate edge related to the Konenkov flexural edge wave is presented in Figure 2.4. In this case we take the value $\lambda_0 = 1$. Here and below all the
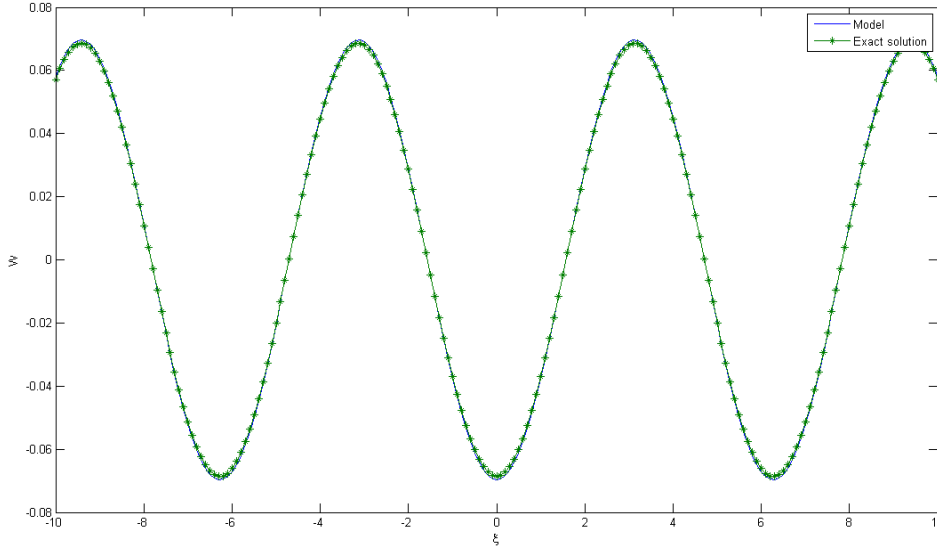
Figure 2.4: Konenkov flexural edge wave in isotropic plate ($\lambda_0 = 1$). Comparison of exact (2.35) and approximate (2.40) solutions

solutions were obtained numerically using Matlab 7.1. Figure 2.4 clearly demonstrates that both methods give similar results, as predicted. Also note that we take the value $\hat{M}_0 = \sqrt{2\pi}$ so that the expression $\dfrac{\hat{M}_0}{\sqrt{2\pi}} = 1$.

To find an overall solution in the dimensionless form $W^*(\xi, \eta)$, we need to evaluate the following integral

$$W^*(\xi, \eta) = \frac{1}{\sqrt{2\pi}} \int_{-\infty}^{\infty} \hat{W}(\eta, p) e^{ip\xi} dp. \tag{2.41}$$

(The method of integrating was described in Section 1.2.3.)

Note that there exist two branch points $p = \pm\sqrt{\lambda_0}$ on the real axis of the solution $\hat{W}(\eta, p)$ (see (2.31)). In the interval between them (when $-\sqrt{\lambda_0} \leq p \leq \sqrt{\lambda_0}$) the quantity α takes the value $\alpha = -i\sqrt{\lambda_0 - p^2}$ to satisfy the Sommerfeld radiation condition at ∞. It is obvious that for $-\infty < p < -\lambda_0$ and $\lambda_0 < p < \infty$ $\alpha = \sqrt{p^2 - \lambda_0}$ is real-valued to ensure the exponential decay.

The obtained numerical solution along with the explicit contribution of the Konenkov flexural edge wave given by (2.40) is shown below for different values of the frequency parameter $\lambda_0 = 0.1$ (Figure 2.5), $\lambda_0 = 1$ (Figure 2.6) and $\lambda_0 = 10$ (Figure 2.7) (at the plate edge $\eta = 0$). Figures 2.5-2.7 show that the Konenkov flexural edge wave makes a dominating contribution to the overall deflection of the plate edge. The only region where the overall deflection is larger than that in the Konenkov flexural edge wave is the vicinity of the point

moment. This is similar to the far-field assumption for the asymptotic model of the Rayleigh wave (see Kaplunov et al. (2006)). Note also that the above vicinity is rather narrow since ξ is the original coordinate x, normalised by the plate half-thickness.
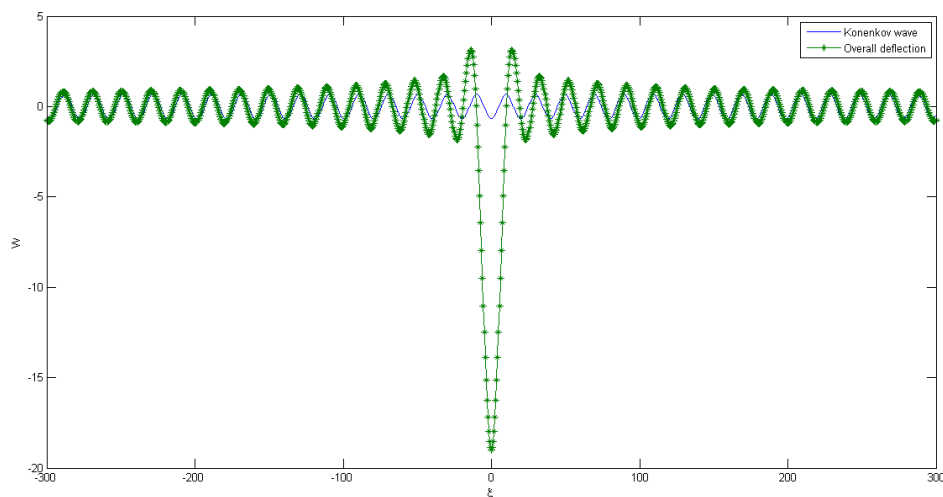
Figure 2.5: Edge deflection in isotropic plate ($\lambda_0 = 0.1$). Overall solution (2.41) and Konenkov flexural edge wave contribution (2.40)
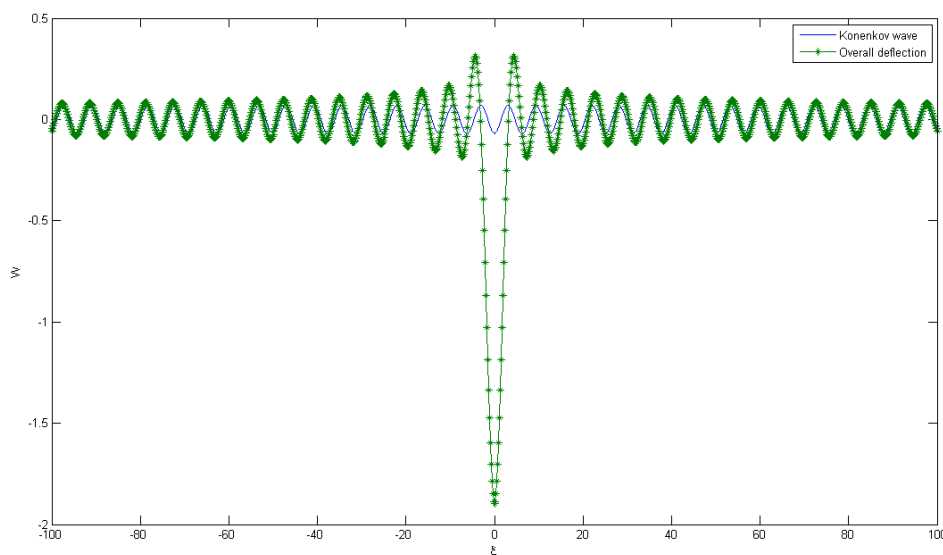
Figure 2.6: Edge deflection in isotropic plate ($\lambda_0 = 1$). Overall solution (2.41) and Konenkov flexural edge wave contribution (2.40)

A similar approach as described above was used to obtain the solutions over the interior domain. Instead of a parabolic equation at the edge, elliptic problem (2.27)-(2.29) is analysed.
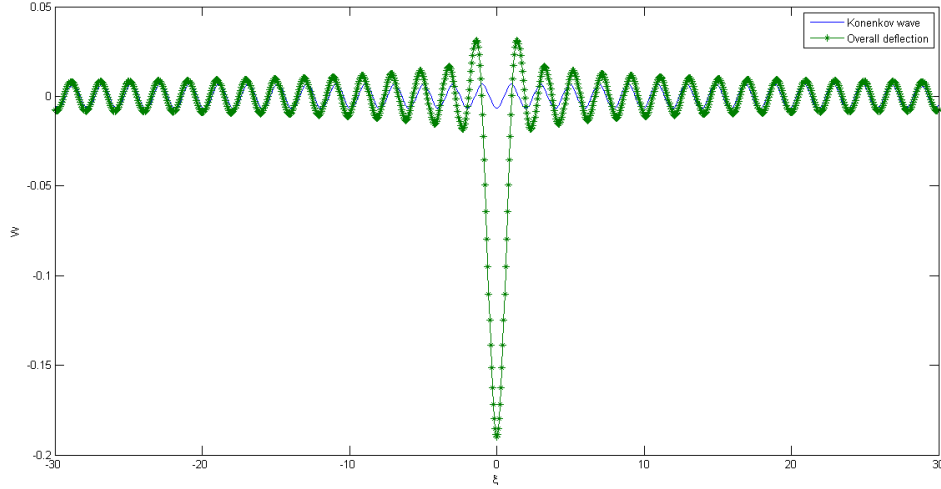
Figure 2.7: Edge deflection in isotropic plate ($\lambda_0 = 10$). Overall solution (2.41) and Konenkov flexural edge wave contribution (2.40)

The solution of this problem is given in terms of the integral transforms. It is

$$
\hat{W}_{in}(\eta, p) = \frac{Q_e^{(1)} \hat{M}_0}{2c_k^2} \frac{p^2}{p^4 - p_k^4} \left[[(1 - \nu) + c_k^2] p^2 e^{-\alpha_c(c_k)p\eta} - [(1 - \nu) - c_k^2] p^2 e^{-\beta_c(c_k)p\eta} \right]. \quad (2.42)
$$

This function may be integrated using the residue theory (see Section 1.2.4), and the final solution for the Konenkov flexural edge wave deflection over the interior domain becomes

$$
W_{in}^*(\xi, \eta) = \sqrt{2\pi} i \frac{Q_e^{(1)} \hat{M}_0}{c_k^2} \frac{1}{4p_k} \left[[(1 - \nu)p_k^2 + \lambda_0] e^{-\alpha(p_k)\eta} - [(1 - \nu)p_k^2 - \lambda_0] e^{-\beta(p_k)\eta} \right] e^{ip_k\xi}. \quad (2.43)
$$

We plot the graphs only for the single value of the frequency parameter $\lambda_0 = 1$ due to the similarity of all the deflection profiles. Numerical solutions, obtained by the scheme described in Section 1.2.3, were also plotted for the various values of the coordinate η. The results are presented in Figures 2.8-2.9. They confirm an intuitive expectation that the Konenkov flexural edge wave makes a key contribution into the exact solution near the edge.

Finally, 3D profiles of the dimensionless deflection associated with the Konenkov flexural edge wave, obtained by the integration of the solutions (2.40) and (2.43) and the profile of the overall deflection are produced (see Figures 2.10-2.11).
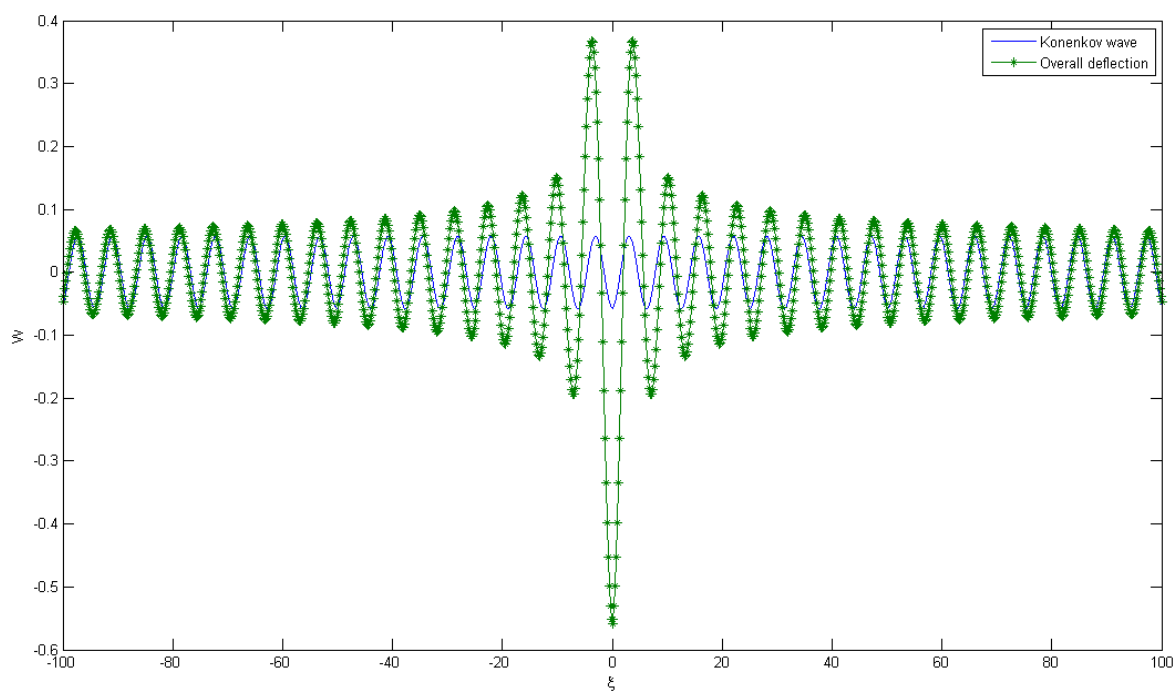
Figure 2.8: Overall deflection of isotropic plate ($\eta = 1$). Overall solution (2.41) and dual parabolic-elliptic model (2.43) for $\lambda_0 = 1$
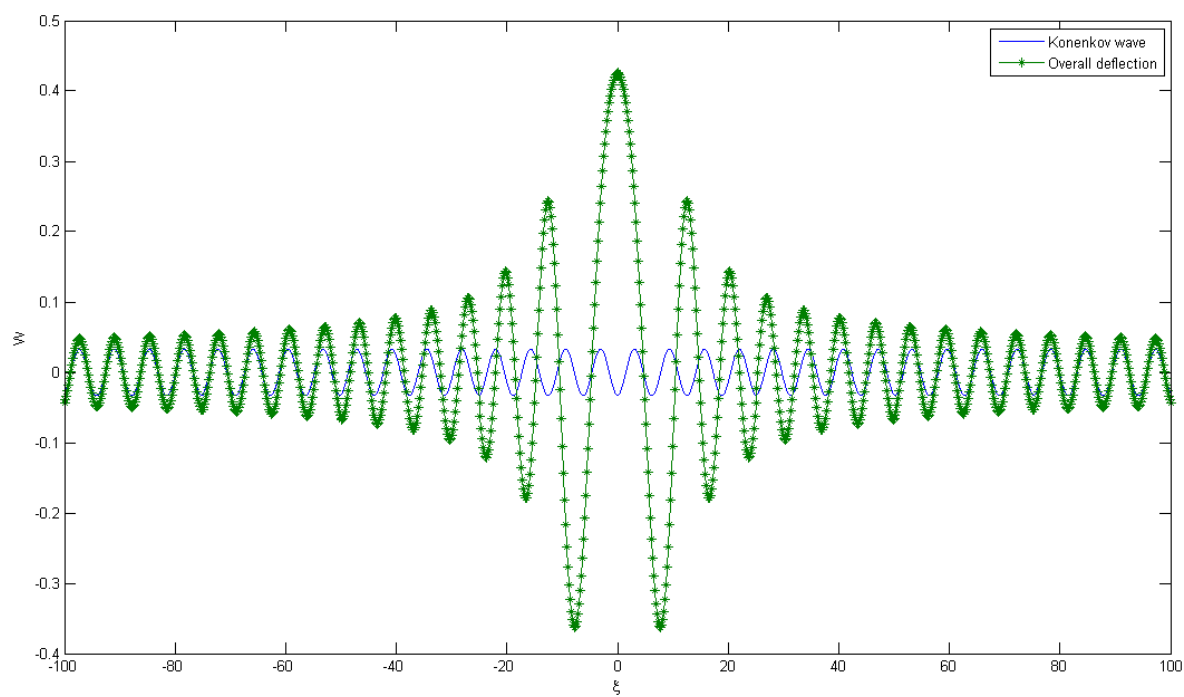
Figure 2.9: Overall deflection of isotropic plate ($\eta = 10$). Overall solution (2.41) and dual parabolic-elliptic model (2.43) for $\lambda_0 = 1$
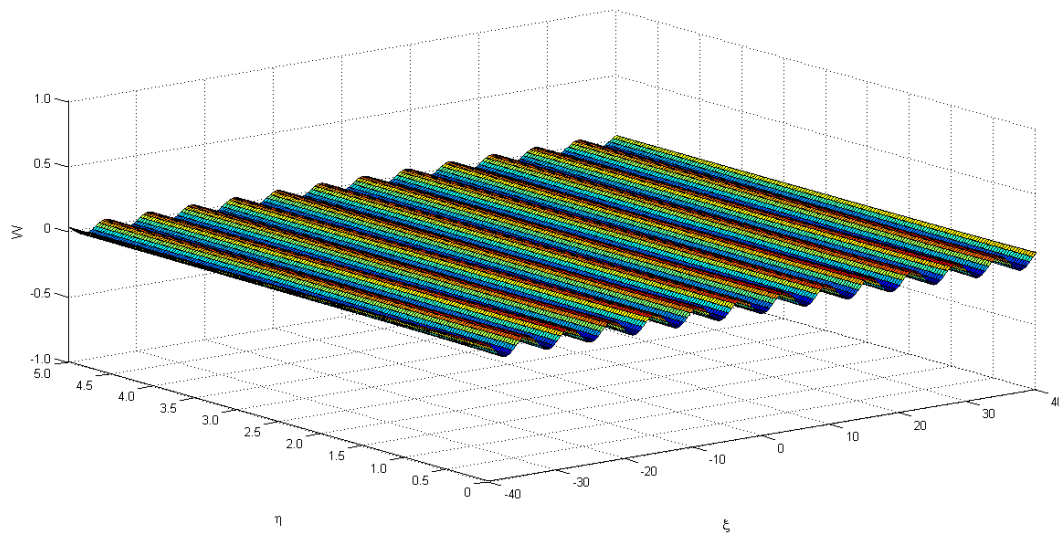
Figure 2.10: Konenkov flexural edge wave in isotropic plate. 3D profile for dual parabolic-elliptic model (2.40) and (2.43) for $\lambda_0 = 1$
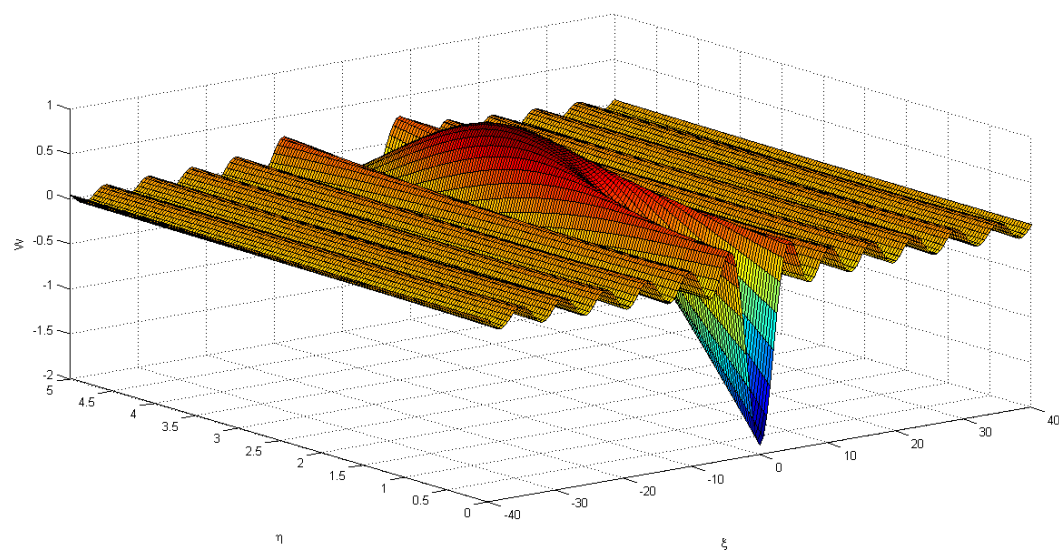
Figure 2.11: Overall deflection of isotropic plate. 3D profile for exact solution (2.41) for $\lambda_0 = 1$

2.1.3 Transverse shear force at plate edge

In this section we consider another type of edge loading in the form of a transverse shear force (see Figure 1.6).

2.1.3.1 Formulation of problem

The equation of motion for w deflection takes the form (1.25) or (1.26) as before, whereas the boundary conditions are given now by (1.43).

By introducing dimensionless quantities (2.1) and applying integral transforms, the sought for equation of motion takes form (2.2); in doing so, boundary conditions (1.43) at $\eta = 0$ become

$$
\begin{aligned}
\frac{d^2\hat{W}}{d\eta^2} - \nu p^2 \hat{W} &= 0, \\
\frac{d^3\hat{W}}{d\eta^3} - (2-\nu)p^2\frac{d\hat{W}}{d\eta} &= -\hat{N}_0,
\end{aligned}
\tag{2.44}
$$

where $\hat{N}_0(p,s)$ is the transformed dimensionless analogue of the original transverse shear force which may be treated as a constant depending only on parameters p and s. It is

$$
\hat{N}_0(p,s) = \frac{h^2}{\sqrt{2\pi}D}\int_{-\infty}^{\infty} e^{-ip\xi}\left(\int_0^{\infty} N_0^*(\xi,\tau)e^{-s\tau}d\tau\right)dp.
\tag{2.45}
$$

As above, the solution of problem (2.2) and (2.44) takes form (2.6)-(2.7). Now we introduce a new function, $v(x,y,t)$, which can be interpreted as the rotation angle about the x-axis.

$$
v(x,y,t) = \frac{\partial w}{\partial y}.
\tag{2.46}
$$

For the latter, an equation of motion may be written in the same form, i.e.

$$
\frac{\partial^4 v}{\partial x^4} + 2\frac{\partial^4 v}{\partial x^2\partial y^2} + \frac{\partial^4 v}{\partial y^4} + \frac{2\rho h}{D}\frac{\partial^2 v}{\partial t^2} = 0.
\tag{2.47}
$$

In terms of the dimensionless quantities (2.1) its transformed analogue becomes

$$
\frac{d^4\hat{V}}{d\eta^4} - 2p^2\frac{d^2\hat{V}}{d\eta^2} + (p^4 + \lambda_0^2 s^2)\hat{V} = 0.
\tag{2.48}
$$

Next, we need to formulate the boundary conditions for the transformed function $\hat{V}(\eta)$. This is expressed through the function $\hat{W}$ as (see (2.6) and (2.7))

$$
\hat{V}(\eta) = -\alpha A e^{-\alpha\eta} - \beta B e^{-\beta\eta}.
\tag{2.49}
$$

On using boundary conditions (2.44) for $\hat{W}$ we conclude that at $\eta = 0$

$$
\begin{aligned}
\frac{d\hat{V}}{d\eta} - \nu p^2 \hat{W}(0) &= 0, \\
\frac{d^2\hat{V}}{d\eta^2} - (2-\nu)p^2 \hat{V}(0) &= -\hat{N}_0.
\end{aligned}
\tag{2.50}
$$

Then we express $\hat{W}(\eta)$ through $\hat{V}(\eta)$ at the plate edge $\eta = 0$. From (2.49) we deduce that

$$
\hat{V}(0) = -\alpha A - \beta B.
$$

Substitution of (2.49) into the second equation (2.50) yields

$$
-(\alpha^2 - (2-\nu)p^2)\alpha A - (\beta^2 - (2-\nu)p^2)\beta B = -\hat{N}_0.
$$

As a result, we get a system for the unknown constants A and B as follows

$$
\begin{aligned}
\alpha A + \beta B &= -\hat{V}(0), \\
\left(\alpha^2 - (2-\nu)p^2\right)\alpha A + \left(\beta^2 - (2-\nu)p^2\right)\beta B &= \hat{N}_0.
\end{aligned}
$$

The solution of this system is given by

$$
\begin{aligned}
A &= -\frac{\beta\left(\hat{V}(0)\left(\beta^2 - (2-\nu)p^2\right) + \hat{N}_0\right)}{\alpha\beta(\beta^2 - \alpha^2)}, \\
B &= \frac{\alpha\left(\hat{V}(0)\left(\alpha^2 - (2-\nu)p^2\right) + \hat{N}_0\right)}{\alpha\beta(\beta^2 - \alpha^2)}.
\end{aligned}
$$

On inserting the expressions for A and B into the formula for $\hat{W}(0)$ we get

$$
\hat{W}(0) = A + B = -\frac{\hat{N}_0}{\alpha\beta(\alpha+\beta)} - \hat{V}(0)\frac{\beta^2 + \alpha\beta + \alpha^2 - (2-\nu)p^2}{\alpha\beta(\alpha+\beta)}.
$$

Thus, we expressed the transformed deflection $\hat{W}(0)$ at the plate edge through the transformed rotation angle $\hat{V}(0)$. The sought for boundary conditions for $\hat{V}(\eta)$ at $\eta = 0$ take the form

$$
\begin{aligned}
\alpha\beta(\alpha+\beta)\frac{d\hat{V}}{d\eta} + \nu p^2 Y(p)\hat{V}(0) &= -\nu p^2 \hat{N}_0, \\
\frac{d^2\hat{V}}{d\eta^2} - (2-\nu)p^2 \hat{V}(0) &= -\hat{N}_0,
\end{aligned}
\tag{2.51}
$$

where

$$
Y(p) = \beta^2 + \alpha\beta + \alpha^2 - (2-\nu)p^2.
\tag{2.52}
$$

2.1.3.2 Exact solution in terms of integral transforms

We take the solution of the problem, formulated in the previous section, as

$$\hat{V}(\eta) = A_1 e^{-\alpha\eta} + B_1 e^{-\beta\eta}. \tag{2.53}$$

It can be easily verified that it satisfies the above equation of motion (2.48), and we can proceed with finding the unknown constants A_1 and B_1 using boundary conditions (2.51). The substitution of (2.53) into (2.51) leads to a system for A_1 and B_1, which may be presented in a matrix form as

$$\begin{bmatrix} -Y(p)\nu p^2 + \alpha^2\beta(\alpha+\beta) & -Y(p)\nu p^2 + \alpha\beta^2(\alpha+\beta) \\ \alpha^2 - (2-\nu)p^2 & \beta^2 + (2-\nu)p^2 \end{bmatrix} \begin{bmatrix} A_1 \\ B_1 \end{bmatrix} = \begin{bmatrix} \nu p^2 \hat{N}_0 \\ -\hat{N}_0 \end{bmatrix}.$$

As shown above, the formulae for A_1 and B_1 are given by

$$A_1 = \frac{\Delta_1}{\Delta}, \quad B_1 = \frac{\Delta_2}{\Delta}, \tag{2.54}$$

where

$$\Delta = -(\beta - \alpha)\left[\alpha^2\beta^2 - (\alpha^2 + \beta^2)\nu p^2 - 2(1-\nu)\alpha\beta p^2 + \nu(2-\nu)p^4\right], \tag{2.55}$$

and

$$\begin{aligned} \Delta_1 &= \hat{N}_0 \alpha(\beta^2 - \nu p^2), \\ \Delta_2 &= -\hat{N}_0 \beta(\alpha^2 - \nu p^2). \end{aligned} \tag{2.56}$$

Next, we determine the zeroes of the denominator Δ in (2.55). Comparison with equation (2.9) shows that it has the same zeros (2.14).

On introducing the parameter c from (2.11), we present the solution for $\hat{V}(\eta)$ as

$$\hat{V}(\eta) = \frac{\hat{N}_0}{-is\lambda_0} \frac{c^2}{(c^4 - c_k^4)} \frac{\Delta_1(c)e^{-\frac{\sqrt{-is\lambda_0}}{c}\alpha_c\eta} + \Delta_2(c)e^{-\frac{\sqrt{-is\lambda_0}}{c}\beta_c\eta}}{\Delta(c)} X(c), \tag{2.57}$$

where

$$\begin{aligned} \Delta(c) &= -(\beta_c - \alpha_c)(c^4 - c_2^4), \\ \Delta_1(c) &= -\left[(1-\nu) + c^2\right]\sqrt{1 - c^2}, \\ \Delta_2(c) &= \left[(1-\nu) - c^2\right]\sqrt{1 + c^2}. \end{aligned} \tag{2.58}$$

Here, α_c and β_c were given previously in (2.20) and the function $X(c)$ was presented by equality (2.13).

2.1.3.3   Derivation of explicit dual parabolic-elliptic model

To investigate the contribution of the poles associated with the Konenkov flexural edge wave, we set $c = \pm c_k$ in the formula (2.57). The result is ($\eta = 0$)

$$\hat{V}_e = A_1 + B_1 = \frac{\hat{N}_0}{-is\lambda_0}\frac{c^2}{\left(c^4 - c_k^4\right)}Q_e^{(2)},$$

where

$$Q_e^{(2)} = \frac{\Delta_1(c_k) + \Delta_2(c_k)}{\Delta(c_k)}X(c_k), \tag{2.59}$$

or, in terms of parameter p

$$\hat{V}_e = -\hat{N}_0\frac{p^2}{c_k^4 p^4 + \lambda_0^2 s^2}Q_e^{(2)}. \tag{2.60}$$

This solution rewritten in the original variables corresponds to the equation for the rotation angle around the x-axis

$$c_k^4\frac{\partial^4 v_e(x,t)}{\partial x^4} + \frac{2\rho h}{D}\frac{\partial^2 v_e}{\partial t^2} = Q_e^{(2)}\frac{1}{D}\frac{\partial^2 N_0}{\partial x^2}, \tag{2.61}$$

where $v_e(x,t)$ is the rotation angle at the plate edge.

To obtain an equation for the rotation angle over the interior domain we can substitute the expression for the Konenkov flexural edge wave poles $s^2 = -\dfrac{c_k^4}{\lambda_0^2}p^4$ into the transformed equation of motion (2.48), resulting in

$$\frac{d^4\hat{V}_{int}}{d\eta^4} - 2p^2\frac{d^2\hat{V}_{int}}{d\eta^2} + (1 - c_k^4)p^4\hat{V}_{int}(\eta) = 0,$$

which corresponds to the equation in the original variables

$$\frac{\partial^4 v_{int}}{\partial y^4} + 2\frac{\partial^4 v_{int}}{\partial x^2 \partial y^2} + (1 - c_k^4)\frac{\partial^4 v_{int}}{\partial x^4} = 0, \tag{2.62}$$

where $v_{int}(x,y)$ is the rotation angle for the Konenkov flexural edge wave over the interior domain.

The first boundary condition for $v_{int}(x,y)$ is

$$v_{int}(x,0) = v_e(x), \tag{2.63}$$

while the second one follows from the second boundary condition (2.51) at $y = 0$

$$\frac{\partial^2 v_{int}}{\partial y^2} = -(2 - \nu)\frac{\partial^2 v_e}{\partial x^2}.$$

(2.64)

The remark about the right hand side of the above boundary conditions is similar to the one described above in Section 2.1.2. The idea of model construction is that these models reveal deformations caused only by the Konenkov wave, and omit those of bulk waves of any types.

Derived model (2.61)-(2.64) also reveals the dual parabolic-elliptic nature of the Konenkov flexural edge wave. However, in the case of transverse shear force, it is derived for the rotation angle v.

2.1.3.4   Explicit model for edge wave induced by transverse shear force. Attempt of alternative formulation

As yet we have derived no model in terms of deflections for this type of loading (see Figure 1.6). Further we will try to reveal our reasons for this choice.

Let the equation of motion for the plate deflection w again be given by (1.25) or (1.26), and the boundary conditions take form (1.43). In dimensionless quantities (2.1) the transformed equation and boundary conditions take form (2.2) and (2.44), respectively.

This time we express the sought for solution in terms of the transformed deflection $\hat{W}(\eta)$. As above, the solution of problem (2.2), (2.44) can be found in form (2.6)-(2.7). On substituting solution (2.6) into boundary conditions (2.44) we get a system of linear equations for the unknown constants A and B. In a matrix form, the latter can be written as

$$\begin{bmatrix} \alpha^2 - \nu p^2 & \beta^2 - \nu p^2 \\ (\alpha^2 - (2 - \nu)p^2)\alpha & (\beta^2 - (2 - \nu)p^2)\beta \end{bmatrix} \begin{bmatrix} A \\ B \end{bmatrix} = \begin{bmatrix} 0 \\ -\hat{N}_0 \end{bmatrix}.$$

(2.65)

On introducing the parameter c from (2.11) and the function $X(c)$ from (2.13), we present the above constants as

$$\begin{aligned} A &= \frac{c^3}{(-is\lambda_0)^{3/2}(c^4 - c_k^4)}\hat{N}_0\frac{\Delta_1(c)}{\Delta(c)}X(c), \\ B &= \frac{c^3}{(-is\lambda_0)^{3/2}(c^4 - c_k^4)}\hat{N}_0\frac{\Delta_2(c)}{\Delta(c)}X(c), \end{aligned}$$

(2.66)

where

$$\begin{aligned} \Delta_1(c) &= \left[(1 - \nu) + c^2\right], \\ \Delta_2(c) &= -\left[(1 - \nu) - c^2\right], \\ \Delta(c) &= -(\beta_c - \alpha_c)(c^4 - c_2^4). \end{aligned}$$

(2.67)

Finally, the transformed deflection of the plate becomes

$$\hat{W}(\eta) = \frac{\hat{N}_0}{(-is\lambda_0)^{3/2}} \frac{c^3}{c^4 - c_k^4} \frac{\Delta_1(c)e^{-\frac{\sqrt{-is\lambda_0}}{c}\alpha_c\eta} + \Delta_2(c)e^{-\frac{\sqrt{-is\lambda_0}}{c}\beta_c\eta}}{\Delta(c)} X(c). \qquad (2.68)$$

It is remarkable that the last formula does not allow an elegant explicit model for the Konenkov flexural edge wave to be derived, as it has been done above, due to the c^3 factor because the odd power does not lead to the sought for real-valued differential operator (see Section 1.2.2). Such a model may be derived from the expression for the transformed rotation angle. On using the relation between the functions $\hat{W}(\eta)$ and $\hat{V}(\eta)$, we get a formula for the transformed rotation angle. As it might be expected, it takes the same form (see (2.57) and (2.58) above).

2.1.3.5   Comparison with exact solution

Comparison of the derived model (2.61)-(2.64) and the exact formulation (2.57) utilises the same methodology as in Section 2.1.2. Below, the shear force is taken in the form $N_0(x,t) = N_0\delta(x)e^{-i\omega t}$.

The edge rotation angle, associated with the Konenkov flexural edge wave, may be found in two ways. First, we calculate the contribution to the exact solution related to the poles. Let us evaluate the integrals

$$V_e^* = \frac{1}{\sqrt{2\pi}}\left[\int_2 \hat{V}(\eta, z_1)e^{iz_1\xi}dz_1 + \int_4 \hat{V}(\eta, z_2)e^{iz_2\xi}dz_2\right]. \qquad (2.69)$$

In this case the exact solution may be further rewritten in terms of the parameter p as

$$\hat{V}(\eta, p) = \hat{N}_0 \frac{p^2}{p^4 - p_k^4} \frac{\Delta_1(p)e^{-\alpha\eta} + \Delta_2(p)e^{-\beta\eta}}{\Delta(p)} X(p), \qquad (2.70)$$

with

$$\begin{aligned} \Delta_1(p) &= -[(1-\nu)p^2 + \lambda_0]\sqrt{p^2 - \lambda_0}, \\ \Delta_2(p) &= [(1-\nu)p^2 - \lambda_0]\sqrt{p^2 + \lambda_0}, \\ \Delta(p) &= -c_k^4 c_2^4(\beta - \alpha)(p^4 - p_2^4), \end{aligned} \qquad (2.71)$$

where the function $X(p)$ takes the same form (2.33) as above, λ_0 is (2.30) and the quantities α and β are expressed through (2.32).

The solution of the parabolic equation (2.61) is found using the residue theory as

$$V_e^* = \frac{1}{\sqrt{2\pi}}\int_{-\infty}^{\infty} \hat{V}_e(\eta, p)e^{ipx}dp = \frac{2\pi i}{\sqrt{2\pi}}Res_{z=p_k}(\hat{V}_e(\eta, z)e^{iz\xi}). \qquad (2.72)$$

The constant $Q_e^{(2)}$ of the transformed angle $\hat{V}_e$ also can be rewritten in the following form

$$Q_e^{(2)} = \frac{\Delta_1(p_k) + \Delta_2(p_k)}{\Delta(p_k)} X(p_k). \tag{2.73}$$

Finally, the solution for V_e^* induced by the Konenkov flexural edge wave can be written in the form

$$V_e^*(\eta, \xi) = \sqrt{2\pi} i Q_e^{(2)} \hat{N}_0 \frac{1}{2p_k} e^{ip_k\xi}. \tag{2.74}$$

As shown above, the small radius of the integration semi-circle (2.69) is taken as (2.36). Here and below the numerical solutions are created for one value of the frequency parameter $\lambda_0 = 1$ due to the similarity of the rotation profiles. Also, $\hat{N}_0 = \sqrt{2\pi}$ similar to $\hat{M}_0$ in the previous Section 2.1.2.4.

The methodology of obtaining the overall solution is the same as in Section 2.1.2. Also, as above, the integration involves the choice of the branch cuts. The overall numerical solution in the form

$$V^*(\xi, \eta) = \frac{1}{\sqrt{2\pi}} \int_{-\infty}^{\infty} \hat{V}(\eta, p) e^{ip\xi} dp \tag{2.75}$$

compared with the Konenkov flexural edge wave contribution (2.74) is demonstrated in Figure 2.12. It shows that the Konenkov flexural edge wave makes the dominating contribution to the overall edge rotation angle. The only region where the overall angle is larger than that for Konenkov flexural edge wave is the vicinity of the point force. We note again that here ξ is the original coordinate normalised by the plate half-thickness. Therefore, the above vicinity is rather narrow.

A similar approach was used to obtain the solutions over the interior domain. Instead of a parabolic equation at the edge, an elliptic problem (2.62)-(2.64) is analyzed. The solution of this problem is given below in terms of the integral transforms. It is

$$\hat{V}_{in}(\eta, p) = \frac{Q_e^{(2)} \hat{N}_0}{2c_k^2} \frac{p^2}{p^4 - p_k^4} \left[-[(1-\nu) - c_k^2]p^2 e^{-\alpha_c(c_k)p\eta} + [(1-\nu) + c_k^2]p^2 e^{-\beta_c(c_k)p\eta} \right]. \tag{2.76}$$

The above function can be integrated using the residue theory, and the final solution for the Konenkov flexural edge wave rotation angle over the interior domain is presented in the following form

$$V_{in}^*(\xi, \eta) = \sqrt{2\pi} i \frac{Q_e^{(2)} \hat{N}_0}{c_k^2} \frac{1}{4p_k} \left[-[(1-\nu)p_k^2 - \lambda_0]e^{-\alpha(p_k)\eta} + [(1-\nu)p_k^2 + \lambda_0]e^{-\beta(p_k)\eta} \right] e^{ip_k\xi}. \tag{2.77}$$

The numerical data for the interior domain is given in Figures 2.13-2.14. They confirm an intuitive expectation that the Konenkov flexural edge wave makes a key contribution to the exact solution near the edge.

Comparison of the 3D profiles corresponding to the proposed dual parabolic-elliptic model and the exact solution are presented in Figures 2.15-2.16.

Figure 2.12: Edge rotation angle in isotropic plate ($\lambda_0 = 1$). Overall solution (2.75) and Konenkov flexural edge wave contribution (2.74)

Figure 2.13: Overall rotation angle of isotropic plate ($\eta = 1$). Overall solution (2.75) and Konenkov flexural edge wave contribution (2.77)
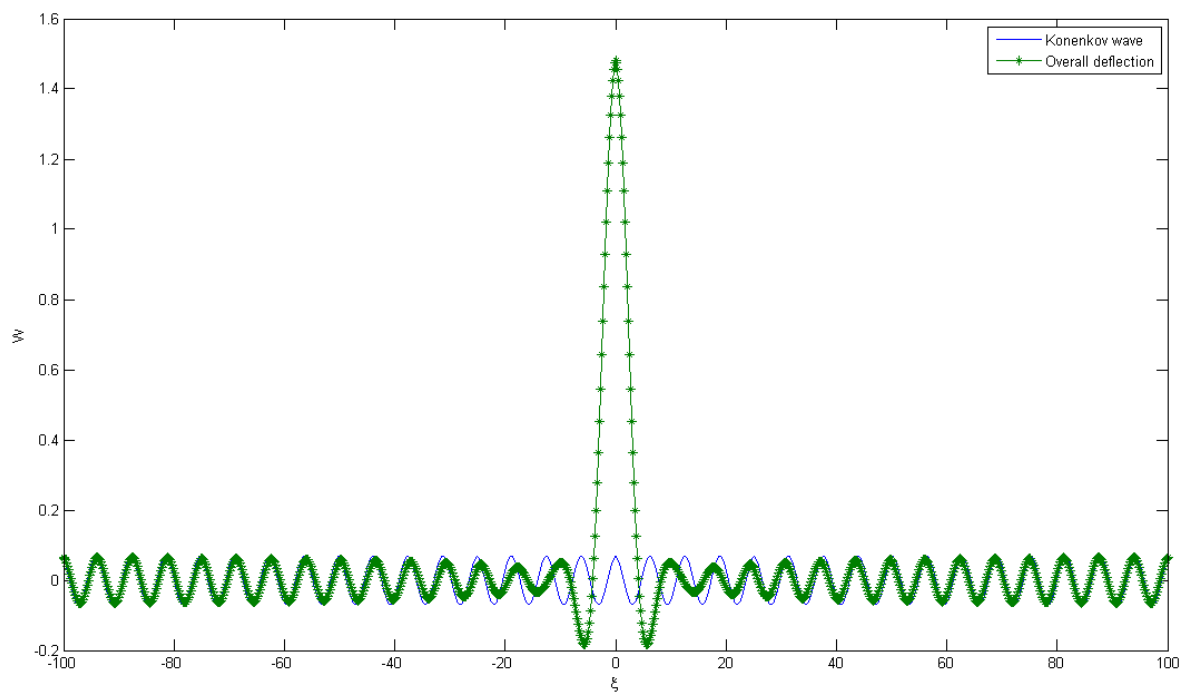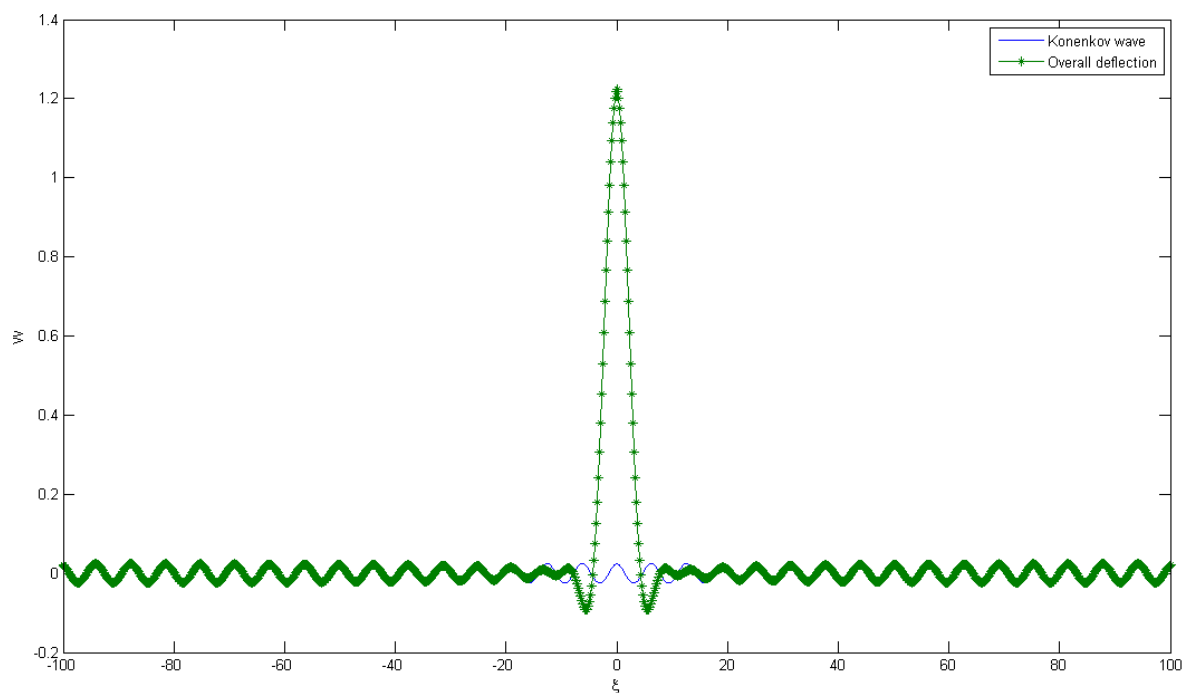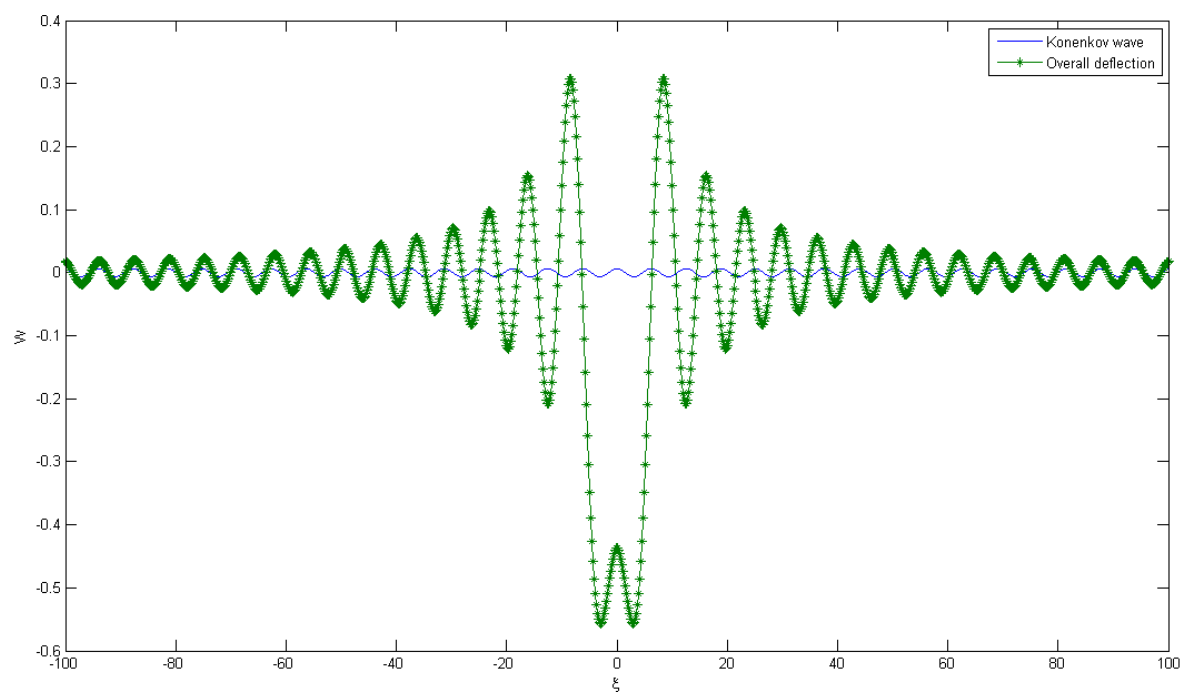

Figure 2.14: Overall rotation angle of isotropic plate ($\eta = 10$). Overall solution (2.75) and Konenkov flexural edge wave contribution (2.77)
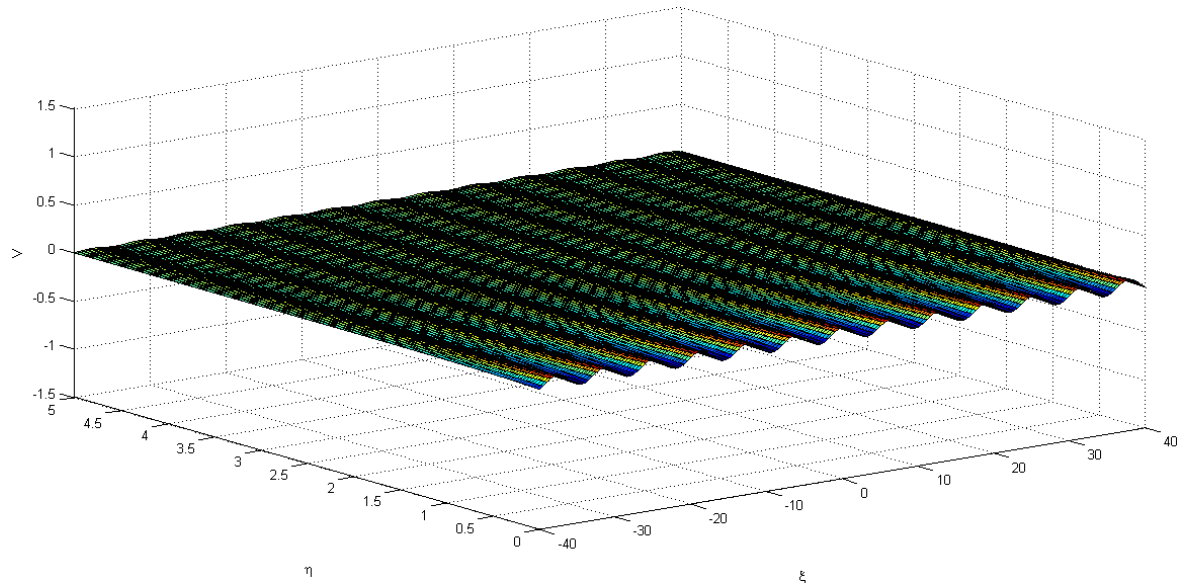
Figure 2.15: Konenkov flexural edge wave in isotropic plate. 3D profile of the parabolic-elliptic model (2.74), (2.77)
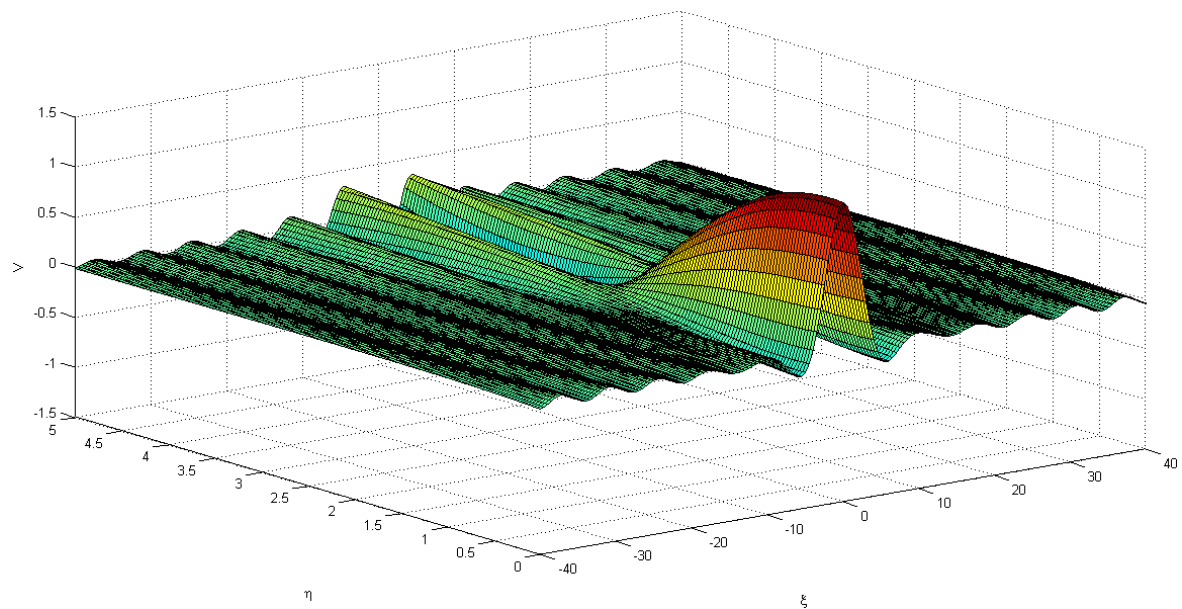
Figure 2.16: Overall rotation angle of isotropic plate. 3D profile of the exact solution (2.75)

2.2 Konenkov flexural edge wave in isotropic circular plates

In this section we consider the edge vibrations in the thin circular plate of radius R and thickness $2h$.

2.2.1 Basic equations

The equation of motion for the deflection w is given by equation (1.33). Taking into account that the plate edge is free from any forces, the boundary conditions are presented in (1.48). The solution for the original plate deflection w can be taken in the following form

$$w(r, \phi, t) = W(r, t)e^{inR\phi}, \tag{2.78}$$

where n is the wave number. Equation of motion (1.33) and boundary conditions (1.48) become

$$\frac{\partial^4 W}{\partial r^4} + \frac{2}{r}\frac{\partial^3 W}{\partial r^3} - \frac{1 + 2n^2 R^2}{r^2}\frac{\partial^2 W}{\partial r^2} + \frac{1 + 2n^2 R^2}{r^3}\frac{\partial W}{\partial r} + \frac{n^4 R^4 - 2n^2 R^2}{r^4}W(r, t) + \frac{2\rho h}{D}\frac{\partial^2 W}{\partial t^2} = 0,$$

and at $r = R$

$$\frac{\partial^2 W}{\partial r^2} + \nu\left(\frac{1}{r}\frac{\partial W}{\partial r} - \frac{n^2 R^2}{r^2}W(r, t)\right) = 0,$$

$$\frac{\partial^3 W}{\partial r^3} + \frac{1}{r}\frac{\partial^2 W}{\partial r^2} - \frac{1 + n^2 R^2}{r^2}\frac{\partial W}{\partial r} + \frac{2n^2 R^2}{r^3}W + (1 - \nu)\left(-\frac{n^2 R^2}{r^2}\frac{\partial W}{\partial r} + \frac{n^2 R^2}{r^3}W\right) = 0.$$

Now, we introduce new dimensionless quantities

$$r = R(1 - \varepsilon\eta), \quad t = T\tau, \quad w = hW^*, \tag{2.79}$$

where $\varepsilon = \dfrac{1}{nR}$.

With (2.79) and after applying the Laplace integral transform to the τ variable ($\tau \to s$) we obtain the equation for the transformed deflection $\hat{W}(\eta)$ as

$$\frac{d^4\hat{W}}{d\eta^4} - \frac{2\varepsilon}{1 - \varepsilon\eta}\frac{d^3\hat{W}}{d\eta^3} - \frac{\varepsilon^2 + 2}{(1 - \varepsilon\eta)^2}\frac{d^2\hat{W}}{d\eta^2} - \frac{\varepsilon^3 + 2\varepsilon}{(1 - \varepsilon\eta)^3}\frac{d\hat{W}}{d\eta} + \left[\frac{1 - 2\varepsilon^2}{(1 - \varepsilon\eta)^4} + \lambda_0^2 s^2\varepsilon^4\right] = 0, \tag{2.80}$$

where

$$\lambda_0^2 = \frac{R^4}{T^2}\frac{2\rho h}{D}. \tag{2.81}$$

The boundary conditions at $\eta = 0$ (that is $r = R$) are given by

$$\frac{d^2\hat{W}}{d\eta^2} - \nu\hat{W} - \nu\varepsilon\frac{d\hat{W}}{d\eta} = 0,$$

$$\frac{d^3\hat{W}}{d\eta^3} - (2-\nu)\frac{d\hat{W}}{d\eta} - \varepsilon\left[\frac{d^2\hat{W}}{d\eta^2} + (3-\nu)\hat{W}\right] - \varepsilon^2\frac{d\hat{W}}{d\eta} = 0. \quad (2.82)$$

We consider the case when the edge wave length is much smaller than R and larger than h, i.e. the parameter $\dfrac{h}{R} \ll \varepsilon \ll 1$. Then equation (2.81) and boundary conditions (2.82) become (here we neglect all the terms of order $O(\varepsilon^2)$ and higher)

$$\frac{d^4\hat{W}}{d\eta^4} - 2\frac{d^2\hat{W}}{d\eta^2} + (1-c^4)\hat{W} - \varepsilon\left[2\frac{d^3\hat{W}}{d\eta^3} + 4\eta\frac{d^2\hat{W}}{d\eta^2} + 2\frac{d\hat{W}}{d\eta} - \varepsilon\eta\hat{W}\right] = 0, \quad (2.83)$$

and

$$\frac{d^2\hat{W}}{d\eta^2} - \nu\hat{W} - \varepsilon\nu\frac{d\hat{W}}{d\eta} = 0,$$

$$\frac{d^3\hat{W}}{d\eta^3} - (2-\nu)\frac{d\hat{W}}{d\eta} - \varepsilon\left[\frac{d^2\hat{W}}{d\eta^2} + (3-\nu)\hat{W}\right] = 0, \quad (2.84)$$

where we define c as

$$c^4 = -s^2\lambda_0^2\varepsilon^4. \quad (2.85)$$

2.2.2   Solution of problem

We look for the transformed deflection $\hat{W}(\eta)$ in the form

$$\hat{W}(\eta) = \hat{W}_0(\eta) + \varepsilon\hat{W}_1(\eta), \quad (2.86)$$

so that the equation of motion can be split into two: for $\hat{W}_0$ and $\hat{W}_1$ respectively. This results in

$$\frac{d^4\hat{W}_0}{d\eta^4} - 2\frac{d^2\hat{W}_0}{d\eta^2} + (1-c^4)\hat{W}_0 = 0, \quad (2.87)$$

and

$$\frac{d^4\hat{W}_1}{d\eta^4} - 2\frac{d^3\hat{W}_0}{d\eta^3} - 2\frac{d^2\hat{W}_1}{d\eta^2} - 4\eta\frac{d\hat{W}_0}{d\eta} + \left[(1-c^4)\hat{W}_1 + 4\eta\hat{W}_0\right] = 0. \quad (2.88)$$

We start with the equation for $\hat{W}_0$ (2.87). We seek solution in the form

$$\hat{W}_0 = Ce^{-\gamma\eta},$$

substitution of which into (2.87) gives

$$\hat{W}_0 = Ae^{-\alpha\eta} + Be^{-\beta\eta}, \quad (2.89)$$

where

$$\alpha = \sqrt{1 - c^2},$$
$$\beta = \sqrt{1 + c^2},$$

(2.90)

and A and B are arbitrary constants.

Now, as we have found the expression for $\hat{W}_0$, we may obtain a non-homogeneous ordinary differential equation for $\hat{W}_1$

$$\frac{d^4\hat{W}_1}{d\eta^4} - 2\frac{d^2\hat{W}_1}{d\eta^2} + (1 - c^4)\hat{W}_1 = \left[-2\sqrt{1 - c^2}(2 - c^2) - 4\eta c^2\right] Ae^{-\alpha\eta}$$
$$+ \left[-2\sqrt{1 + c^2}(2 + c^2) + 4\eta c^2\right] Be^{-\beta\eta}.$$

(2.91)

Solution of (2.91) may be taken in the form

$$\hat{W}_1 = (A_1\eta + A_2\eta^2)Ae^{-\alpha\eta} + (B_1\eta + B_2\eta^2)Be^{-\beta\eta}.$$

(2.92)

On substituting it into (2.91), we arrive at the explicit expressions for unknown constants A_1, A_2, B_1, B_2

$$A_1 = -\frac{c^2}{2(1 - c^2)}, \quad A_2 = -\frac{1}{2\sqrt{1 - c^2}},$$
$$B_1 = \frac{c^2}{2(1 + c^2)}, \quad B_2 = -\frac{1}{2\sqrt{1 + c^2}}.$$

(2.93)

Knowing that $\hat{W}(\eta)$ can be found in form (2.86), where all the components $\hat{W}_0$ and $\hat{W}_1$ are from (2.89)-(2.90) and (2.92)-(2.93), we can deduce that

$$\hat{W}(\eta) = \left[1 - \varepsilon\left(\frac{c^2}{2(1 - c^2)}\eta + \frac{1}{2\sqrt{1 - c^2}}\eta^2\right)\right] Ae^{-\alpha\eta}$$
$$+ \left[1 + \varepsilon\left(\frac{c^2}{2(1 + c^2)}\eta - \frac{1}{2\sqrt{1 + c^2}}\eta^2\right)\right] Be^{-\beta\eta}.$$

(2.94)

To find A and B, we substitute (2.94) into boundary conditions (2.84). In doing so we obtain the following system of linear equations

$$\left[(1 - \nu - c^2) - \varepsilon(1 - \nu)\sqrt{1 - c^2}\right] A + \left[(1 - \nu + c^2) - \varepsilon(1 - \nu)\sqrt{1 + c^2}\right] B = 0,$$
$$\left[(1 - \nu + c^2)\sqrt{1 - c^2} + \varepsilon\left(-\frac{1}{2}c^2 - (1 - \nu) + \frac{(2 - \nu)c^2}{2(1 - c^2)}\right)\right] A$$
$$+ \left[(1 - \nu - c^2)\sqrt{1 + c^2} + \varepsilon\left(-\frac{5}{2}c^2 - (1 - \nu) - \frac{(2 - \nu)c^2}{2(1 + c^2)}\right)\right] B = 0.$$

(2.95)

2.2.3 Homogeneous edge wave. Curvature correction

System (2.95) has non-zero solutions provided that

$$(1 - \nu - c^2)^2\sqrt{1 + c^2} - (1 - \nu + c^2)^2\sqrt{1 - c^2}$$
$$+ \varepsilon\left[2c^2(1 - \nu)\sqrt{1 - c^4} + 2(1 - \nu)c^2 - \frac{(1 - \nu - c^2)^2c^2}{2(1 + c^2)} - \frac{(1 - \nu + c^2)^2c^2}{2(1 - c^2)}\right] = 0.$$

(2.96)

Here we neglect the terms of order $O(\varepsilon^2)$ and higher. The solution of the above equation can be found only using numerical methods. Note that if we also neglect terms of order $O(\varepsilon)$, this equation can be reduced to the form similar to (1.1), i.e. to the Konenkov dispersion equation (see Konenkov (1960)) for the semi-infinite plate. In the latter case its solution can be easily found analytically.

As it has been previously mentioned at the beginning of this section, the exact equation and solution of this problem were obtained by Destrade and Fu (2008). Written in terms of parameters used in the thesis, their equation is

$$(1 - \nu - c^2)^2 B_i - (1 - \nu + c^2)^2 B_j + 2c^2(1 + B_i B_j)(1-\nu)\varepsilon - (B_i - B_j)(1-\nu)^2\varepsilon^2 = 0, \ (2.97)$$

where

$$
\begin{aligned}
B_i &= \frac{c\left(I_\alpha\left(\frac{1}{\varepsilon}+1,\alpha\right) + \frac{1}{\varepsilon}\frac{I_\alpha\left(\frac{1}{\varepsilon},\alpha\right)}{\alpha}\right)}{I_\alpha\left(\frac{1}{\varepsilon},\alpha\right)}, \\[2em]
B_j &= \frac{c\left(\frac{1}{\varepsilon}\frac{J_\alpha\left(\frac{1}{\varepsilon},\alpha\right)}{\alpha} - J_\alpha\left(\frac{1}{\varepsilon}+1,\alpha\right)\right)}{J_\alpha\left(\frac{1}{\varepsilon},\alpha\right)},
\end{aligned}
\tag{2.98}
$$

and $\alpha = \dfrac{c}{\varepsilon}$. It can be easily checked that, using Debye series expansions from Abramowitz and Stegun (1965), in the first-order approximation equation (2.97) can be reduced to form (2.96).

We compare our first-order approximation solution with the exact one using the fzero function from Matlab 7.1. The obtained solutions are plotted against the parameter nR and are presented in Figures 2.17-2.19 for the various values of the Poisson's ratio. For $nR = 300$ in Figure 2.20, we create solutions as functions of Poisson's ratio. As it can be seen from these Figures, the equations approximation depends only on the parameter nR, and not on the material properties of the plate. It also can be noticed from Figure 2.17 that Matlab 7.1 function fzero, which has been utilised while obtaining these numerical solutions, does not give a good approximation for small values of the parameter nR under the condition of small Poisson's ratio. This resulted in the small leap of solution for first-order approximation.
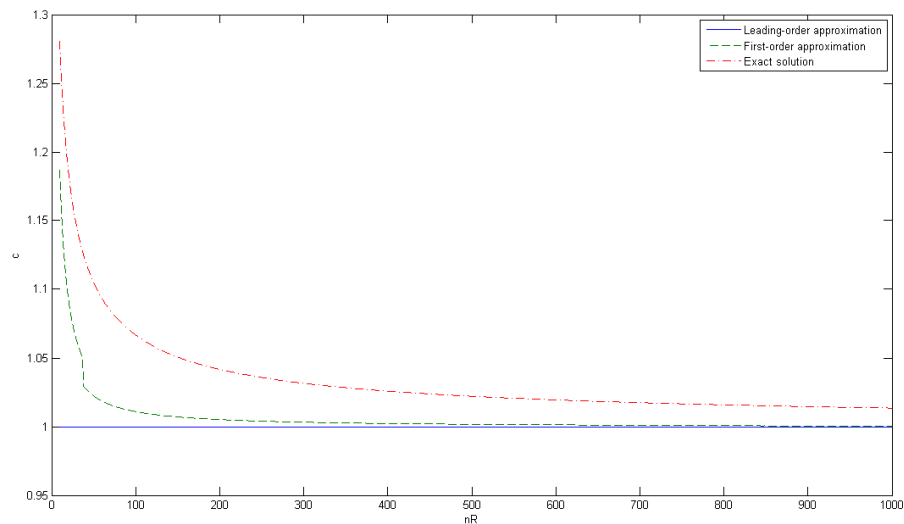
Figure 2.17: Solutions of dispersion equations for $\nu = 0.2$. Exact solution, first order approximation and leading order approximation corresponding to the semi-infinite plate
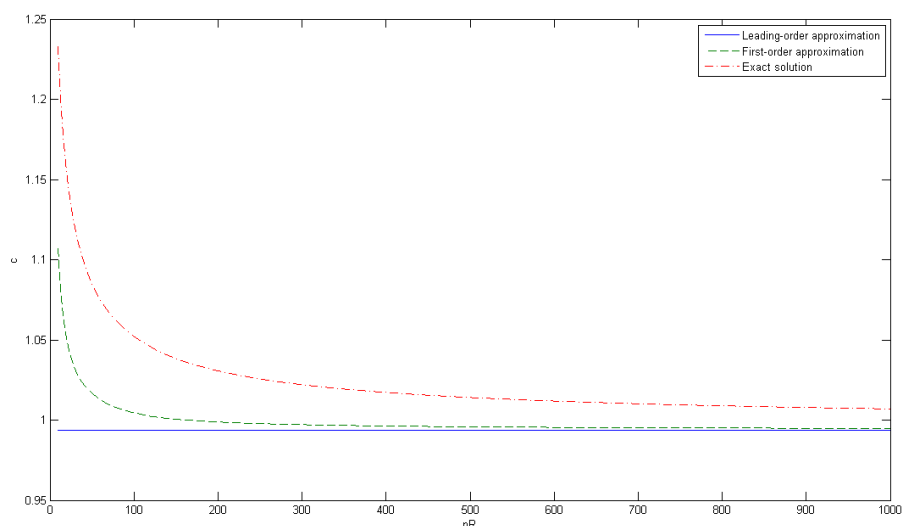
Figure 2.18: Solutions of dispersion equations for $\nu = \dfrac{1}{3}$. Exact solution, first order approximation and leading order approximation corresponding to the semi-infinite plate
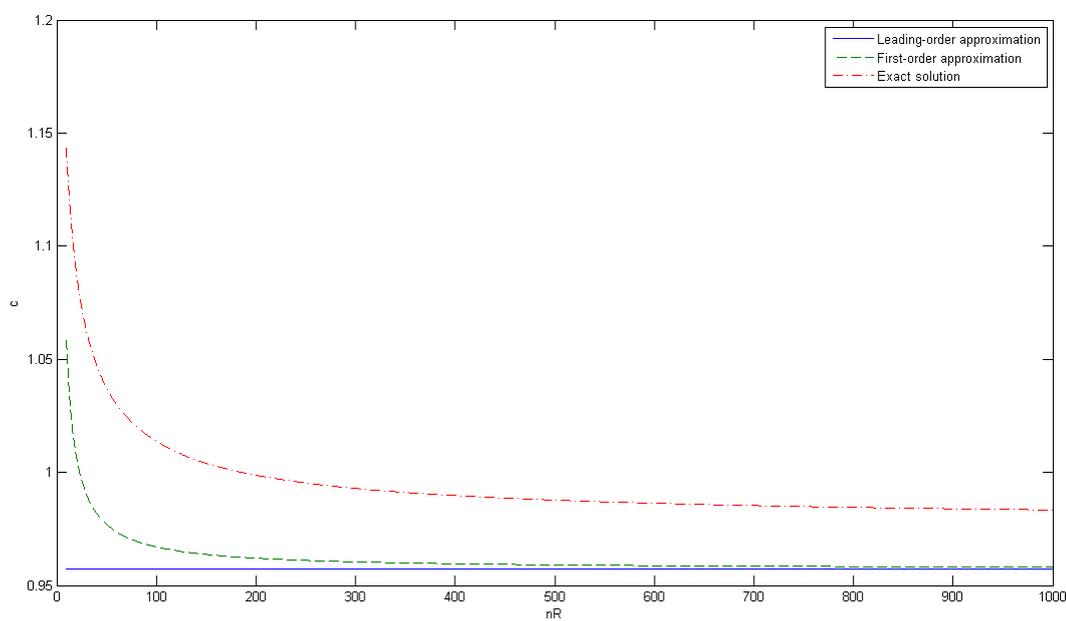
Figure 2.19: Solutions of dispersion equations for $\nu = 0.5$. Exact solution, first order approximation and leading order corresponding to the semi-infinite plate
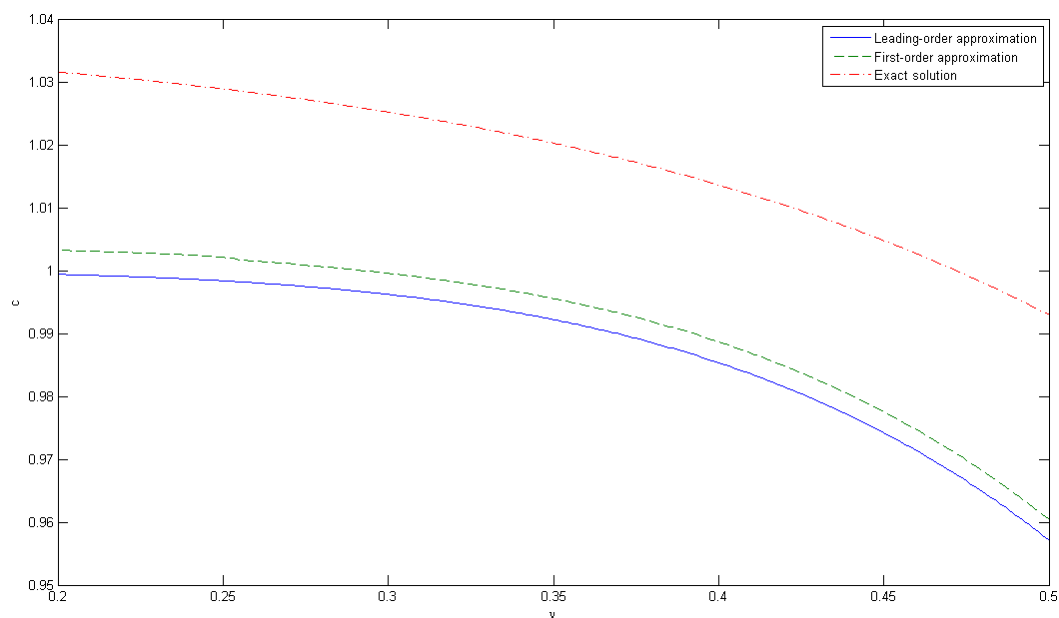
Figure 2.20: Solutions of dispersion equations for $nR = 300$. Exact solution, first order approximation and leading order corresponding to the semi-infinite plate versus Poisson's ratio

Chapter 3

Konenkov flexural edge wave in orthotropic plate

3.1 Homogeneous edge wave

In this section we investigate a homogeneous flexural edge wave propagating along the edge of a semi-infinite orthotropic plate.

3.1.1 Basic equations

In this case, the equation of motion for the deflection $w(x, y, t)$ is given by (1.30). The boundary conditions for a traction-free edge are presented by formulae (1.38).

First we introduce dimensionless quantities in the following form

$$
\begin{aligned}
x &= h\xi, & y &= h\eta, & t &= T\tau, \\
w &= hW^*, & D_x &= D\hat{D}_x, & D_y &= D\hat{D}_y, \\
D_1 &= D\hat{D}_1, & D_{xy} &= D\hat{D}_{xy},
\end{aligned}
\tag{3.1}
$$

where h is the half-thickness of the plate, D is a typical stiffness of the plate (for a number of problems it is natural to take $D = D_y$. However in the thesis we are going to leave it in the general form as D) and T is a typical time scale.

After introducing (3.1) and applying integral transforms to equation (1.30) and the boundary conditions (1.38), we get a problem for the transformed deflection $\hat{W}(\eta)$. It is

$$
\hat{D}_y \frac{d^4\hat{W}}{d\eta^4} - 2(\hat{D}_1 + 2\hat{D}_{xy})p^2 \frac{d^2\hat{W}}{d\eta^2} + (\hat{D}_x p^4 + \lambda_0^2 s^2)\hat{W} = 0,
\tag{3.2}
$$

where $\lambda_0^2 = \dfrac{2\rho h^5}{DT^2}$ has the same form as above (see (2.3)).

The boundary conditions at $\eta = 0$ become

$$
\begin{aligned}
\hat{D}_y \frac{d^2 \hat{W}}{d\eta^2} - \hat{D}_1 p^2 \hat{W} &= 0, \\
\hat{D}_y \frac{d^3 \hat{W}}{d\eta^3} - (\hat{D}_1 + 4\hat{D}_{xy})p^2 \frac{d\hat{W}}{d\eta} &= 0.
\end{aligned}
\tag{3.3}
$$

3.1.2 Konenkov flexural edge wave coefficient in orthotropic plate

The solution of the problem (3.2)-(3.3) can be taken in the form (2.6). Substitution of (2.6) into equation (3.2) leads to the expressions for the parameters α and β; they are

$$
\begin{aligned}
\alpha &= \frac{1}{\hat{D}_y^{1/2}} \sqrt{(\hat{D}_1 + 2\hat{D}_{xy})p^2 - \sqrt{\left[(\hat{D}_1 + 2\hat{D}_{xy})^2 - \hat{D}_x \hat{D}_y\right] p^4 - \hat{D}_y s^2 \lambda_0^2}}, \\
\beta &= \frac{1}{\hat{D}_y^{1/2}} \sqrt{(\hat{D}_1 + 2\hat{D}_{xy})p^2 + \sqrt{\left[(\hat{D}_1 + 2\hat{D}_{xy})^2 - \hat{D}_x \hat{D}_y\right] p^4 - \hat{D}_y s^2 \lambda_0^2}}.
\end{aligned}
\tag{3.4}
$$

As in Section 2.1, the system for the unknown constants A and B can be obtained by the substitution of (2.6) with (3.4) into the boundary conditions (3.3). In a matrix form it is given by

$$
\begin{bmatrix}
\hat{D}_y \alpha^2 - \hat{D}_1 p^2 & \hat{D}_y \beta^2 - \hat{D}_1 p^2 \\
\left[\hat{D}_y \alpha^2 - (\hat{D}_1 + 4\hat{D}_{xy})p^2\right]\alpha & \left[\hat{D}_y \beta^2 - (\hat{D}_1 + 4\hat{D}_{xy})p^2\right]\beta
\end{bmatrix}
\begin{bmatrix}
A \\
B
\end{bmatrix}
=
\begin{bmatrix}
0 \\
0
\end{bmatrix}.
\tag{3.5}
$$

The above system of linear equations has a non-trivial solution only in the case when its determinant equals to zero, i.e.

$$
(\beta - \alpha)\left[\hat{D}_y^2 \alpha^2 \beta^2 - \hat{D}_y(\beta^2 + \alpha^2)\hat{D}_1 p^2 + 4\hat{D}_y \alpha\beta \hat{D}_{xy} p^2 + \hat{D}_1(\hat{D}_1 + 4\hat{D}_{xy})p^4\right] = 0,
\tag{3.6}
$$

or, in terms of p

$$
(\hat{D}_x \hat{D}_y - \hat{D}_1^2)p^4 + \hat{D}_y s^2 \lambda_0^2 + 4\hat{D}_{xy}\sqrt{\hat{D}_x \hat{D}_y p^4 + \hat{D}_y s^2 \lambda_0^2}\, p^2 = 0.
\tag{3.7}
$$

Now, we introduce a new parameter c by the following equality

$$
c = \frac{\sqrt{-is\lambda_0 \sqrt{\hat{D}_y}}}{p}.
\tag{3.8}
$$

Formula (3.7) expressed in terms of c becomes

$$
(\hat{D}_x \hat{D}_y - \hat{D}_1^2) - \hat{D}_y c^4 + 4\hat{D}_{xy}\sqrt{\hat{D}_x \hat{D}_y - \hat{D}_y c^4} = 0.
\tag{3.9}
$$

On multiplying by the function $X(c)$

$$X(c) = (\hat{D}_x\hat{D}_y - \hat{D}_1^2) - c^4 - 4\hat{D}_{xy}\sqrt{\hat{D}_x\hat{D}_y - c^4} \tag{3.10}$$

we find the explicit expression of the solutions of (3.9)

$$
\begin{aligned}
c_k &= \left(\hat{D}_x\hat{D}_y - (\sqrt{\hat{D}_1^2 + 4\hat{D}_{xy}^2} - 2\hat{D}_{xy})^2\right)^{\frac{1}{4}}, \\
c_2 &= \left(\hat{D}_x\hat{D}_y - (\sqrt{\hat{D}_1^2 + 4\hat{D}_{xy}^2} + 2\hat{D}_{xy})^2\right)^{\frac{1}{4}}.
\end{aligned} \tag{3.11}
$$

As above, c_k corresponds to the Konenkov flexural edge wave coefficient in the case of an orthotropic plate, and c_2 is the second root of the equation, which has no physical meaning.

3.1.2.1 Dependence of Konenkov flexural edge wave coefficient on orthotropy

As was shown in Chapter 2, the Konenkov flexural edge wave coefficient c_k depends on the problem parameters including the plate stiffness. For an isotropic plate its stiffness is a function of two parameters, namely Poisson's ratio ν and Young's modulus E. In the case of an orthotropic plate, instead of Poisson's ratio ν and Young's modulus E, we have to consider four stiffnesses D_x, D_y, D_1 and D_{xy} (or their dimensionless analogues, specified in (3.1)). Further we study their effect on the value of Konenkov flexural edge wave coefficient c_k.

First, we show that the expression for c_k from (3.11) involves an isotropic plate as a particular case. We recall that the parameters D_x, D_y, D_1 and D_{xy} are connected with E and ν by equalities (1.32). Substitution of these parameters into formula (3.11) gives exactly the same expressions as those obtained in Chapter 2 for an isotropic plate, namely formulae (2.14).

Let us investigate the behavior of the coefficient c_k for the varying stiffnesses, D_x, D_y, D_1 and D_{xy}. First, we assume that D_y, D_1 and D_{xy} take the same values as in (1.32) in terms of ν and D, whereas D_x varies between $\frac{1}{5}D \le D_x \le 5D$. The graph of $\frac{c_{k,orthotropic}}{c_{k,isotropic}}$ versus $\hat{D}_x$ is presented in Figure 3.1. It is clear that the coefficient c_k tends to infinity as the parameter D_x increases. This fact will also be further discussed when considering the explicit dual parabolic-elliptic models for different types of boundary conditions.

The further graphs are obtained for the variation of D_y ($\frac{1}{5}D \le D_y \le 5D$) (see Figure 3.1), D_1 ($\frac{1}{10}D \le D_1 \le 0.99D$) (see Figure 3.2) and D_{xy} ($\frac{1}{5}D \le D_{xy} \le 5D$) (see Figure

Figure 3.1: Konenkov flexural edge wave coefficient versus D_x
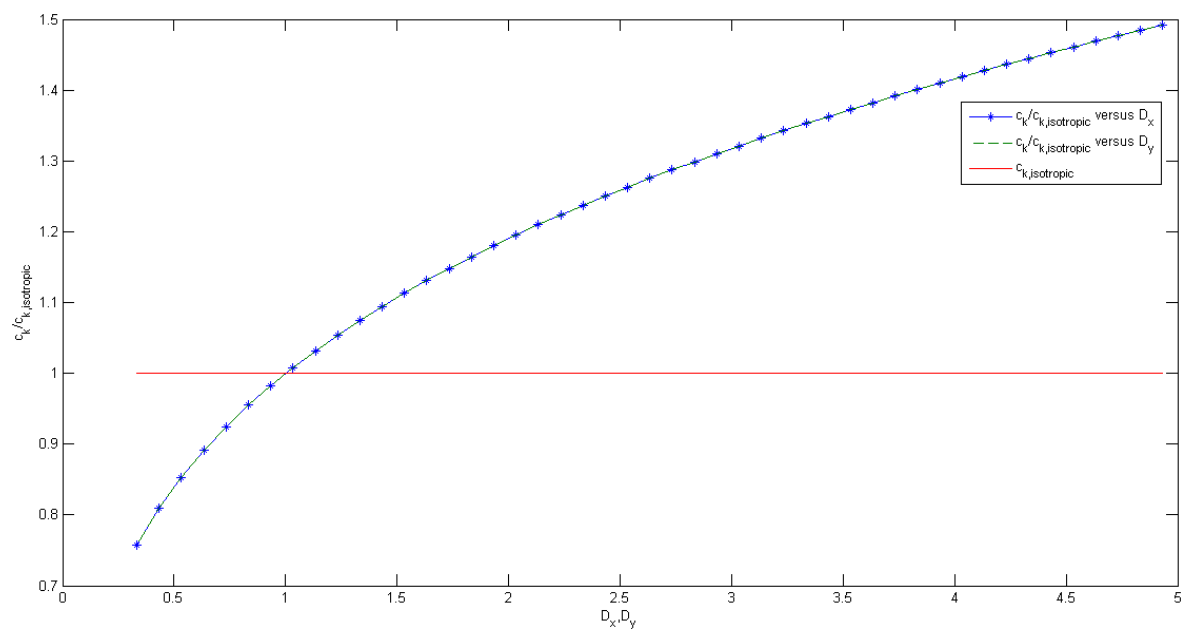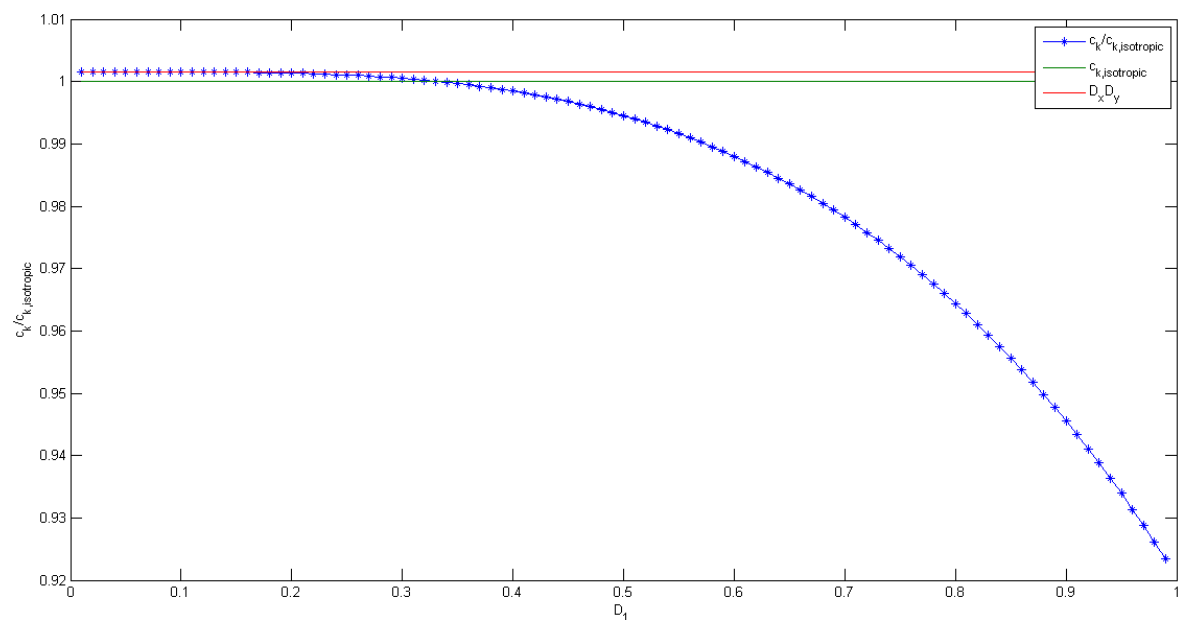

Figure 3.2: Konenkov flexural edge wave coefficient versus D_1
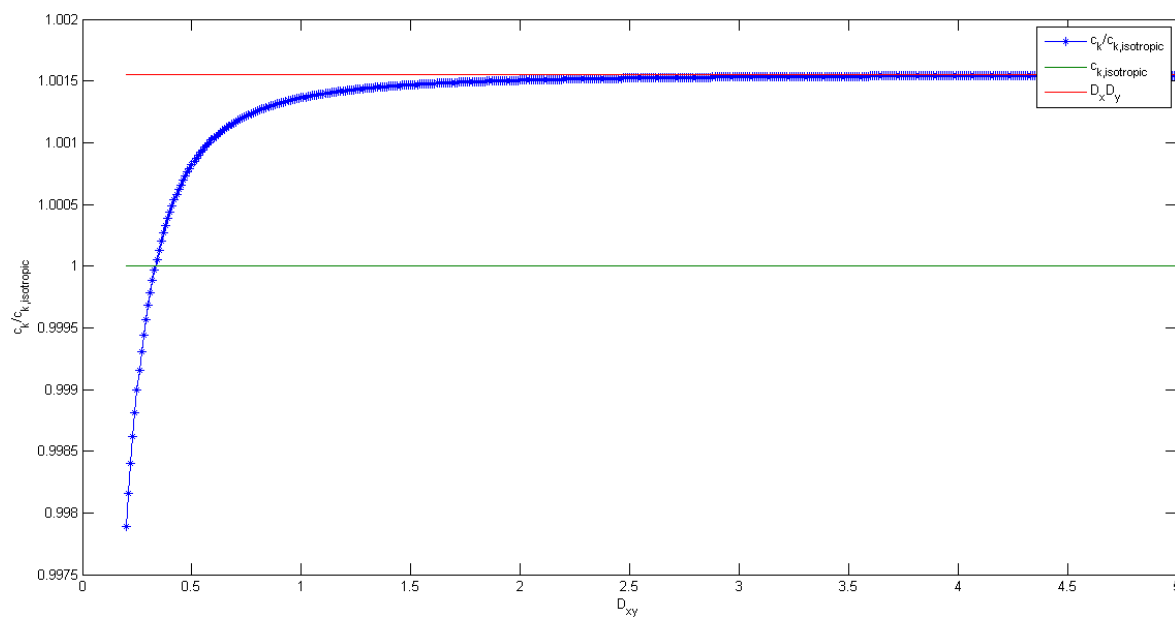
Figure 3.3: Konenkov flexural edge wave coefficient versus D_{xy}

3.3). It is also noted that c_k decreases as $\hat{D}_1$ grows whereas c_k versus $\hat{D}_{xy}$ becomes almost constant and equals to the asymptote $\sqrt[4]{\hat{D}_x \hat{D}_y}$. This asymptote is demonstrated in the last two Figures.

3.2   Bending moment at plate edge

In this section we discuss propagation of the Konenkov flexural edge wave induced by a bending moment applied at the edge of an orthotropic plate.

3.2.1   Basic equations

The equation of motion for the deflection w remains the same as in (1.29), and the boundary conditions appear as (1.41). On using quantities (3.1) and applying integral transforms we get equation (3.2) with the following boundary conditions at the plate edge $\eta = 0$

$$
\begin{aligned}
\hat{D}_y \frac{d^2\hat{W}}{d\eta^2} - \hat{D}_1 p^2 \hat{W} &= -\hat{M}_0, \\
\hat{D}_y \frac{d^3\hat{W}}{d\eta^3} - (\hat{D}_1 + 4\hat{D}_{xy})p^2 \frac{d\hat{W}}{d\eta} &= 0,
\end{aligned}
\tag{3.12}
$$

where $\hat{M}_0 = \hat{M}_0(s,p)$ is the transformed dimensionless analogue of the bending moment applied at the plate edge.

3.2.2   Derivation of transformed solution

The solution of problem (3.2), (3.12) may be found in form (2.6), where parameters α and β are given by (3.4). Omitting the algebra, which is fairly similar to what has been done for an isotropic plate, we get for the sought for exact solution

$$
\hat{W}(\eta) = \frac{\hat{M}_0}{-is\lambda_0\sqrt{\hat{D}_y}} \frac{c^2}{c^4 - c_k^4} \frac{\Delta_1(c)e^{-\frac{\sqrt{-is\lambda_0\sqrt{\hat{D}_y}}}{c}\alpha_c\eta} + \Delta_2(c)e^{-\frac{\sqrt{-is\lambda_0\sqrt{\hat{D}_y}}}{c}\beta_c\eta}}{\Delta(c)} X(c),
\tag{3.13}
$$

where

$$
\begin{aligned}
\alpha_c &= \frac{1}{\sqrt{\hat{D}_y}}\sqrt{\hat{D}_1 + 2\hat{D}_{xy} - \sqrt{(\hat{D}_1 + 2\hat{D}_{xy})^2 - \hat{D}_x\hat{D}_y + c^4}}, \\
\beta_c &= \frac{1}{\sqrt{\hat{D}_y}}\sqrt{\hat{D}_1 + 2\hat{D}_{xy} + \sqrt{(\hat{D}_1 + 2\hat{D}_{xy})^2 - \hat{D}_x\hat{D}_y + c^4}},
\end{aligned}
\tag{3.14}
$$

and also

$$
\begin{aligned}
\Delta_1(c) &= -\left[2\hat{D}_{xy} - \sqrt{(\hat{D}_1 + 2\hat{D}_{xy})^2 - \hat{D}_x\hat{D}_y + c^4}\right]\beta_c, \\
\Delta_2(c) &= \left[2\hat{D}_{xy} + \sqrt{(\hat{D}_1 + 2\hat{D}_{xy})^2 - \hat{D}_x\hat{D}_y + c^4}\right]\alpha_c, \\
\Delta(c) &= (\beta_c - \alpha_c)(c^4 - c_2^4),
\end{aligned}
\tag{3.15}
$$

with the function $X(c)$ from (3.10).

3.2.3   Derivation of explicit dual parabolic-elliptic model

Our main aim now is to identify the Konenkov flexural edge wave contribution to the exact solution (3.14). For this purpose we use a similar methodology as that described in Section 2.1.2. First, we introduce several new quantities to simplify the formulation of the model.

The expressions for the dimension counterparts of the coefficients c_k and the second root c_2 in (3.11) are

$$
\begin{aligned}
c_k^* &= \left(D_x D_y - (\sqrt{D_1^2 + 4D_{xy}^2} - 2D_{xy})^2\right)^{\frac{1}{4}}, \\
c_2^* &= \left(D_x D_y - (\sqrt{D_1^2 + 4D_{xy}^2} + 2D_{xy})^2\right)^{\frac{1}{4}}.
\end{aligned}
\tag{3.16}
$$

Also, we use the equality

$$
Q_e^{(1)*} = \frac{\Delta_1(c_k^*) + \Delta_2(c_k^*)}{\Delta(c_k^*)}.
\tag{3.17}
$$

where

$$
\begin{aligned}
\Delta_1(c_k^*) &= -\left[2D_{xy} - \sqrt{(D_1 + 2D_{xy})^2 - D_x D_y + c_k^{*4}}\right]\beta_c(c_k^*), \\
\Delta_2(c_k^*) &= \left[2D_{xy} + \sqrt{(D_1 + 2D_{xy})^2 - D_x D_y + c_k^{*4}}\right]\alpha_c(c_k^*), \\
\Delta(c_k^*) &= (\beta_c(c_k^*) - \alpha_c(c_k^*))(c_k^{*4} - c_2^{*4}).
\end{aligned}
\tag{3.18}
$$

with

$$
\begin{aligned}
\alpha_c(c_k^*) &= \frac{1}{\sqrt{D_y}}\sqrt{D_1 + 2D_{xy} - \sqrt{(D_1 + 2D_{xy})^2 - D_x D_y + c_k^{*4}}}, \\
\beta_c(c_k^*) &= \frac{1}{\sqrt{D_y}}\sqrt{D_1 + 2D_{xy} + \sqrt{(D_1 + 2D_{xy})^2 - D_x D_y + c_k^{*4}}},
\end{aligned}
\tag{3.19}
$$

After these preliminaries, we finally come to the model equations of interest. In particular, the parabolic equation at the plate edge in the original variables becomes

$$
\frac{c_k^{*4}}{D_y^2}\frac{\partial^4 w_e}{\partial x^4} + \frac{2\rho h}{D_y}\frac{\partial^2 w_e}{\partial t^2} = Q_e^{(1)*}\frac{1}{D_y}\frac{\partial^2 M_0}{\partial x^2},
\tag{3.20}
$$

whereas the elliptic problem over the interior domain is

$$
\left(D_x - \frac{c_k^{*4}}{D_y}\right)\frac{\partial^4 w_{in}}{\partial x^4} + 2(D_1 + 2D_{xy})\frac{\partial^4 w_{in}}{\partial x^2\partial y^2} + D_y\frac{\partial^4 w_{in}}{\partial y^4} = 0,
\tag{3.21}
$$

with the boundary conditions at the plate edge $y = 0$

$$
\begin{aligned}
w_{in}(x,0) &= w_e(x), \\
D_y\frac{\partial^2 w_{in}}{\partial y^2} &= -D_1\frac{\partial^2 w_e}{\partial x^2}.
\end{aligned}
\tag{3.22}
$$

We may notice that, using equalities (1.32) which are the connection of the parameters D_x, D_y, D_1 and D_{xy} with E and ν, we can obtain a dual parabolic-elliptic model (2.25), (2.27)-(2.29) for the isotropic plate.

3.2.4   Comparison with exact solution

We obtained exact solution (3.13) for the transformed deflection $\hat{W}(\eta)$ and also derived the explicit dual parabolic-elliptic model for Konenkov flexural edge wave in an orthotropic plate (see (3.20)-(3.22)). The next step is the comparison of the obtained solutions by applying the inverse Fourier transform and plotting the results. We again investigate the case of the bending point-moment M_0 (see Section 2.1.2 above for more details) applied at the plate edge. The assumption of the solution form remains the same and so does the form of the frequency parameter λ_0 (see (2.30)).

As in Section 2.1.2, here the comparison of the model with the exact solutions is performed using a similar methodology. First, in terms of the transform parameter p, the exact solution for the deflection $\hat{W}(\eta, p)$ is

$$\hat{W}(\eta, p) = \hat{M}_0 \frac{p^2}{p^4 - p_k^4} \frac{\Delta_1(p)e^{-\alpha\eta} + \Delta_2(p)e^{-\beta\eta}}{\Delta(p)} X(p), \tag{3.23}$$

where

$$\begin{aligned}
\alpha &= \frac{1}{\hat{D}_y^{1/2}} \sqrt{(\hat{D}_1 + 2\hat{D}_{xy})p^2 - \sqrt{\left[(\hat{D}_1 + 2\hat{D}_{xy})^2 - \hat{D}_x\hat{D}_y\right]p^4 + \hat{D}_y\lambda_0^2}}, \\
\beta &= \frac{1}{\hat{D}_y^{1/2}} \sqrt{(\hat{D}_1 + 2\hat{D}_{xy})p^2 + \sqrt{\left[(\hat{D}_1 + 2\hat{D}_{xy})^2 - \hat{D}_x\hat{D}_y\right]p^4 + \hat{D}_y\lambda_0^2}},
\end{aligned} \tag{3.24}$$

with

$$\begin{aligned}
\Delta_1(p) &= -\left[2\hat{D}_{xy}p^2 - \sqrt{\left[(\hat{D}_1 + 2\hat{D}_{xy})^2 - \hat{D}_x\hat{D}_y\right]p^4 + \hat{D}_y\lambda_0^2}\right]\beta, \\
\Delta_2(p) &= \left[2\hat{D}_{xy}p^2 + \sqrt{\left[(\hat{D}_1 + 2\hat{D}_{xy})^2 - \hat{D}_x\hat{D}_y\right]p^4 + \hat{D}_y\lambda_0^2}\right]\alpha, \\
\Delta(p) &= (\beta - \alpha)c_k^4 c_2^4(p^4 - p_2^4),
\end{aligned} \tag{3.25}$$

and the parameters c_k, c_2, p_k and p_2 are connected by the equalities

$$p_k = \frac{\sqrt{\lambda_0\sqrt{\hat{D}_y}}}{c_k}, \quad p_2 = \frac{\sqrt{\lambda_0\sqrt{\hat{D}_y}}}{c_2}. \tag{3.26}$$

Also, $X(c)$ function transforms into

$$X(p) = (\hat{D}_x\hat{D}_y - \hat{D}_1^2)p^4 + \hat{D}_y s^2\lambda_0^2 - 4\hat{D}_{xy}\sqrt{\hat{D}_x\hat{D}_y p^4 + \hat{D}_y s^2\lambda_0^2}p^2. \tag{3.27}$$

The contribution $\hat{W}_e$ of the Konenkov flexural edge wave at the plate edge is given by

$$\hat{W}_e = Q_e^{(1)}\hat{M}_0 \frac{p^2}{p^4 - p_k^4}, \tag{3.28}$$

where

$$Q_e^{(1)} = \frac{\Delta_1(p_k) + \Delta_2(p_k)}{\Delta(p_k)} X(p_k), \tag{3.29}$$

and, according to the residue theory, the dimensionless deflection at the plate edge is given by the formula (2.40) with $Q_e^{(1)}$ defined by (3.29).

It should be mentioned that the exact solution has branch points at $p = \pm\sqrt{\dfrac{\lambda_0}{\sqrt{\hat{D}_x \hat{D}_y}}}$.

Then, over the interval $-\sqrt{\dfrac{\lambda_0}{\sqrt{\hat{D}_x \hat{D}_y}}} \leq p \leq \sqrt{\dfrac{\lambda_0}{\sqrt{\hat{D}_x \hat{D}_y}}}$, we take the branch with

$$\alpha = -i \frac{1}{\hat{D}_y^{1/2}} \sqrt{\sqrt{\left[(\hat{D}_1 + 2\hat{D}_{xy})^2 - \hat{D}_x \hat{D}_y\right] p^4 + \hat{D}_y \lambda_0^2} - (\hat{D}_1 + 2\hat{D}_{xy})p^2}. \tag{3.30}$$

As before, the radius r is taken by (2.36) when integrating the exact solution along the small semi-circles (see Sections 1.2.3 and 2.1.1).

We solve the elliptic problem (3.21)-(3.22) over the interior domain. In this case the deflection takes the following form

$$\hat{W}_{in} = \hat{M}_0 \frac{p^2}{p^4 - p_k^4} Q_e^{(1)} \frac{\Delta_{1,in}(p)e^{-\alpha_c(c_k)p\eta} + \Delta_{2,in}(p)e^{-\beta_c(c_k)p\eta}}{\hat{D}_y(\beta_c^2(c_k) - \alpha_c^2(c_k))}, \tag{3.31}$$

where

$$\begin{aligned}
\Delta_{1,in}(p) &= \left(2\hat{D}_{xy} + \sqrt{(\hat{D}_1 + 2\hat{D}_{xy})^2 - \hat{D}_x \hat{D}_y + c_k^4}\right) p^2, \\
\Delta_{2,in}(p) &= -\left(2\hat{D}_{xy} - \sqrt{(\hat{D}_1 + 2\hat{D}_{xy})^2 - \hat{D}_x \hat{D}_y + c_k^4}\right) p^2.
\end{aligned} \tag{3.32}$$

Finally, the dimensionless deflection corresponding to Konenkov flexural edge wave over the interior domain follows from the residue theory and is given by

$$W_{in}^*(\xi, \eta) = \sqrt{2\pi} i Q_e^{(1)} \hat{M}_0 \frac{1}{4p_k} \frac{\Delta_{1,in}(p_k)e^{-\alpha_c(c_k)p\eta} + \Delta_{2,in}(p_k)e^{-\beta_c(c_k)p\eta}}{\hat{D}_y(\beta_c^2(c_k) - \alpha_c^2(c_k))} e^{ip_k\xi}. \tag{3.33}$$

It should be noted that for all the following numerical results the frequency parameter is taken as $\lambda_0 = 1$ and $\hat{M}_0 = \sqrt{2\pi}$.

The analysis of the deflection is presented below using the results of Section 3.1.2.1 related to the dependence of the Konenkov flexural edge wave coefficient on the stiffness parameters D_x, D_y, D_1 and D_{xy}. Using Figures 3.1-3.3, we can show how different values of the stiffness parameters affect the Konenkov wave contribution into the overall plate deformation.

First, we study the effect of parameter D_x on Konenkov wave propagation. The following Figures 3.4-3.7 are created for $\hat{D}_x = \dfrac{1}{5}$ and clearly demonstrate that the flexural edge wave contribution into the overall plate deflection is rather significant.

Figure 3.4: Edge deflection in orthotropic plate ($\hat{D}_x = \frac{1}{5}$). Overall solution (3.23) and Konenkov flexural
edge wave contribution (2.40)
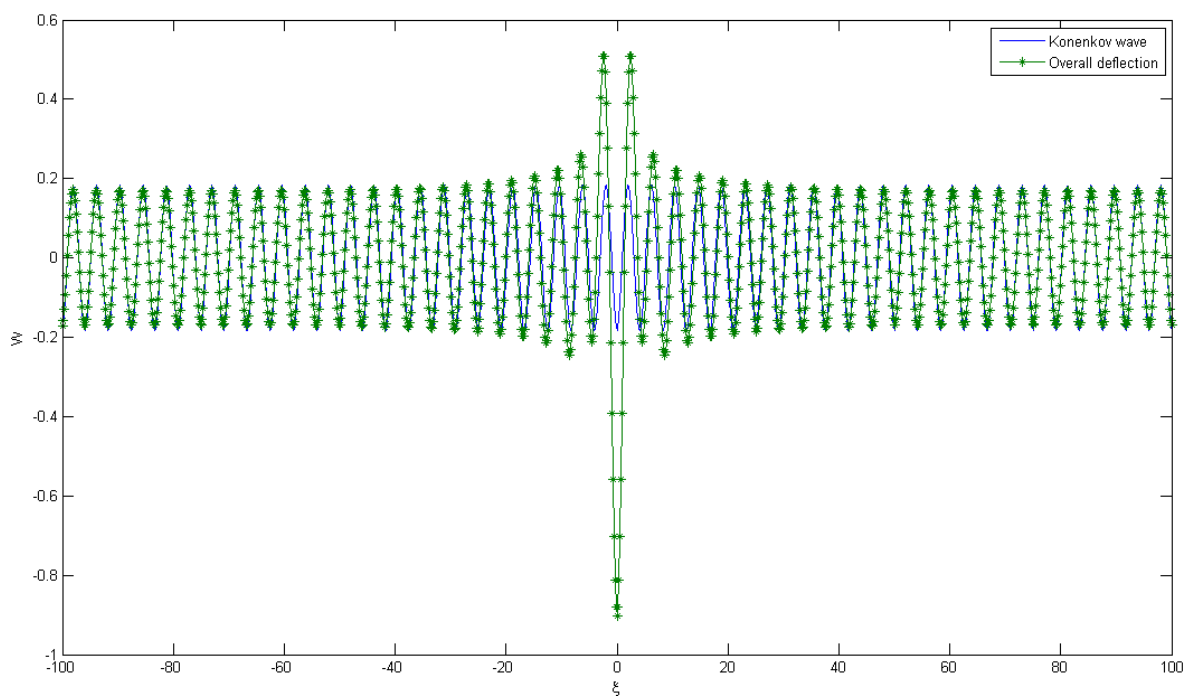
Figure 3.5: Deflection in orthotropic plate ($\hat{D}_x = \frac{1}{5}$) for $\eta = 1$ Overall solution (3.23) and Konenkov flexural
edge wave contribution (3.33)

Figure 3.6: Konenkov flexural edge wave in orthotropic plate ($\hat{D}_x = \frac{1}{5}$). 3D profile of the parabolic-elliptic model (2.40), (3.33)

Figure 3.7: Overall deflection in orthotropic plate ($\hat{D}_x = \frac{1}{5}$). 3D profile of the exact solution (3.23)

For the value $\hat{D}_x = 5$, when the Konenkov flexural edge wave coefficient c_k takes the largest value (see Figure 3.1) the deflection at the plate edge is demonstrated in Figure 3.8 while the solutions over the interior domain are shown in Figure 3.9. In addition, the 3D profiles of the deflection corresponding to the Konenkov flexural edge wave, based on parabolic-elliptic model, and the overall deflection profiles are shown in Figures 3.10-3.11. Note that as it follows from the analysis of the numerical results presented in Figures 3.4-3.11 larger values of Konenkov flexural edge wave coefficient c_k correspond to smaller deflections. In this case the vicinity of the point moment has the most contribution to the overall deflection field.
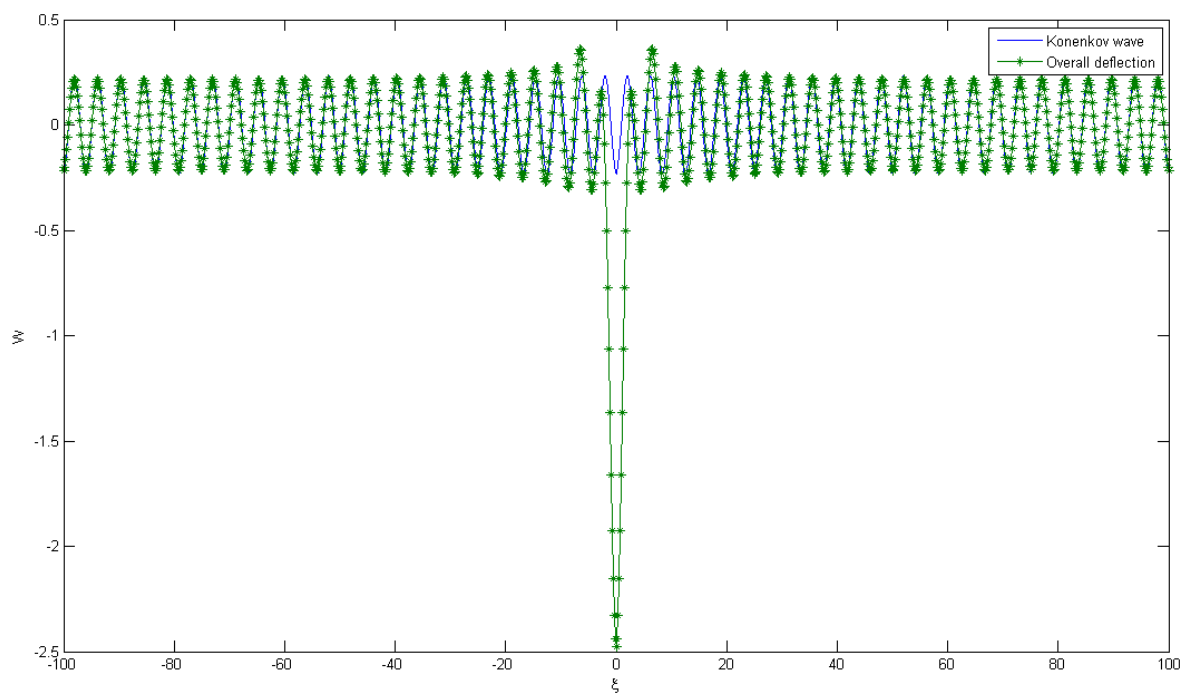

Figure 3.8: Edge deflection in orthotropic plate ($\hat{D}_x = 5$). Overall solution (3.23) and Konenkov flexural edge wave contribution (2.40)

The effect of the parameter D_y is similar to D_x, although the behavior of the solutions against D_x and D_y is not symmetric despite the symmetry of the coefficient c_k with respect to D_x and D_y. Therefore we believe there is no need to present the solution dependence on D_y graphically.

As it can be seen from the above figures, propagation of the Konenkov flexural edge wave and its contribution to the plate deflection is rather material-sensitive. The following cases show this dependence even more clear.

For example, one can choose the plate material so that the Konenkov wave contribution

Figure 3.9: Deflection in orthotropic plate ($\hat{D}_x = 5$) for $\eta = 1$ Overall solution (3.23) and Konenkov flexural edge wave contribution (3.33)

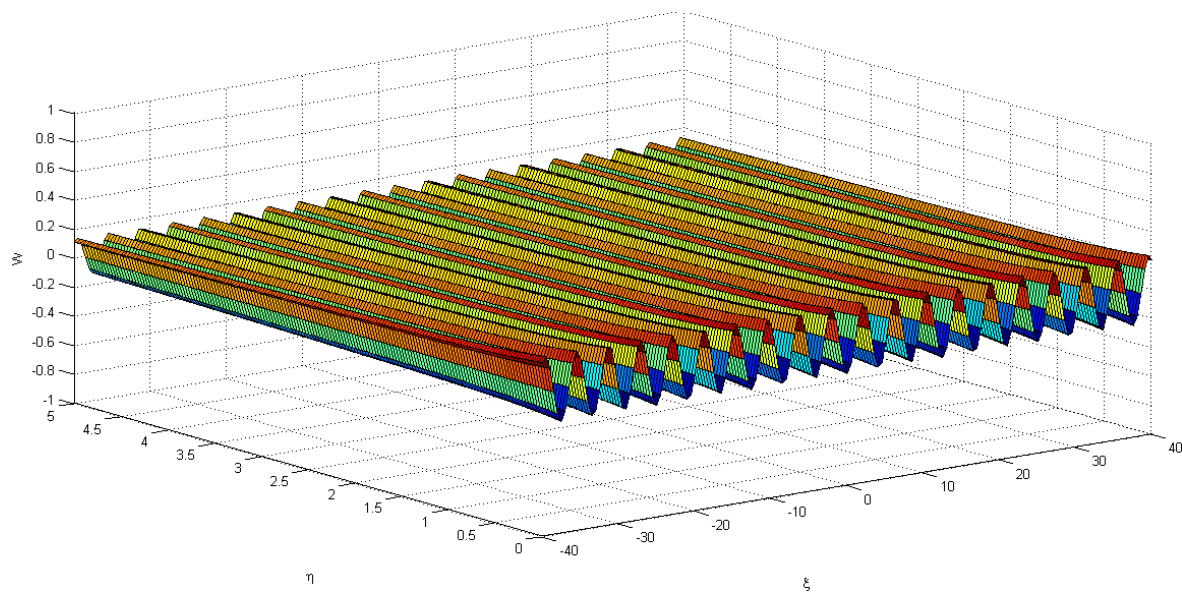Figure 3.10: Konenkov flexural edge wave in orthotropic plate ($\hat{D}_x = 5$). 3D profile of the parabolic-elliptic model (2.40), (3.33)
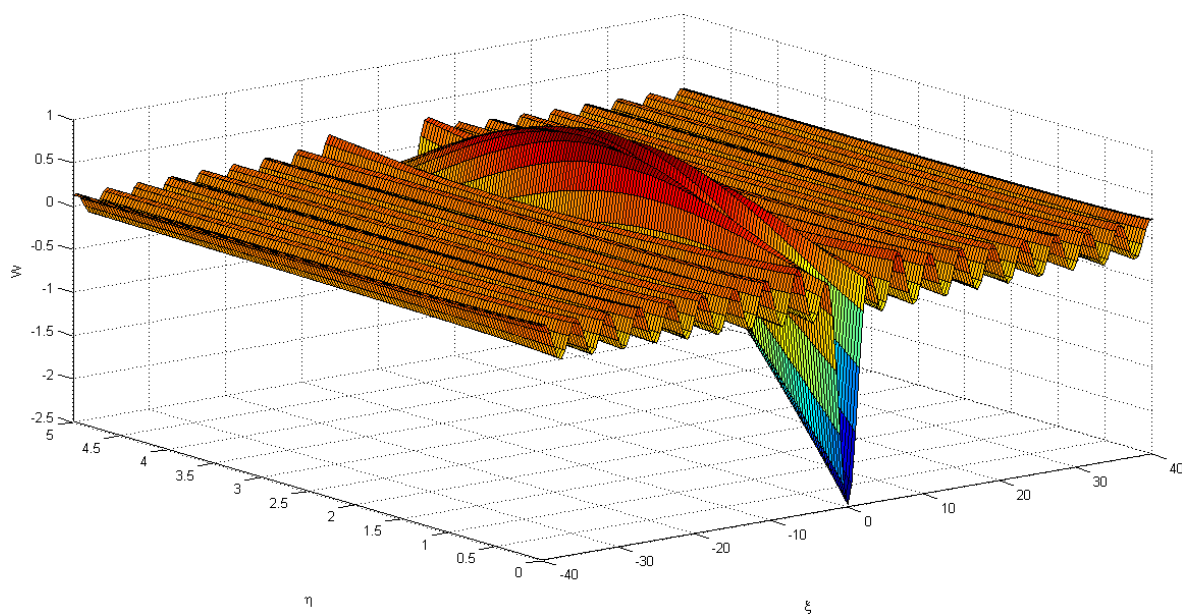
Figure 3.11: Overall deflection in orthotropic plate ($\hat{D}_x = 5$). 3D profile of the exact solution (3.23)

will be the dominating. This material can be the material where all the other parameters are as of an isotropic plate, but $\hat{D}_1 = 0.99$. The following Figures 3.12-3.14 clearly demonstrate the fact that Konenkov wave now has a dominating contribution into the overall plate deflection. The only exception is the vicinity of the applied force.

On the other hand, there exist and can be found using the model such materials, for which when propagating, the flexural edge wave has a negligible contribution. One of the examples is the material with large values of the D_{xy} stiffness. In this case the value for c_k is close to the asymptote $\sqrt[4]{\hat{D}_x \hat{D}_y}$. The following Figures 3.15-3.17, plotted for the material with $\hat{D}_{xy} = 5$, clearly demonstrate that the model allows us to find such a material.
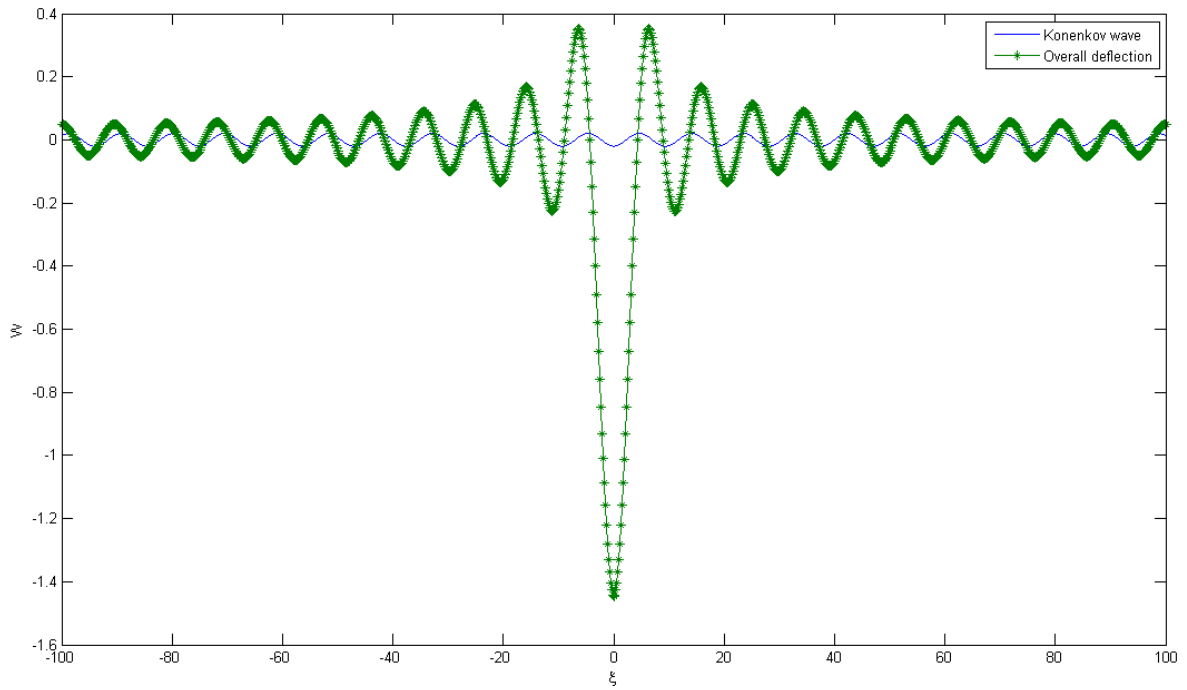
Figure 3.12: Edge deflection in orthotropic plate ($\hat{D}_1 = 0.99$). Overall solution (3.23) and Konenkov flexural edge wave contribution (2.40)

Figure 3.13: Konenkov flexural edge wave in orthotropic plate ($\hat{D}_1 = 0.99$). 3D profile of the parabolic-elliptic model (2.40), (3.33)
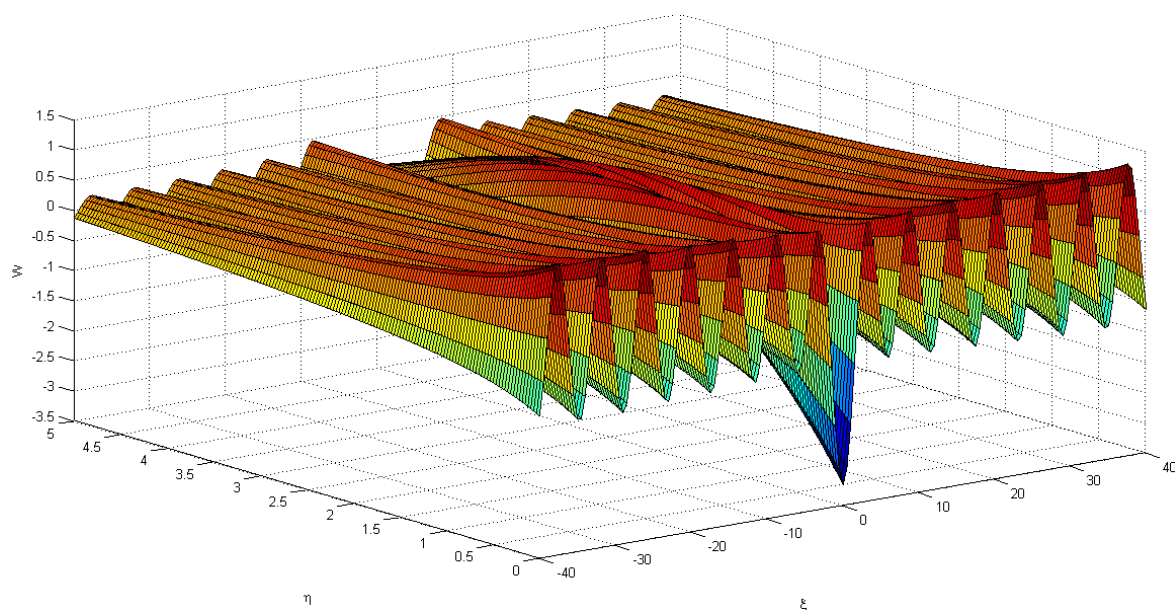
Figure 3.14: Overall deflection in orthotropic plate ($\hat{D}_1 = 0.99$). 3D profile of the exact solution (3.23)
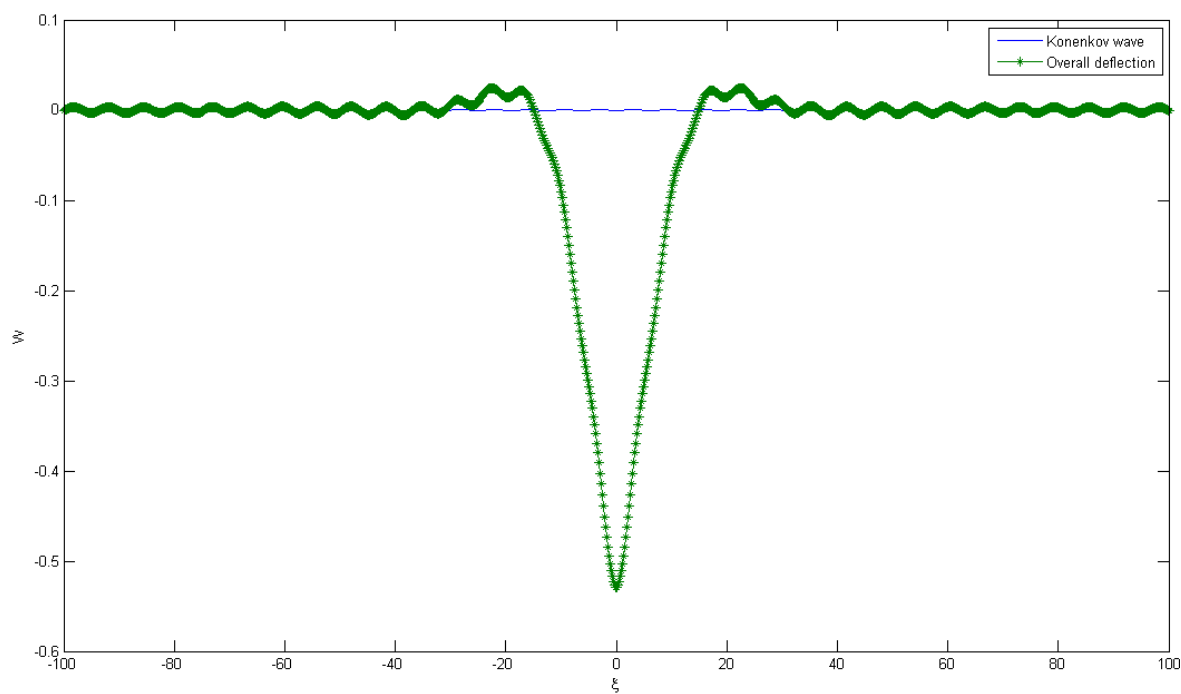
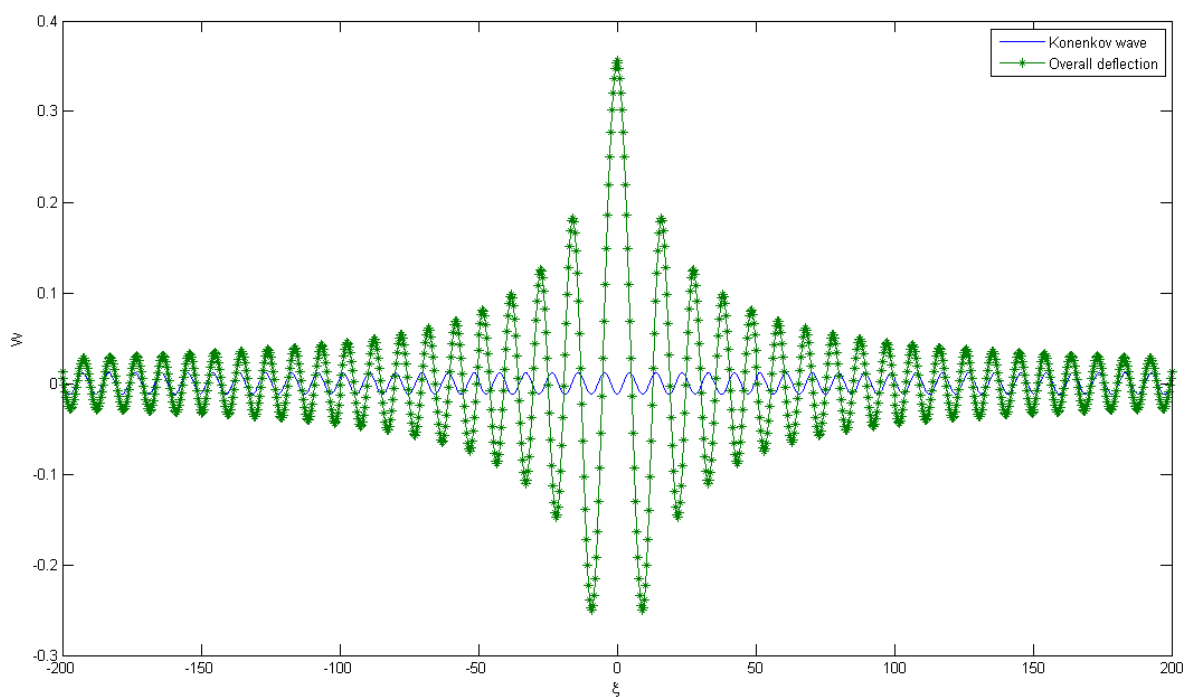Figure 3.15: Edge deflection in orthotropic plate ($\hat{D}_{xy} = 5$). Overall solution (3.23) and Konenkov flexural edge wave contribution (2.40)
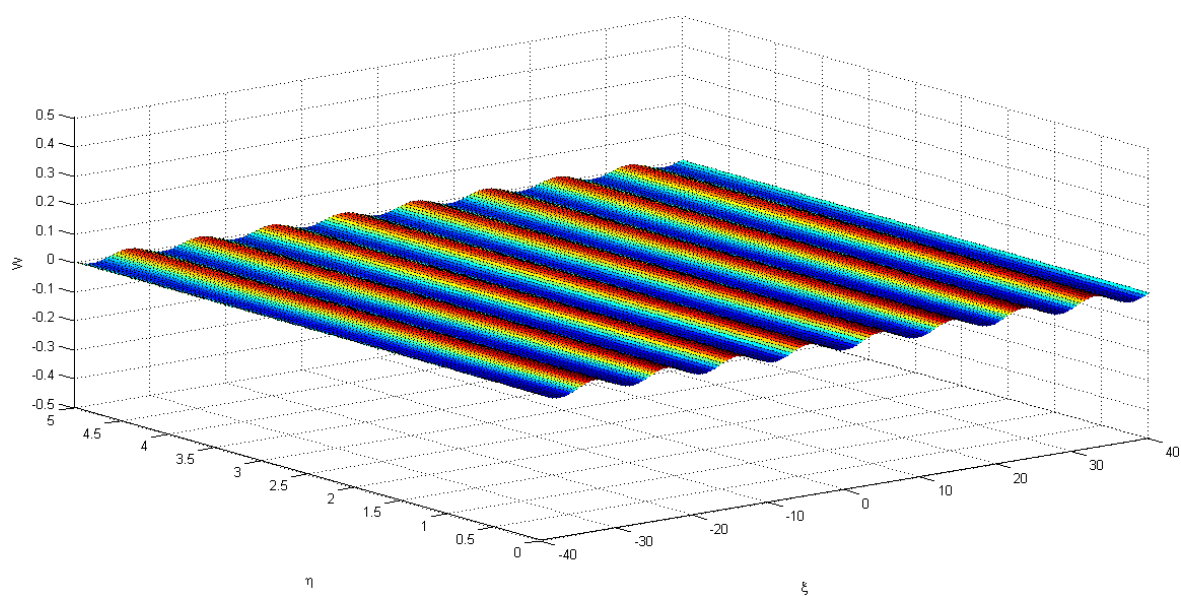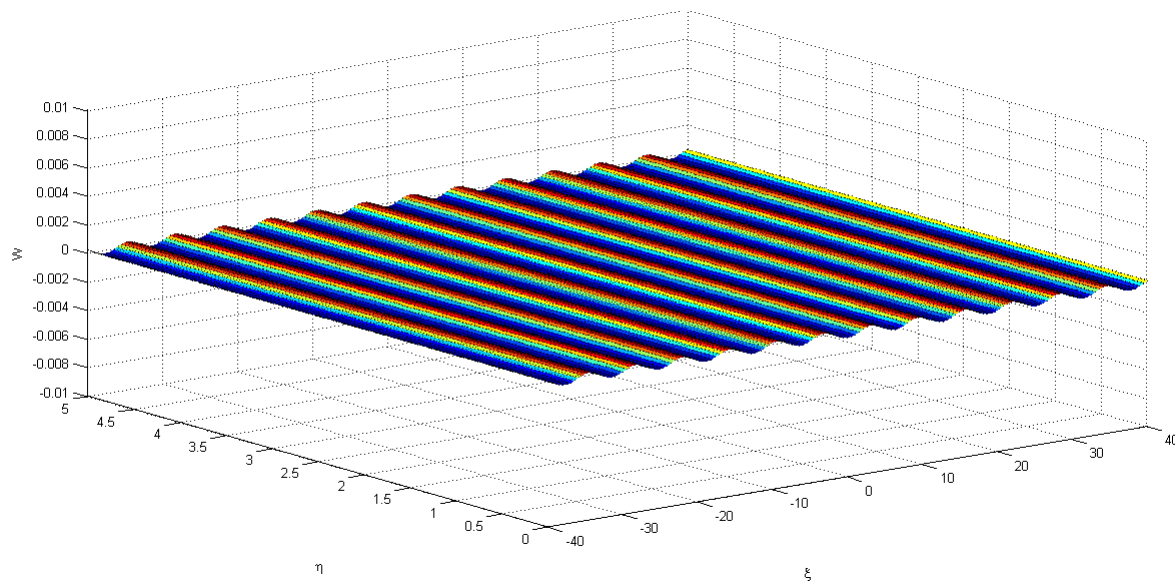
Figure 3.16: Konenkov flexural edge wave in orthotropic plate ($\hat{D}_{xy} = 5$). 3D profile of the parabolic-elliptic model (2.40), (3.33)
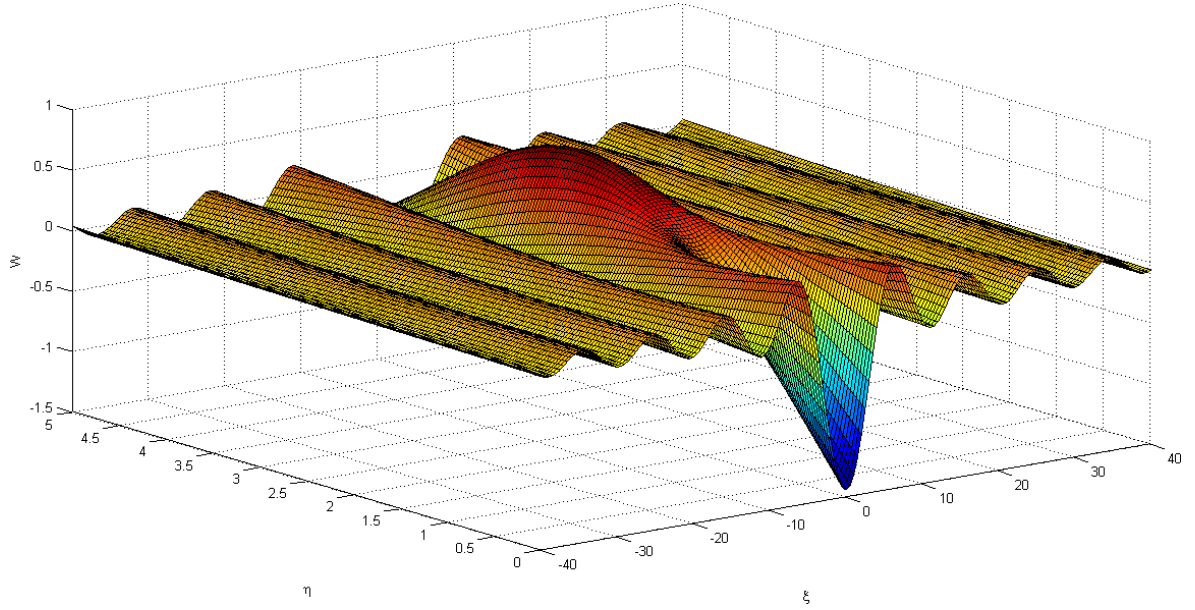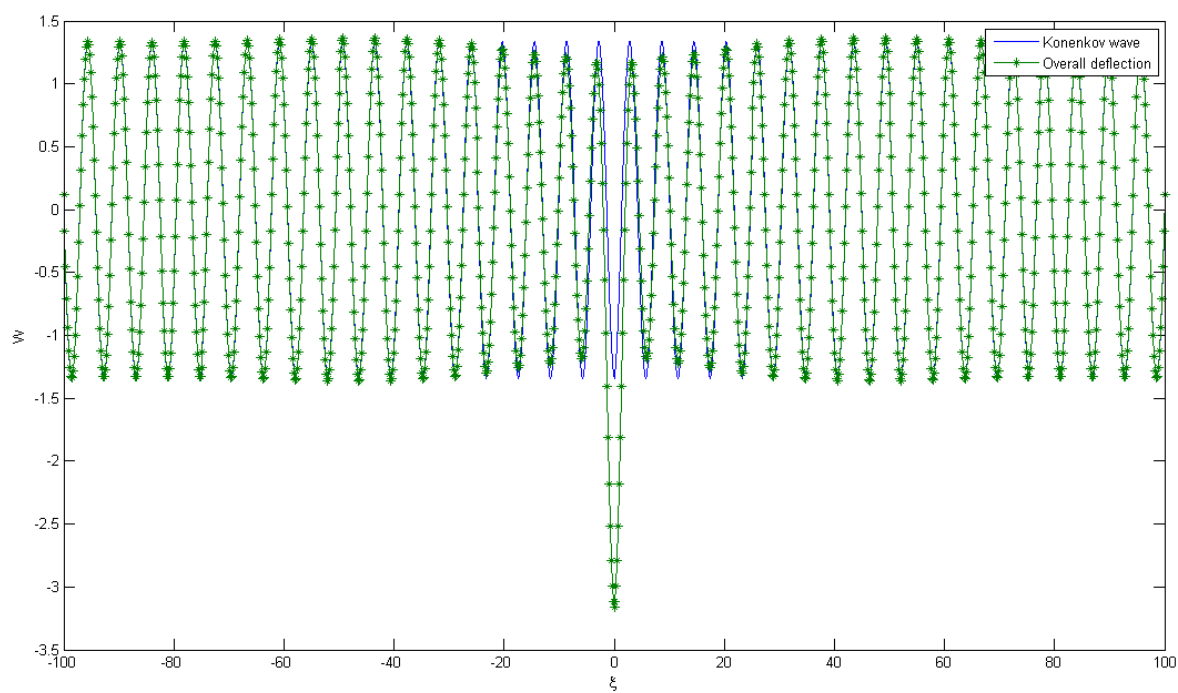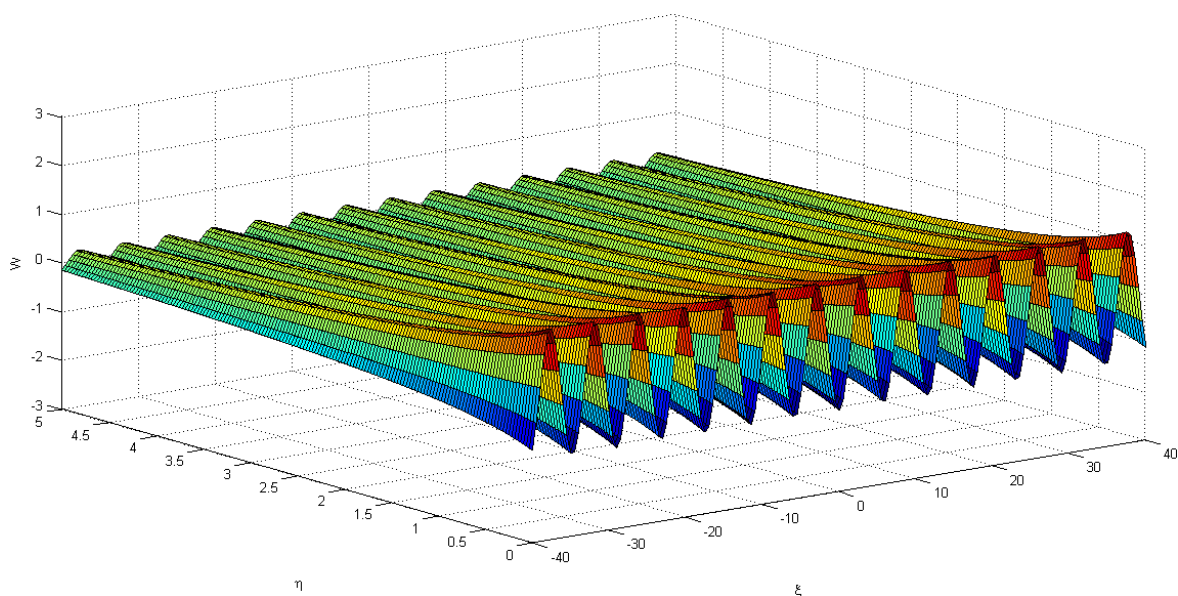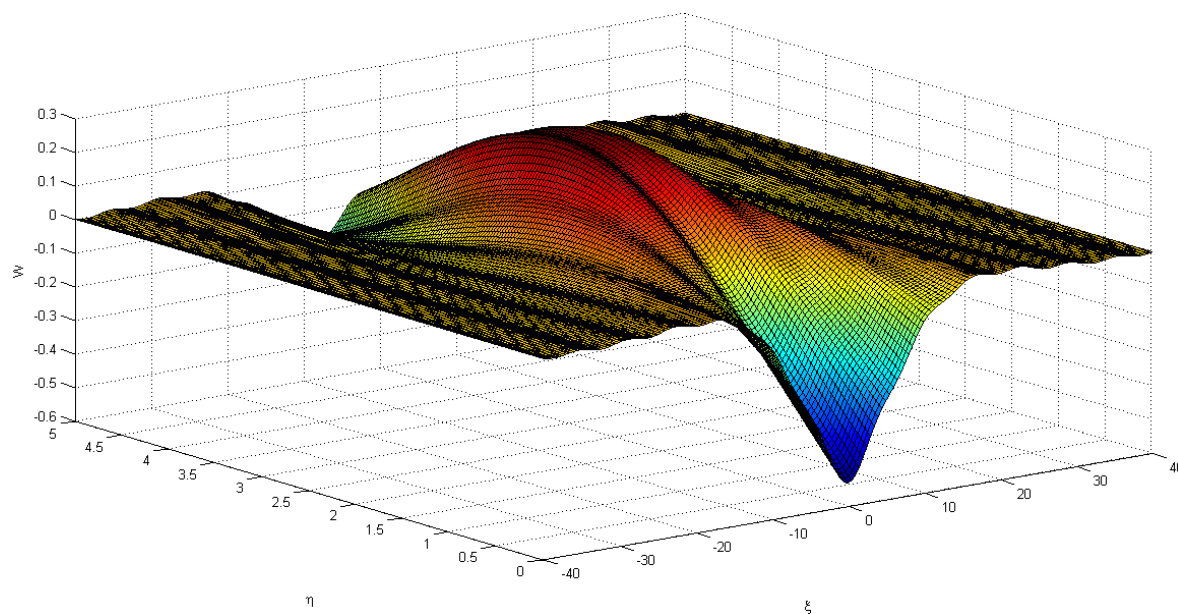

Figure 3.17: Overall deflection in orthotropic plate ($\hat{D}_{xy} = 5$). 3D profile of the exact solution (3.23)

3.3 Transverse shear force at plate edge

This section is dedicated to an edge loading in the form of a transverse shear force (see Figure 1.6).

3.3.1 Formulation of problem

The equation of motion for the deflection w is taken in the form (1.29) as above, while the boundary conditions are given now by relations (1.44). On using the dimensionless quantities (3.1) and applying the integral transforms, the sought for transformed equation takes the form of (3.2) and the boundary conditions at $\eta = 0$ become

$$\begin{aligned}
\hat{D}_y \frac{d^2\hat{W}}{d\eta^2} - \hat{D}_1 p^2 \hat{W} &= 0, \\
\hat{D}_y \frac{d^3\hat{W}}{d\eta^3} - (\hat{D}_1 + 4\hat{D}_{xy})p^2 \frac{d\hat{W}}{d\eta} &= -\hat{N}_0,
\end{aligned} \tag{3.34}$$

where $\hat{N}_0$ is the transformed dimensionless analogue of the original transverse point shear force.

3.3.2 Exact solution

The exact solution for the rotation angle $v(x, y, t)$ around the x-axis (or its transform $\hat{V}(\eta)$) can be obtained using the similar method as that described in Section 2.1.2. Omitting messy but pretty straightforward algebra, we present the final result as

$$\hat{V}(\eta) = \frac{\hat{M}_0}{-is\lambda_0\sqrt{\hat{D}_y}} \frac{c^2}{c^4 - c_k^4} \frac{\Delta_1(c)e^{-\frac{\sqrt{-is\lambda_0\sqrt{\hat{D}_y}}}{c}\alpha_c\eta} + \Delta_2(c)e^{-\frac{\sqrt{-is\lambda_0\sqrt{\hat{D}_y}}}{c}\beta_c\eta}}{\Delta(c)} X(c), \tag{3.35}$$

where α_c and β_c are given by (3.14), the function $X(c)$ is expressed by (3.10) and

$$\begin{aligned}
\Delta_1(c) &= \left[2\hat{D}_{xy} + \sqrt{(\hat{D}_1 + 2\hat{D}_{xy})^2 - \hat{D}_x\hat{D}_y + c^4}\right]\alpha_c, \\
\Delta_2(c) &= -\left[2\hat{D}_{xy} - \sqrt{(\hat{D}_1 + 2\hat{D}_{xy})^2 - \hat{D}_x\hat{D}_y + c^4}\right]\beta_c, \\
\Delta(c) &= -(\beta_c - \alpha_c)(c^4 - c_2^4).
\end{aligned} \tag{3.36}$$

3.3.3 Derivation of model

As it was mentioned above, the investigation of the Konenkov flexural edge wave contribution into the overall solution (3.35) is based on the derivation of an explicit dual parabolic-elliptic model. The method of its derivation is basically the same as that described in Section 2.1.2.

In the case under study, the parabolic equation at the plate edge becomes

$$\frac{c_k^{*4}}{D_y^2}\frac{\partial^4 v_e}{\partial x^4} + \frac{2\rho h}{D_y}\frac{\partial^2 v_e}{\partial t^2} = Q_e^{(2)*}\frac{1}{D_y}\frac{\partial^2 N_0}{\partial x^2}, \tag{3.37}$$

where

$$Q_e^{(2)*} = \frac{\Delta_1(c_k^*) + \Delta_2(c_k^*)}{\Delta(c_k^*)}, \tag{3.38}$$

with

$$\begin{aligned}
\Delta_1(c_k^*) &= \left[2D_{xy} + \sqrt{(D_1 + 2D_{xy})^2 - D_x D_y + c_k^{*4}}\right]\alpha_c(c_k^*),\\
\Delta_2(c_k^*) &= -\left[2D_{xy} - \sqrt{(D_1 + 2D_{xy})^2 - D_x D_y + c_k^{*4}}\right]\beta_c(c_k^*),\\
\Delta(c_k^*) &= -(\beta_c(c_k^*) - \alpha_c(c_k^*))(c_k^{*4} - c_2^{*4}),
\end{aligned} \tag{3.39}$$

and $\alpha_c(c_k^*)$, $\beta_c(c_k^*)$ are presented by relations (3.19), c_k^* and c_2^* are given by (3.16); also, as above, v_e is the rotation angle at the plate edge related to the Konenkov flexural edge wave.

The elliptic equation for the rotation angle v_{in} over the interior domain has now the form

$$\left(D_x - \frac{c_k^{*4}}{D_y}\right)\frac{\partial^4 v_{in}}{\partial x^4} + 2(D_1 + 2D_{xy})\frac{\partial^4 v_{in}}{\partial x^2 \partial y^2} + D_y\frac{\partial^4 v_{in}}{\partial y^4} = 0. \tag{3.40}$$

with the boundary conditions at $y = 0$

$$\begin{aligned}
v_{in}(x,0) &= v_e(x),\\
D_y\frac{\partial^2 v_{in}}{\partial y^2} &= -(D_1 + 4D_{xy})\frac{\partial^2 v_e}{\partial x^2}.
\end{aligned} \tag{3.41}$$

This concludes the formulation of the model.

3.3.4 Comparison with exact solution

Thus, we have obtained the exact solution (3.35) for the transformed angle $\hat{V}(\eta)$ and also derived the explicit dual parabolic-elliptic model for the Konenkov flexural edge wave in an orthotropic plate (see (3.37) and (3.40)-(3.41)). The next step is to compare the obtained solutions by analyzing the inverse Fourier transform and computing graphical illustrations.

We use now the case of the transverse shear point force N_0 (see Section 2.1.3) applied at the plate edge. As before, we operate with the same frequency parameter λ_0 (see (2.30)). Let us derive the formulae we need for computations. First we present the exact solution for the rotation angle $\hat{V}(\eta, p)$ in terms of the transform parameter p

$$\hat{V}(\eta, p) = \hat{N}_0 \frac{p^2}{p^4 - p_k^4}\frac{\Delta_1(p)e^{-\alpha\eta} + \Delta_2(p)e^{-\beta\eta}}{\Delta(p)}X(p), \tag{3.42}$$

where parameters $\alpha(p)$ and $\beta(p)$ are given by relations (3.24), p_k and p_2 take form (3.26), the function $X(p)$ is given by (3.27) and

$$
\begin{aligned}
\Delta_1(p) &= \left[2\hat{D}_{xy}p^2 + \sqrt{\left[(\hat{D}_1 + 2\hat{D}_{xy})^2 - \hat{D}_x\hat{D}_y\right]p^4 + \hat{D}_y\lambda_0^2}\right]\alpha, \\
\Delta_2(c) &= -\left[2\hat{D}_{xy}p^2 - \sqrt{\left[(\hat{D}_1 + 2\hat{D}_{xy})^2 - \hat{D}_x\hat{D}_y\right]p^4 + \hat{D}_y\lambda_0^2}\right]\beta, \\
\Delta(p) &= (\beta - \alpha)c_k^4 c_2^4(p^4 - p_2^4),
\end{aligned}
\tag{3.43}
$$

The solution at the plate edge for the Konenkov flexural edge wave is given by the following expression (where $\hat{V}_e(p)$ is the transformed angle of interest)

$$
\hat{V}_e = Q_e^{(2)}\hat{N}_0\frac{p^2}{p^4 - p_k^4},
\tag{3.44}
$$

where

$$
Q_e^{(2)} = \frac{\Delta_1(p_k) + \Delta_2(p_k)}{\Delta(p_k)}X(p_k),
\tag{3.45}
$$

and, according to the residue theory, the dimensionless rotation angle at the plate edge takes form (2.74) with $Q_e^{(2)}$ defined by (3.45). The branch points and the cut remain the same as in the previous Section 3.2.4.

To integrate the exact solution over the small semi-circles (see Sections 1.2.3 and 2.1.1 for more details), radius r is taken by (2.36).

As above, for the interior domain we solve the elliptic problem (3.40)-(3.41). The sought for solution takes the following form

$$
\hat{V}_{in} = \hat{N}_0\frac{p^2}{p^4 - p_k^4}Q_e^{(2)}\frac{\Delta_{1,in}(p)e^{-\alpha_c(c_k)p\eta} + \Delta_{2,in}(p)e^{-\beta_c(c_k)p\eta}}{\hat{D}_y(\beta_c^2(c_k) - \alpha_c^2(c_k))},
\tag{3.46}
$$

where

$$
\begin{aligned}
\Delta_{1,in}(p) &= -\left(2\hat{D}_{xy} - \sqrt{(\hat{D}_1 + 2\hat{D}_{xy})^2 - \hat{D}_x\hat{D}_y + c_k^4}\right)p^2, \\
\Delta_{2,in}(p) &= \left(2\hat{D}_{xy} + \sqrt{(\hat{D}_1 + 2\hat{D}_{xy})^2 - \hat{D}_x\hat{D}_y + c_k^4}\right)p^2.
\end{aligned}
\tag{3.47}
$$

Finally, the dimensionless rotation angle corresponding to Konenkov flexural edge wave over the interior domain can be found using the residue theory resulting in

$$
V_{in}^*(\xi, \eta) = \sqrt{2\pi}iQ_e^{(2)}\hat{N}_0\frac{1}{4p_k}\frac{\Delta_{1,in}(p_k)e^{-\alpha_c(c_k)p\eta} + \Delta_{2,in}(p_k)e^{-\beta_c(c_k)p\eta}}{\hat{D}_y(\beta_c^2(c_k) - \alpha_c^2(c_k))}e^{ip_k\xi}.
\tag{3.48}
$$

The results of computations are given in Figures 3.18-3.21. We set $\lambda_0 = 1$ and $\hat{N}_0 = \sqrt{2\pi}$ in all the graphs. The general conclusion is that the effect of orthotropy on the magnitude of the Konenkov component is analogous to that for the excitation by a point-bending moment.

Note also that the form of the approximate solution at the plate edge in the case of orthotropic plate is similar to the one of the isotropic plate (see (2.74)). The only difference is the coefficient $Q_e^{(2)}$ which depends on the material parameters. Therefore, below we present only the 3D profiles for two most significant cases of wave propagation.
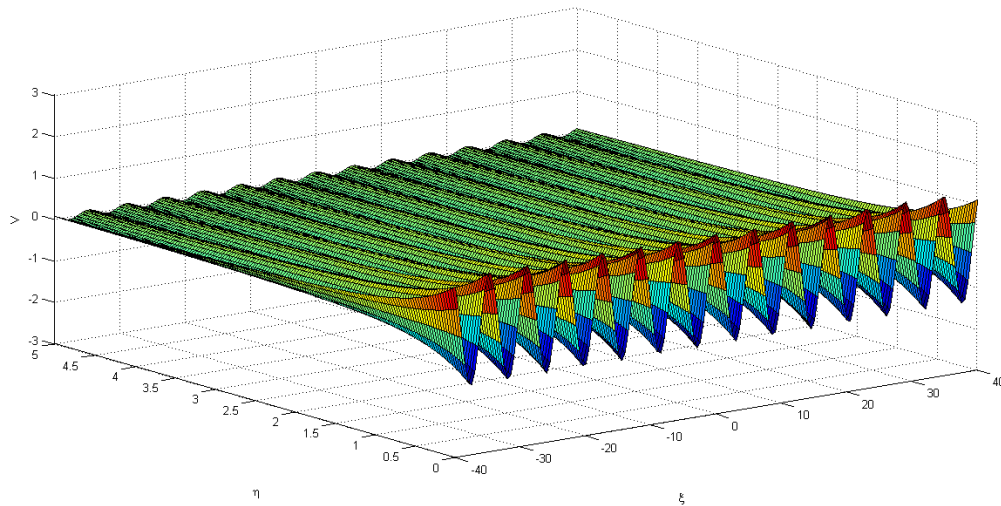
Figure 3.18: Konenkov flexural edge wave in orthotropic plate ($\hat{D}_1 = 0.99$). 3D profile of the parabolic-elliptic model (2.74), (3.48)
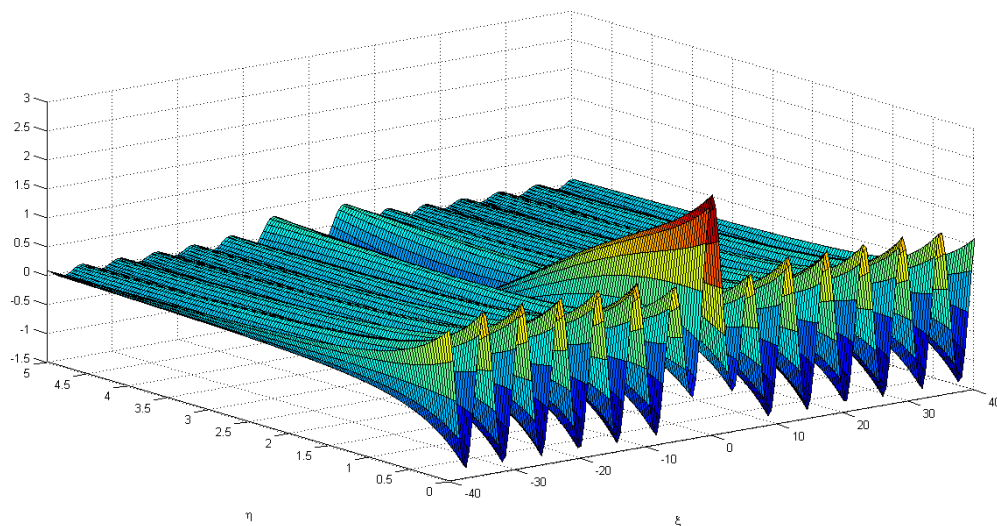
Figure 3.19: Overall rotation angle in orthotropic plate ($\hat{D}_1 = 0.99$). 3D profile of the exact solution (3.42)
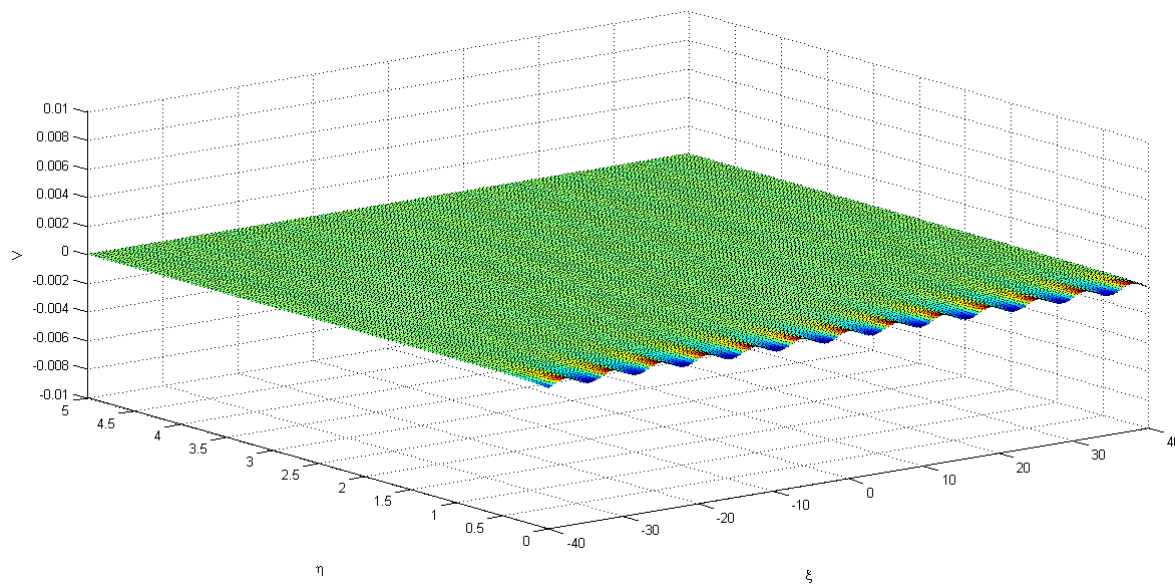
Figure 3.20: Konenkov flexural edge wave in orthotropic plate ($\hat{D}_{xy} = 5$). 3D profile of the parabolic-elliptic model (2.74), (3.48)
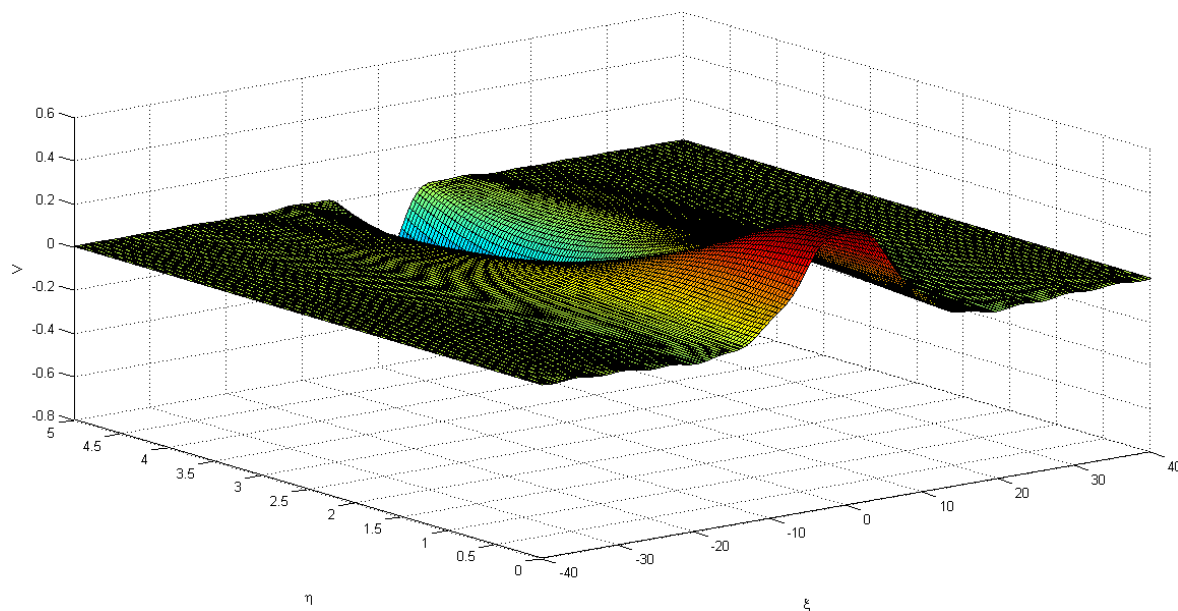
Figure 3.21: Overall rotation angle in orthotropic plate ($\hat{D}_{xy} = 5$). 3D profile of the exact solution (3.42)

Chapter 4

Stoneley-type flexural interfacial waves

4.1 Homogeneous interfacial wave

In this section we study homogeneous Stoneley-type flexural interfacial waves appearing at a junction of two semi-infinite isotropic plates.

4.1.1 Basic equations

For the interfacial vibrations of two semi-infinite plates, it is natural to state a joint problem for deflections of the plates participating in the junction. In this thesis we consider two plates (see Figure 4.1).
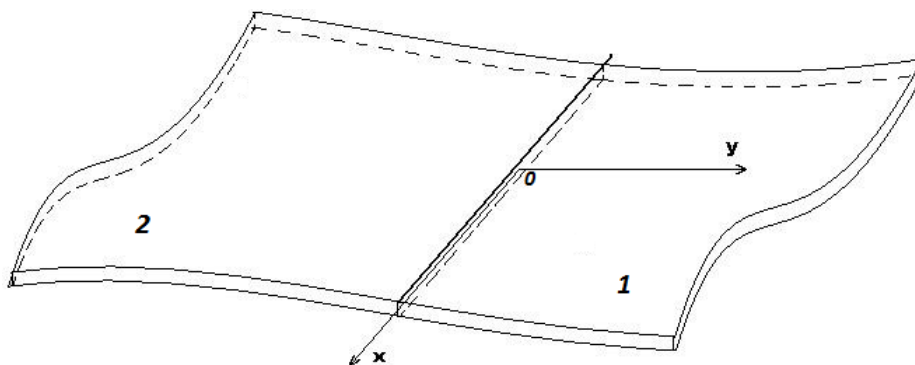
Figure 4.1: Junction of two semi-infinite plates. Directions of coordinate system

Equations of motion may be taken as (1.25) or (1.26), leading to two equations for de-

flections $w_1(x, y, t)$ and $w_2(x, y, t)$ of plates 1 and 2 respectively. They are

$$\frac{\partial^4 w_i}{\partial x^4} + 2\frac{\partial^4 w_i}{\partial x^2 \partial y^2} + \frac{\partial^4 w_i}{\partial y^4} + \frac{2\rho_i h}{D_i}\frac{\partial^2 w_i}{\partial t^2} = 0, \quad i = 1, 2, \tag{4.1}$$

where ρ_i are the material densities of plates 1 and 2, h is the half-thickness of plates (we assume that thickness is the same for both plates) and D_i are the bending stiffnesses.

By assuming that the junction $y = 0$ is continuous, and both plates are perfectly bonded (i.e. perfect contact), contact conditions would now consist of four main components listed below:

- equality of both plates deflections;

- equality of both plates rotation around the x-axis;

- equality of bending moments M_y;

- equality of vertical shear forces.

In terms of equations, these conditions are

$$
\begin{aligned}
w_1 &= w_2, \\
\frac{\partial w_1}{\partial y} &= \frac{\partial w_2}{\partial y}, \\
D_1\left[\frac{\partial^2 w_1}{\partial y^2} + \nu_1\frac{\partial^2 w_1}{\partial x^2}\right] &= D_2\left[\frac{\partial^2 w_2}{\partial y^2} + \nu_2\frac{\partial^2 w_2}{\partial x^2}\right], \\
D_1\left[\frac{\partial^3 w_1}{\partial y^3} + (2 - \nu_1)\frac{\partial^3 w_1}{\partial x^2 \partial y}\right] &= D_2\left[\frac{\partial^3 w_2}{\partial y^3} + (2 - \nu_2)\frac{\partial^3 w_2}{\partial x^2 \partial y}\right],
\end{aligned}
\tag{4.2}
$$

where ν_1 and ν_2 are the Poisson's ratios of plates 1 and 2 respectively.

We non-dimensionalise our equations by introducing the following notation

$$x = h\xi, \quad y = h\eta, \quad w_i = hW_i^*, \quad D_i = D\hat{D}_i, \quad t = T\tau, \tag{4.3}$$

where T is a typical time scale and D is a typical stiffness (which, in many problems, could be taken as D_1).

After using (4.3) and applying the integral transforms to (4.1), the transformed equations of motion become

$$\frac{d^4\hat{W}_i}{d\eta^4} - 2p^2\frac{d^2\hat{W}_i}{d\eta^2} + (p^4 + s^2\lambda_i^2)\hat{W}_i = 0, \quad i = 1, 2, \tag{4.4}$$

where

$$\lambda_i^2 = \frac{2\rho_i h^5}{D_i T^2} \tag{4.5}$$

- are the frequency parameters of plates 1 and 2.

In doing so, the contact conditions at the junction of plates take the form of

$$
\begin{aligned}
\hat{W}_1 &= \hat{W}_2, \\
\frac{d\hat{W}_1}{d\eta} &= \frac{d\hat{W}_2}{d\eta}, \\
\frac{d^2\hat{W}_1}{d\eta^2} - \nu_1 p^2 \hat{W}_1 &= \frac{\hat{D}_2}{\hat{D}_1}\left[\frac{d^2\hat{W}_2}{d\eta^2} - \nu_2 p^2 \hat{W}_2\right], \\
\frac{d^3\hat{W}_1}{d\eta^3} - (2-\nu_1)p^2\frac{d\hat{W}_1}{d\eta} &= \frac{\hat{D}_2}{\hat{D}_1}\left[\frac{d^3\hat{W}_2}{d\eta^2} - (2-\nu_2)p^2\frac{d\hat{W}_2}{d\eta}\right].
\end{aligned}
\tag{4.6}
$$

4.1.2 Stoneley-type flexural interfacial wave in isotropic plates

Due to the nature of the above problem we introduce its solutions as

$$
\hat{W}_i = C_i e^{-\gamma_i |\eta|}, \quad i = 1, 2.
\tag{4.7}
$$

Substitution of (4.7) into equations (4.4) suggests that the solution of the above problem takes form

$$
\hat{W}_j = A_j e^{-\alpha_j |\eta|} + B_j e^{-\beta_j |\eta|}, \quad j = 1, 2,
\tag{4.8}
$$

where parameters α_j and β_j are

$$
\alpha_j = \sqrt{p^2 + i\lambda_j s}, \quad \beta_j = \sqrt{p^2 - i\lambda_j s}, \quad j = 1, 2,
\tag{4.9}
$$

and A_j, B_j are arbitrary constants which can be found by substitution of (4.8) into contact conditions (4.6). The obtained system of linear equations for A_j and B_j, $j = 1, 2$, expressed in a matrix form, is

$$
\begin{bmatrix} A_1 & B_1 & A_2 & B_2 \end{bmatrix}
$$

$$
\times \begin{bmatrix}
1 & \alpha_1 & \alpha_1^2 - \nu_1 p^2 & \left(\alpha_1^2 - (2-\nu_1)p^2\right)\alpha_1 \\
1 & \beta_1 & \beta_1^2 - \nu_1 p^2 & \left(\beta_1^2 - (2-\nu_1)p^2\right)\beta_1 \\
-1 & -\alpha_2 & -\dfrac{\hat{D}_2}{\hat{D}_1}\left(\alpha_2^2 - \nu_2 p^2\right) & -\dfrac{\hat{D}_2}{\hat{D}_1}\left(\alpha_2^2 - (2-\nu_2)p^2\right)\alpha_2 \\
-1 & -\beta_2 & -\dfrac{\hat{D}_2}{\hat{D}_1}\left(\beta_2^2 - \nu_2 p^2\right) & -\dfrac{\hat{D}_2}{\hat{D}_1}\left(\beta_2^2 - (2-\nu_2)p^2\right)\beta_2
\end{bmatrix}
\tag{4.10}
$$

$$
= \begin{bmatrix} 0 & 0 & 0 & 0 \end{bmatrix}.
$$

The above system has non-zero solutions only in the case when its determinant equals to

zero. This fact leads to the following equation

$$
\begin{aligned}
&\left[-is\lambda_1 - \tfrac{\hat{D}_2}{\hat{D}_1}is\lambda_2 + \left[(1-\nu_1) - \tfrac{\hat{D}_2}{\hat{D}_1}(1-\nu_2)\right]p^2\right]^2 \sqrt{p^2+is\lambda_1}\sqrt{p^2-is\lambda_2} \\
&+ \left[-is\lambda_1 - \tfrac{\hat{D}_2}{\hat{D}_1}is\lambda_2 - \left[(1-\nu_1) - \tfrac{\hat{D}_2}{\hat{D}_1}(1-\nu_2)\right]p^2\right]^2 \sqrt{p^2-is\lambda_1}\sqrt{p^2+is\lambda_2} \\
&- \left[is\lambda_1 - \tfrac{\hat{D}_2}{\hat{D}_1}is\lambda_2 - \left[(1-\nu_1) - \tfrac{\hat{D}_2}{\hat{D}_1}(1-\nu_2)\right]p^2\right]^2 \sqrt{p^2+is\lambda_1}\sqrt{p^2+is\lambda_2} \\
&- \left[-is\lambda_1 + \tfrac{\hat{D}_2}{\hat{D}_1}is\lambda_2 + \left[(1-\nu_1) - \tfrac{\hat{D}_2}{\hat{D}_1}(1-\nu_2)\right]p^2\right]^2 \sqrt{p^2-is\lambda_1}\sqrt{p^2-is\lambda_2} \\
&+ 4s^2\lambda_1\lambda_2\tfrac{\hat{D}_2}{\hat{D}_1}\left[\sqrt{p^4+s^2\lambda_1^2} + \sqrt{p^4+s^2\lambda_2^2}\right] = 0.
\end{aligned}
\tag{4.11}
$$

It is obvious that equation (4.11) is a very complicated one with many parameters. In order to simplify it, we introduce new quantities by the following expressions

$$
\alpha = \sqrt{\frac{\rho_2}{\rho_1}}, \quad \beta = \sqrt{\frac{\hat{D}_2}{\hat{D}_1}}, \quad c = \frac{\sqrt{-is\lambda_1}}{p}.
\tag{4.12}
$$

Then (4.11) transforms to

$$
\begin{aligned}
&\left[(1+a)c^2+d\right]^2 \sqrt{1-c^2}\sqrt{1+bc^2} + \left[(1+a)c^2-d\right]^2 \sqrt{1+c^2}\sqrt{1-bc^2} \\
&- \left[(1-a)c^2+d\right]^2 \sqrt{1-c^2}\sqrt{1-bc^2} - \left[(1-a)c^2-d\right]^2 \sqrt{1+c^2}\sqrt{1+bc^2} \\
&- 4a\left[\sqrt{1-c^4} + \sqrt{1-b^2c^4}\right]c^4 = 0,
\end{aligned}
\tag{4.13}
$$

where

$$
a = \alpha\beta, \quad b = \frac{\alpha}{\beta}, \quad d = (1-\nu_1) - (1-\nu_2)\beta^2.
\tag{4.14}
$$

As it might be seen from equation (4.13), its most general form does not have analytical solutions, but it is possible to find them numerically. The next 3 plots (see Figures 4.2-4.4) demonstrate the dependence of the solution on the parameters α and β from (4.14) for different values of the plates Poisson's ratios. We may notice that the solution is highly dependent on the material parameters and does not exist for many of their values. Note that the white areas in all Figures 4.2-4.4 correspond to such parameters relation where no flexural interfacial wave exists.

As it can be seen from the pictures, one of the boundaries where the solution disappears is the line $\alpha = \beta$. It corresponds to the value $b = 1$ in the above equation (4.13). Setting $b = 1$ in (4.13), which leads to more simple form of it, we are able to obtain the analytical solutions

$$
c = \pm\frac{\sqrt{(\alpha^2-1)((1-\nu_1)-(1-\nu_2)\alpha^2)}}{1-\alpha^2}
\tag{4.15}
$$

for $\alpha^2 < 1$ and $\alpha^2 < \dfrac{1-\nu_1}{1-\nu_2}$ or

$$
c = \pm\frac{\sqrt{(\alpha^2-1)((1-\nu_1)-(1-\nu_2)\alpha^2)}}{\alpha^2-1}
\tag{4.16}
$$
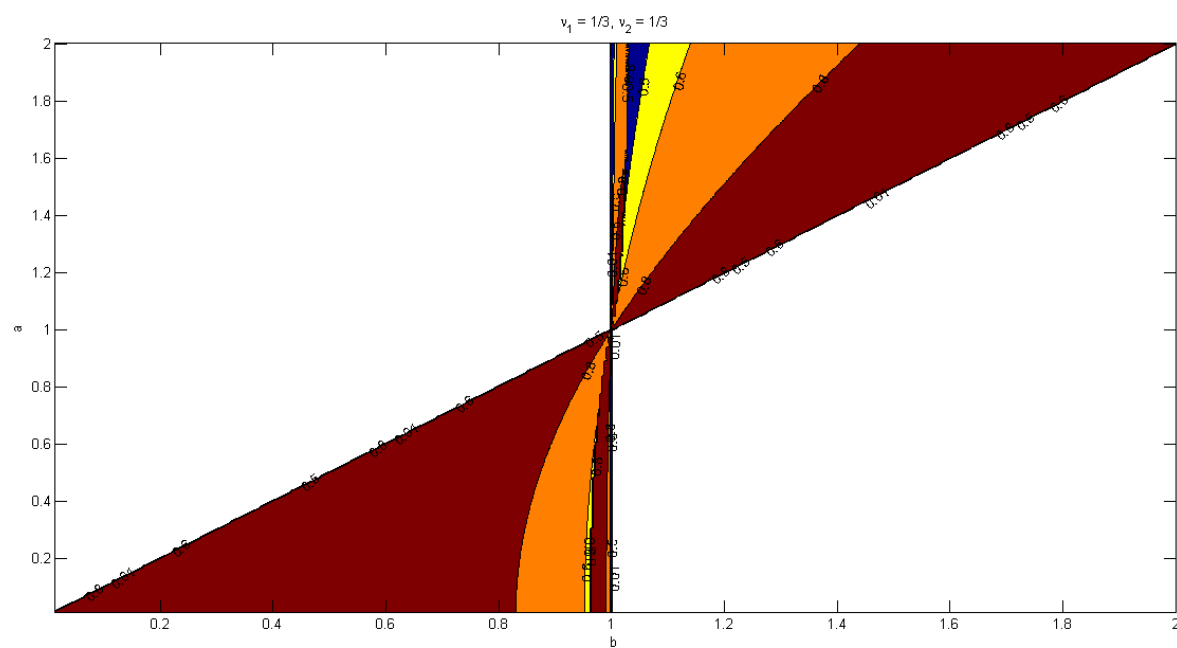
Figure 4.2: Wave coefficient distribution ($\nu_1 = \nu_2 = \frac{1}{3}$). Areas of solution existence
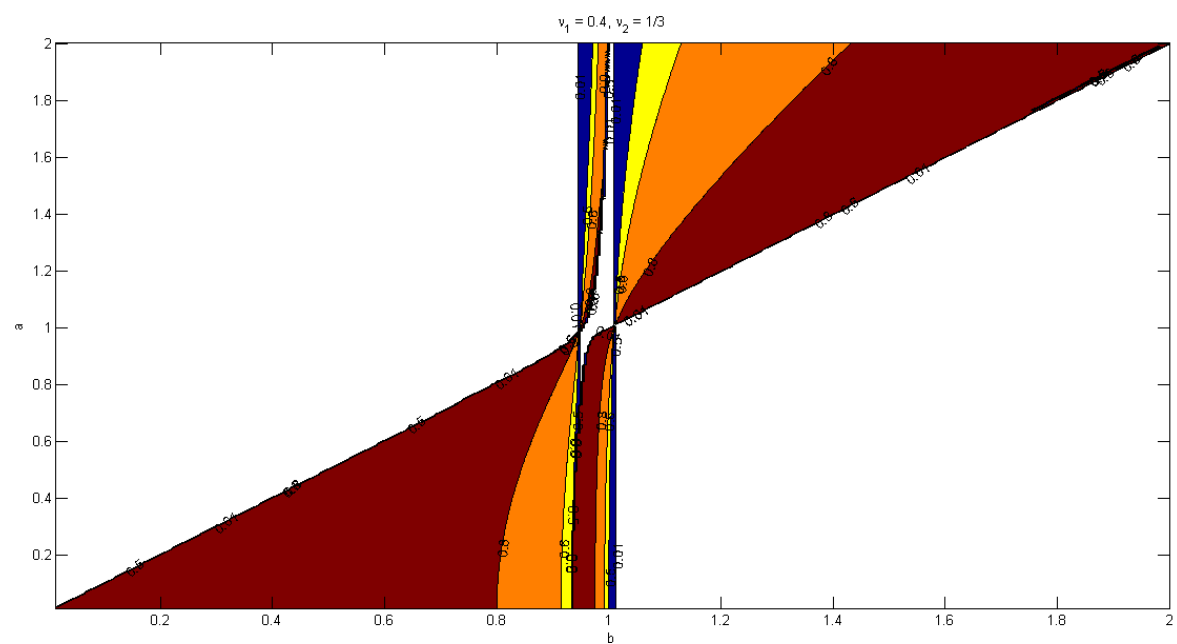
Figure 4.3: Wave coefficient distribution ($\nu_1 = 0.4$, $\nu_2 = \frac{1}{3}$). Areas of solution existence
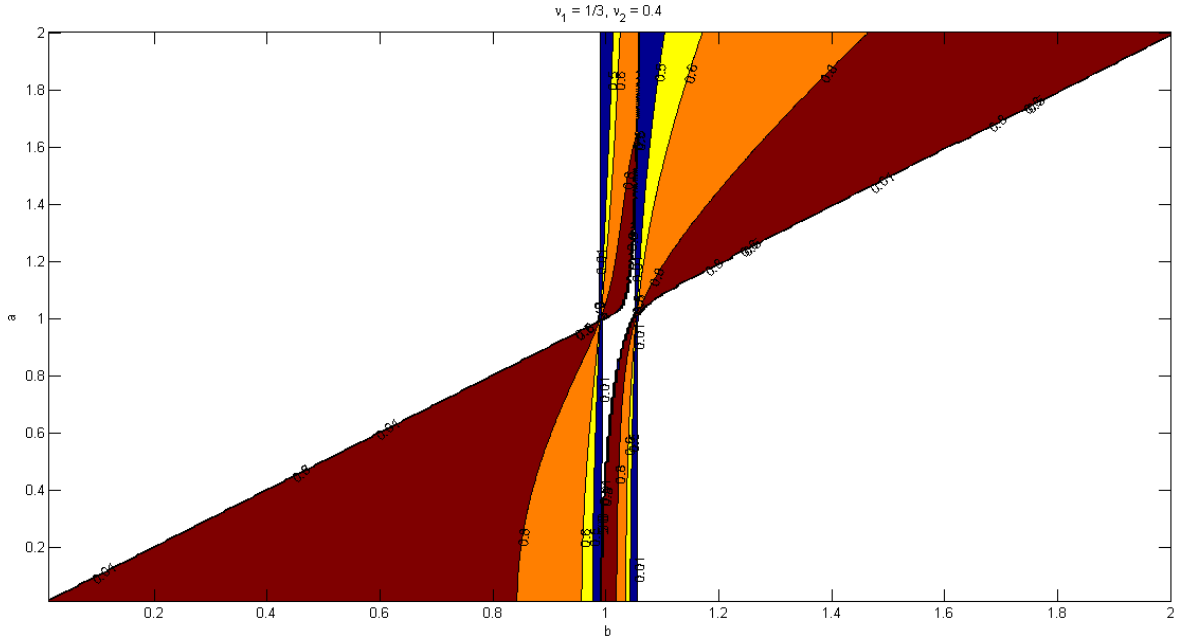
Figure 4.4: Wave coefficient distribution ($\nu_1 = \dfrac{1}{3}$, $\nu_2 = 0.4$). Areas of solution existence

for $\alpha^2 > 1$ and $\alpha^2 > \dfrac{1 - \nu_1}{1 - \nu_2}$.

It is natural to assume that the most general solution of equation (4.13) has a form similar to (4.15)-(4.16) and, therefore, we may predict that the solutions can only exist for the values $\dfrac{\alpha^2}{\beta^2} < 1$ and $\dfrac{\alpha^2}{\beta^2} < \dfrac{1 - \nu_1}{1 - \nu_2}$, or $\dfrac{\alpha^2}{\beta^2} > 1$ and $\dfrac{\alpha^2}{\beta^2} > \dfrac{1 - \nu_1}{1 - \nu_2}$. This dependence can be also noticed in Figures 4.2-4.4.

When the parameter β reaches the value $\beta^2 = \dfrac{1 - \nu_1}{1 - \nu_2}$ (which corresponds to $d = 0$), equation (4.13) appears to have no solutions. It can also be checked by the asymptotic analysis of the above equation by considering the case of $c \to 0$. The above observations explain several boundaries of solution existence. The curved boundary which is seen in the last two Figures may be explained by the fact that parameter β depends on the Poisson's ratios of both plates.

4.2 Bending moment at junction of two plates

This section is dedicated to the analysis of the deflection of two spliced isotropic semi-infinite plates induced by a bending moment at their junction.
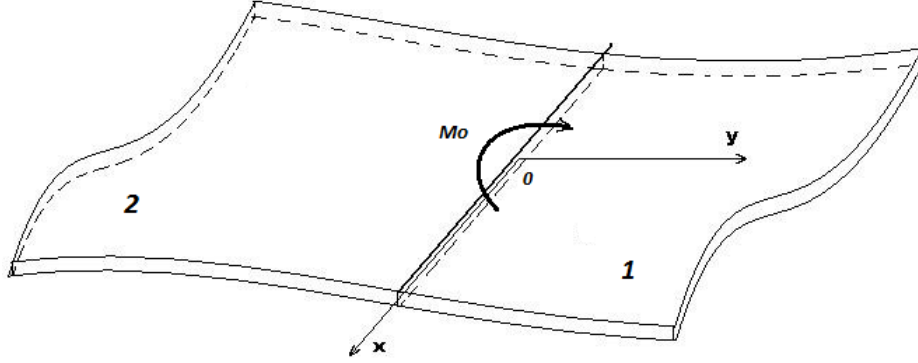
Figure 4.5: Bending moment at the junction. Scheme of loading

4.2.1 Basic equations

For this type of loading (see Figure 4.5) the equations for the deflections w_i, $i = 1, 2$ remain in form (4.1), whereas the boundary conditions at the junction $(y = 0)$ become

$$
\begin{aligned}
w_1 &= w_2, \\
\frac{\partial w_1}{\partial y} &= \frac{\partial w_2}{\partial y}, \\
D_1 \left[\frac{\partial^2 w_1}{\partial y^2} + \nu_1 \frac{\partial^2 w_1}{\partial x^2} \right] &= D_2 \left[\frac{\partial^2 w_2}{\partial y^2} + \nu_2 \frac{\partial^2 w_2}{\partial x^2} \right] - M_0(x, t), \\
D_1 \left[\frac{\partial^3 w_1}{\partial y^3} + (2 - \nu_1) \frac{\partial^3 w_1}{\partial x^2 \partial y} \right] &= D_2 \left[\frac{\partial^3 w_2}{\partial y^3} + (2 - \nu_2) \frac{\partial^3 w_2}{\partial x^2 \partial y} \right],
\end{aligned}
\tag{4.17}
$$

where $M_0(x, t)$ is the applied bending moment.

On using expressions (4.3) and applying the integral transforms to (4.1), we again come to equations of motion (4.4). In doing so to boundary conditions (4.17), at $\eta = 0$ we obtain the following

$$
\begin{aligned}
\hat{W}_1 &= \hat{W}_2, \\
\frac{d\hat{W}_1}{d\eta} &= \frac{d\hat{W}_2}{d\eta}, \\
\frac{d^2\hat{W}_1}{d\eta^2} - \nu_1 p^2 \hat{W}_1 &= \frac{\hat{D}_2}{\hat{D}_1} \left[\frac{d^2\hat{W}_2}{d\eta^2} - \nu_2 p^2 \hat{W}_2 \right] - \frac{\hat{M}_0}{\hat{D}_1}, \\
\frac{d^3\hat{W}_1}{d\eta^3} - (2 - \nu_1)p^2 \frac{d\hat{W}_1}{d\eta} &= \frac{\hat{D}_2}{\hat{D}_1} \left[\frac{d^3\hat{W}_2}{d\eta^2} - (2 - \nu_2)p^2 \frac{d\hat{W}_2}{d\eta} \right],
\end{aligned}
\tag{4.18}
$$

where $\hat{M}_0(s,p)$ is the transformed dimensionless bending moment.

4.2.2 Solution of problem

We take (4.8)-(4.9) as the solution of problem (4.4), (4.18). By substituting them to the boundary conditions (4.18) we obtain a system of linear equations for the unknown constants A_1, B_1, A_2 and B_2. In the matrix form it can be written by

$$
\begin{bmatrix} A_1 & B_1 & A_2 & B_2 \end{bmatrix}
$$

$$
\times \begin{bmatrix}
1 & \alpha_1 & \alpha_1^2 - \nu_1 p^2 & (\alpha_1^2 - (2 - \nu_1)p^2)\,\alpha_1 \\
1 & \beta_1 & \beta_1^2 - \nu_1 p^2 & (\beta_1^2 - (2 - \nu_1)p^2)\,\beta_1 \\
-1 & -\alpha_2 & -\dfrac{\hat{D}_2}{\hat{D}_1}\left(\alpha_2^2 - \nu_2 p^2\right) & -\dfrac{\hat{D}_2}{\hat{D}_1}\left(\alpha_2^2 - (2 - \nu_2)p^2\right)\alpha_2 \\
-1 & -\beta_2 & -\dfrac{\hat{D}_2}{\hat{D}_1}\left(\beta_2^2 - \nu_2 p^2\right) & -\dfrac{\hat{D}_2}{\hat{D}_1}\left(\beta_2^2 - (2 - \nu_2)p^2\right)\beta_2
\end{bmatrix} \tag{4.19}
$$

$$
= \begin{bmatrix} 0 & 0 & -\dfrac{\hat{M}_0}{\hat{D}_1} & 0 \end{bmatrix}.
$$

Without providing quite straightforward algebra, we present the exact solutions for the transformed deflections $\hat{W}_1(\eta)$ and $\hat{W}_2(\eta)$ as

$$
\begin{aligned}
\hat{W}_1(\eta) &= \frac{\hat{M}_0}{\hat{D}_1^2(-is\lambda_1^2)}\frac{c^2}{c^4 - c_k^4}\frac{\Delta_1(c)e^{-\frac{\sqrt{-is\lambda_1}}{c}\alpha_1(c)|\eta|} + \Delta_2(c)e^{-\frac{\sqrt{-is\lambda_1}}{c}\beta_1(c)|\eta|}}{\Delta'(c_k^4)}, \\
\hat{W}_2(\eta) &= \frac{\hat{M}_0}{\hat{D}_1^2(-is\lambda_1^2)}\frac{c^2}{c^4 - c_k^4}\frac{\Delta_3(c)e^{-\frac{\sqrt{-is\lambda_1}}{c}\alpha_2(c)|\eta|} + \Delta_4(c)e^{-\frac{\sqrt{-is\lambda_1}}{c}\beta_2(c)|\eta|}}{\Delta'(c_k^4)},
\end{aligned} \tag{4.20}
$$

where c_k is the solution of equation (4.13), the expressions for $\alpha_j(c)$ and $\beta_j(c)$ $(j = 1, 2)$ are presented below

$$
\begin{aligned}
\alpha_1(c) &= \sqrt{1 - c^2}, & \beta_1(c) &= \sqrt{1 + c^2}, \\
\alpha_2(c) &= \sqrt{1 - bc^2}, & \beta_1(c) &= \sqrt{1 + bc^2},
\end{aligned} \tag{4.21}
$$

with b from (4.14).

And also,

$$
\begin{aligned}
\Delta_1(c) &= \beta^2\left[(\beta_1-\alpha_2)\beta_2((\nu_2-1)+bc^2)+(\beta_2-\beta_1)\alpha_2((\nu_2-1)-bc^2)\right]\\
&\quad +(\alpha_2-\beta_2)\beta_1((\nu_1-1)+c^2),\\
\Delta_2(c) &= -\left[\beta^2\left[(\beta_2-\alpha_1)\alpha_2((\nu_2-1)-bc^2)+(\alpha_1-\alpha_2)\beta_2((\nu_2-1)+bc^2)\right]\right.\\
&\quad \left.+(\alpha_2-\beta_2)\alpha_1((\nu_1-1)-c^2)\right],\\
\Delta_3(c) &= (\alpha_1-\beta_2)\beta_1((\nu_1-1)+c^2)+(\beta_1-\beta_2)\alpha_1((\nu_1-1)-c^2)\\
&\quad +\beta^2(\alpha_1-\beta_1)\beta_2((\nu_2-1)+bc^2),\\
\Delta_4(c) &= -\left[(\alpha_1-\alpha_2)\beta_1((\nu_1-1)+c^2)+(\alpha_2-\beta_1)\alpha_1((\nu_1-1)-c^2)\right.\\
&\quad \left.+\beta^2(\beta_1-\alpha_1)\alpha_2((\nu_2-1)-bc^2)\right].
\end{aligned}
\tag{4.22}
$$

As it was mentioned above, due to the form of equation (4.13), it is impossible to find its solutions analytically. Therefore it becomes impossible to expand the denominator Δ of the original solution in order to find contribution of the interfacial wave coefficient poles. For this reason we use the Taylor series to expand the denominator approximately as $\Delta(c) = (c^4 - c_k^4)\Delta'(c_k^4)$, where c_k is the sought for real zero of denominator and

$$
\begin{aligned}
\Delta'(c_k^4) = &\frac{1}{4c_k^2}\\
&\times\left[((1+a)c_k^2+d)A+((1+a)c_k^2-d)B\right.\\
&\left.-((1-a)c_k^2+d)C-((1-a)c_k^2-d)D\right]\\
&-4a(\sqrt{1-c_k^4}+\sqrt{1-b^2c_k^4})+2ac_k^4\left[\frac{1}{\sqrt{1-c_k^4}}+\frac{b^2}{\sqrt{1-b^2c_k^4}}\right].
\end{aligned}
\tag{4.23}
$$

where

$$
\begin{aligned}
A &= 4(1+a)\sqrt{1-c_k^2}\sqrt{1+bc_k^2}+((1+a)c_k^2+d)\left(-\frac{\sqrt{1+bc_k^2}}{\sqrt{1-c_k^2}}+b\frac{\sqrt{1-c_k^2}}{\sqrt{1+bc_k^2}}\right),\\
B &= 4(1+a)\sqrt{1+c_k^2}\sqrt{1-bc_k^2}+((1+a)c_k^2-d)\left(\frac{\sqrt{1-bc_k^2}}{\sqrt{1+c_k^2}}+b\frac{\sqrt{1+c_k^2}}{\sqrt{1-bc_k^2}}\right),\\
C &= 4(1-a)\sqrt{1-c_k^2}\sqrt{1-bc_k^2}-((1-a)c_k^2+d)\left(\frac{\sqrt{1-bc_k^2}}{\sqrt{1-c_k^2}}+b\frac{\sqrt{1-c_k^2}}{\sqrt{1-bc_k^2}}\right),\\
D &= 4(1-a)\sqrt{1+c_k^2}\sqrt{1+bc_k^2}+((1-a)c_k^2-d)\left(\frac{\sqrt{1+bc_k^2}}{\sqrt{1+c_k^2}}+b\frac{\sqrt{1+c_k^2}}{\sqrt{1+bc_k^2}}\right).
\end{aligned}
\tag{4.24}
$$

4.2.3 Derivation of dual parabolic-elliptic model

The analysis of the Stoneley-type flexural interfacial wave contribution into the exact solution is connected to the derivation of the dual parabolic-elliptic model. It consists of the parabolic equations at the plates junction and the elliptic problem over the interior domain. The nature of the problem and method of model construction allow us to create these equations separately for each plate.

First, at the junction, where $\eta = 0$, we obtain (see Section 2.1.2 for more details) the following expressions in terms of the transform parameter p

$$\hat{W}_{e,i}(p) = -\frac{\hat{M}_0}{\hat{D}_1}\frac{p^2}{p^4 - p_k^4}Q_{e,i}^{(1)}, \quad i = 1, 2, \tag{4.25}$$

where $\hat{W}_{e,i}$ are the transformed deflections of plates 1 and 2 at the junction corresponding to the Stoneley-type flexural interfacial wave and

$$\begin{aligned} Q_{e,1}^{(1)} &= \frac{\Delta_1(c_k) + \Delta_2(c_k)}{\Delta'(c_k^4)}, \\ Q_{e,2}^{(1)} &= \frac{\Delta_3(c_k) + \Delta_4(c_k)}{\Delta'(c_k^4)}. \end{aligned} \tag{4.26}$$

It is easy to check that $Q_{e,1}^{(1)} = Q_{e,2}^{(1)}$ and, therefore, the deflections of both plates at the junction are equal. In the original variables, we have the following parabolic equations:

$$c_k^4\frac{\partial^2 w_{e,i}}{\partial x^4} + \frac{2\rho h}{D_1}\frac{\partial^2 w_{e,i}}{\partial t^2} = \frac{1}{D_1}Q_{e,i}^{(1)}\frac{\partial^2 M_0}{\partial x^2} \tag{4.27}$$

- is the equation for the deflection $w_{e,i}(x,t)$ of plate i ($i = 1, 2$) related to the Stoneley-type flexural interfacial wave.

The elliptic equations over the interior domain for the plates 1 and 2 deflections are shown by

$$\frac{\partial^4 w_{in,i}}{\partial y^4} + 2\frac{\partial^4 w_{in,i}}{\partial x^2 \partial y^2} + (1 - \gamma c_k^4)\frac{\partial^4 w_{in,i}}{\partial x^4} = 0, \tag{4.28}$$

with $w_{in,i}(x,y)$ as the deflection of the plate i ($i = 1, 2$) over the interior domain related to the Stoneley-type flexural interfacial wave, and

$$\gamma = \begin{cases} 1, & i = 1, \\ \dfrac{\rho_2}{\rho_1}, & i = 2. \end{cases} \tag{4.29}$$

The boundary conditions for $w_{in,i}(x,y)$, $i = 1, 2$ can be taken by the following expressions

$$w_{in,i}(x,0) = w_{e,i}(x),$$
$$\frac{\partial^2 w_{in,i}}{\partial y^2} = -\nu_i \frac{\partial^2 w_{e,i}}{\partial x^2}. \tag{4.30}$$

4.2.4 Comparison with exact solution

We obtained exact solutions (4.20) for the transformed deflections $\hat{W}_j(\eta, p)$, and also derived the explicit dual parabolic-elliptic model related to the Stoneley-type flexural interfacial wave (see (4.27)-(4.30)). Now we compare the obtained solutions by applying the inverse Fourier transform and plotting the results. We consider a particular problem of a point bending moment $M_0(x,t) = M_0 \delta(x) e^{-i\omega t}$ applied at the plates junction $y = 0$. Here and below, the Poisson's ratios are assumed to be $\nu_1 = 0.4$, $\nu_2 = 0.3$. The frequency parameters then become

$$\lambda_1 = \sqrt{\frac{2\rho_1 h^5 \omega^2}{D_1}},$$
$$\lambda_2 = \sqrt{\frac{2\rho_2 h^5 \omega^2}{D_2}}. \tag{4.31}$$

Also, for this point moment M_0, we can rewrite the exact solution in a more convenient form in terms of p parameter as follows

$$\hat{W}_1(\eta) = \frac{\hat{M}_0}{D_1} \frac{p^2}{p^4 - p_k^4} \frac{\Delta_1(p) e^{-\alpha_1 |\eta|} + \Delta_2(p) e^{-\beta_1 |\eta|}}{\Delta(p)},$$
$$\hat{W}_2(\eta) = \frac{\hat{M}_0}{D_1} \frac{p^2}{p^4 - p_k^4} \frac{\Delta_3(p) e^{-\alpha_2 |\eta|} + \Delta_4(p) e^{-\beta_2 |\eta|}}{\Delta(p)}, \tag{4.32}$$

Here,

$$\alpha_i = \sqrt{p^2 - \lambda_i}, \quad \beta_i = \sqrt{p^2 + \lambda_i}, \quad i = 1, 2, \tag{4.33}$$

$$
\begin{aligned}
\Delta_1(p) &= \beta^2 \left[(\beta_1 - \alpha_2)\beta_2((\nu_2 - 1)p^2 + \lambda_2) + (\beta_2 - \beta_1)\alpha_2((\nu_2 - 1)p^2 - \lambda_2) \right] \\
&\quad + (\alpha_2 - \beta_2)\beta_1((\nu_1 - 1)p^2 + \lambda_1), \\
\Delta_2(p) &= -\left[\beta^2 \left[(\beta_2 - \alpha_1)\alpha_2((\nu_2 - 1)p^2 - \lambda_2) + (\alpha_1 - \alpha_2)\beta_2((\nu_2 - 1)p^2 + \lambda_2) \right] \right. \\
&\quad \left. + (\alpha_2 - \beta_2)\alpha_1((\nu_1 - 1)p^2 - \lambda_1) \right], \\
\Delta_3(p) &= (\alpha_1 - \beta_2)\beta_1((\nu_1 - 1)p^2 + \lambda_1) + (\beta_1 - \beta_2)\alpha_1((\nu_1 - 1)p^2 - \lambda_1) \\
&\quad + \beta^2(\alpha_1 - \beta_1)\beta_2((\nu_2 - 1)p^2 + \lambda_2), \\
\Delta_4(p) &= -\left[(\alpha_1 - \alpha_2)\beta_1((\nu_1 - 1)p^2 + \lambda_1) + (\alpha_2 - \beta_1)\alpha_1((\nu_1 - 1)p^2 - \lambda_1) \right. \\
&\quad \left. + \beta^2(\beta_1 - \alpha_1)\alpha_2((\nu_2 - 1)p^2 - \lambda_2) \right],
\end{aligned} \tag{4.34}
$$

and also,

$$
\begin{aligned}
\Delta(p) =& \left[(1+a) + dp^2\right]^2 \sqrt{p^2 - \lambda_1}\sqrt{p^2 + \lambda_2} \\
&+ \left[(1+a) - dp^2\right]^2 \sqrt{p^2 + \lambda_1}\sqrt{p^2 - \lambda_2} \\
&- \left[(1-a) + dp^2\right]^2 \sqrt{p^2 - \lambda_1}\sqrt{p^2 - \lambda_2} \\
&- \left[(1-a) - dp^2\right]^2 \sqrt{p^2 + \lambda_1}\sqrt{p^2 + \lambda_2} \\
&- 4a\left[\sqrt{p^4 - \lambda_1^2} + \sqrt{p^4 - \lambda_2^2}\right],
\end{aligned}
\tag{4.35}
$$

with

$$
p_k = \frac{\sqrt{\lambda_1}}{c_k}.
\tag{4.36}
$$

The deflection related to the Stoneley-type flexural interfacial wave may be found from exact solution (4.20) by isolating the contribution of the poles $p = \pm p_k$ in the overall solution. This contribution may be found using the contour integration (see Section 1.2.3 above) and also using the constructed dual parabolic-elliptic model. The solutions of parabolic equations (4.27) immediately follow from the residue theory (e.g. see Section 1.2.4). We find them as

$$
\begin{aligned}
W^*_{e,j} =& \frac{1}{\sqrt{2\pi}} \int_{-\infty}^{\infty} \hat{W}_{e,j}(\eta, p) e^{ip\xi} dp = \frac{2\pi i}{\sqrt{2\pi}} Res_{z=p_k}(\hat{W}_{e,j}(\eta, z)e^{iz\xi}), \\
& j = 1, 2,
\end{aligned}
\tag{4.37}
$$

where

$$
\hat{W}_{e,j}(\eta, p) = Q^{(1)}_{e,j} \hat{M}_0 \frac{p^2}{p^4 - p_k^4}, \quad j = 1, 2,
\tag{4.38}
$$

with

$$
\begin{aligned}
Q^{(1)}_{e,1} &= \frac{\Delta_1(p_k) + \Delta_2(p_k)}{\Delta}, \\
Q^{(1)}_{e,2} &= \frac{\Delta_3(p_k) + \Delta_4(p_k)}{\Delta},
\end{aligned}
\tag{4.39}
$$

and

$$
\begin{aligned}
\Delta =& c_k^4 \left[\frac{1}{4p_k^2} \left[((1+a) + dp_k^2)A + ((1+a) - dp_k^2)B \right.\right. \\
& \left. - ((1-a) + dp_k^2)C - ((1-a) - dp_k^2)D \right] \\
& \left. - 2a \left[\frac{1}{\sqrt{p_k^4 - \lambda_1^2}} + \frac{1}{\sqrt{p_k^4 - \lambda_2^2}} \right] \right],
\end{aligned}
\tag{4.40}
$$

where

$$A = 4d\sqrt{p_k^2 - \lambda_1}\sqrt{p_k^2 + \lambda_2} + ((1+a) + dp_k^2)\left(\frac{\sqrt{p_k^2 + \lambda_2}}{\sqrt{p_k^2 - \lambda_1}} + \frac{\sqrt{p_k^2 - \lambda_1}}{\sqrt{p_k^2 + \lambda_2}}\right),$$

$$B = -4d\sqrt{p_k^2 + \lambda_1}\sqrt{p_k^2 - \lambda_2} + ((1+a) - dp_k^2)\left(\frac{\sqrt{p_k^2 - \lambda_2}}{\sqrt{p_k^2 + \lambda_1}} + \frac{\sqrt{p_k^2 + \lambda_1}}{\sqrt{p_k^2 - \lambda_2}}\right),$$

$$C = 4d\sqrt{p_k^2 - \lambda_1}\sqrt{p_k^2 - \lambda_2} - ((1-a) + dp_k^2)\left(\frac{\sqrt{p_k^2 - \lambda_2}}{\sqrt{p_k^2 - \lambda_1}} + \frac{\sqrt{p_k^2 - \lambda_1}}{\sqrt{p_k^2 - \lambda_2}}\right),$$

$$D = -4d\sqrt{p_k^2 + \lambda_1}\sqrt{p_k^2 + \lambda_2} + ((1-a) - dp_k^2)\left(\frac{\sqrt{p_k^2 + \lambda_2}}{\sqrt{p_k^2 + \lambda_1}} + \frac{\sqrt{p_k^2 + \lambda_1}}{\sqrt{p_k^2 + \lambda_2}}\right). \tag{4.41}$$

Therefore, contribution of the Stoneley-type flexural interfacial wave into the overall deflection at the junction $W_{e,i}^*$ is given by

$$W_{e,j}^*(\xi) = \sqrt{2\pi}iQ_{e,j}^{(1)}\hat{M}_0\frac{1}{2p_k}e^{ip_k\xi}, \quad j = 1, 2. \tag{4.42}$$

In order to find the overall solution for the dimensionless deflection $W_j^*(\xi, \eta)$, $j = 1, 2$, we need to integrate the following expression

$$W_j^*(\xi, \eta) = \frac{1}{\sqrt{2\pi}} \int_{-\infty}^{\infty} \hat{W}_j(\eta, p)e^{ip\xi}dp. \tag{4.43}$$

The method of finding it was described in Section 1.2.3. In this case, the branch points are $p = \pm\sqrt{\lambda_i}$, $i = 1, 2$, and the cut where we take $\alpha_j = -i\sqrt{\lambda_j - p^2}$, is between them, so it is $-\sqrt{\lambda_i} \leq p \leq \sqrt{\lambda_i}$.

For the numerical analysis of the above solutions we choose the parameters so that $\alpha = \sqrt{\frac{\rho_2}{\rho_1}} = 0.4382$ and $\beta = \sqrt{\frac{\hat{D}_2}{\hat{D}_1}} = 0.5477$. Under these conditions the Stoneley coefficient becomes $c_k = 0.9714$. The frequency parameter is assumed to be $\lambda_1 = 1$ whereas $\hat{M}_0 = \sqrt{2\pi}$. The small radius r of the contour semi-circles is again taken as (2.36).

Comparison of the Stoneley-type flexural interfacial wave contribution into the deflections at the junction of plates is demonstrated in Figure 4.6. Since the solutions at the junction are the same because of the problem statement, we provide only one figure for the overall deflections.

A similar approach as described above is used to obtain the solutions over the interior domain. Instead of parabolic equations at the junction, the elliptic problems (4.28)-(4.30)
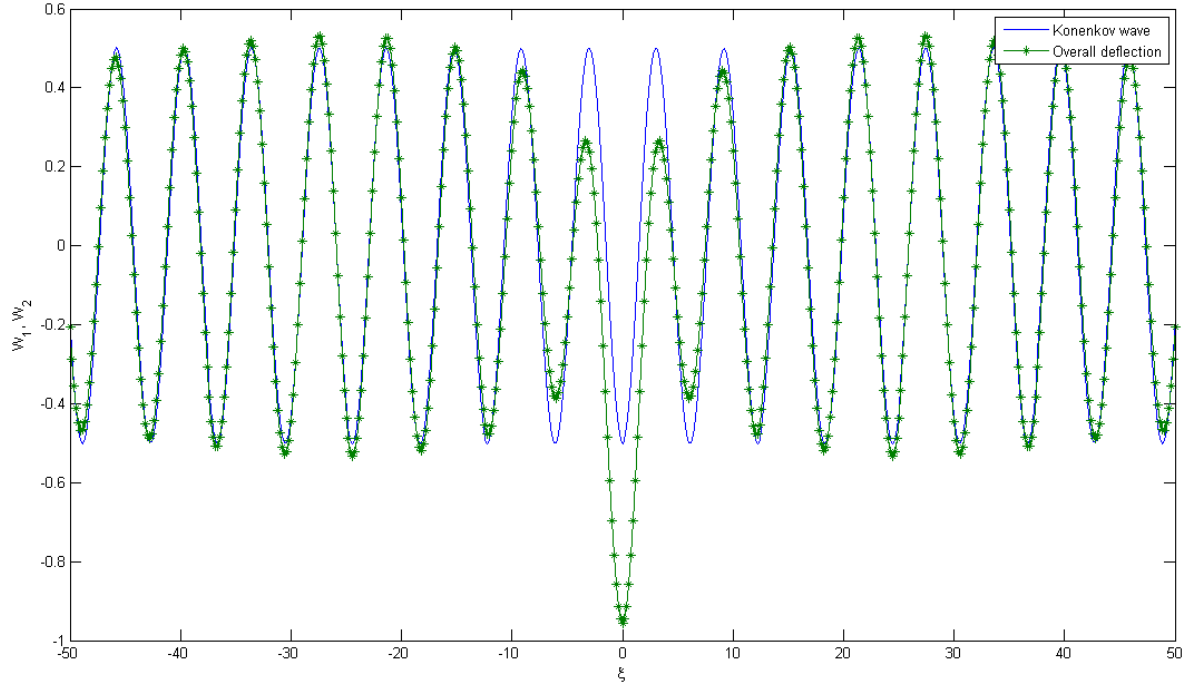
Figure 4.6: Deflection at the junction of isotropic plates. Overall solution (4.43) and Stoneley-type flexural interfacial wave contribution (4.42)

are analyzed. The solutions of these problems are given in terms of the integral transforms. They are

$$
\hat{W}_{in,j}(\eta,p) = \frac{Q_{e,j}^{(1)}\hat{M}_0}{2c_k^2}\frac{p^2}{p^4 - p_k^4}
$$
$$
\times\left[[(1-\nu_j)+c_k^2]p^2 e^{-\alpha_j(c_k)p|\eta|} - [(1-\nu)-c_k^2]p^2 e^{-\beta_j(c_k)p|\eta|}\right] \tag{4.44}
$$

for $j = 1, 2$. The above function can be integrated using the residue theory (see Section 1.2.4), and the final solution for the deflections related to the Stoneley-type flexural interfacial wave become

$$
W_{in,j}^*(\xi,\eta) = \sqrt{2\pi}i\frac{Q_{e,j}^{(1)}\hat{M}_0}{c_k^2}\frac{1}{4p_k}
$$
$$
\times\left[[(1-\nu_j)p_k^2+\lambda_j]e^{-\alpha_j(c_k)p_k|\eta|} - [(1-\nu_j)p_k^2-\lambda_j]e^{-\beta_j(c_k)p_k|\eta|}\right]e^{ip_k\xi}. \tag{4.45}
$$

The numerical solutions found using the scheme from Section 1.2.3 are shown in Figures 4.7-4.10. They confirm an intuitive expectation that the Stoneley-type flexural interfacial wave makes a key contribution into the exact solution near the junction (again, the only exception is the vicinity of the applied point bending moment).

Figure 4.7: Overall deflection in isotropic plates (plate 1). Overall solution (4.43) and the parabolic-elliptic model (4.45) at $\eta = 1$

Figure 4.8: Overall deflection in isotropic plates (plate 2). Overall solution (4.43) and the parabolic-elliptic model (4.45) at $\eta = -1$
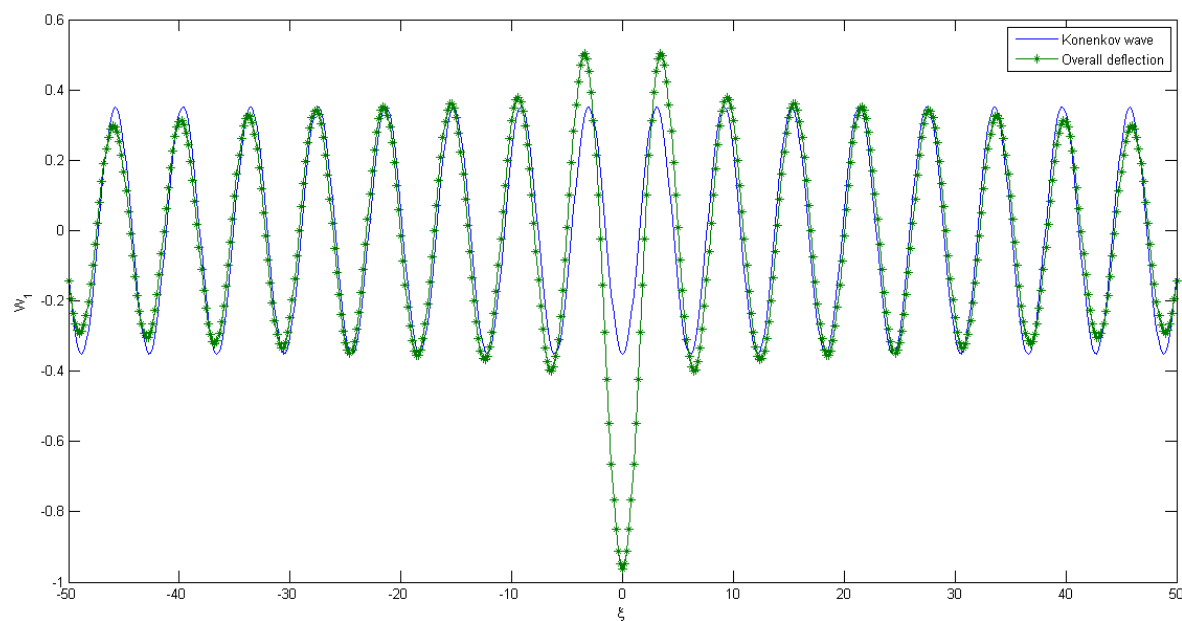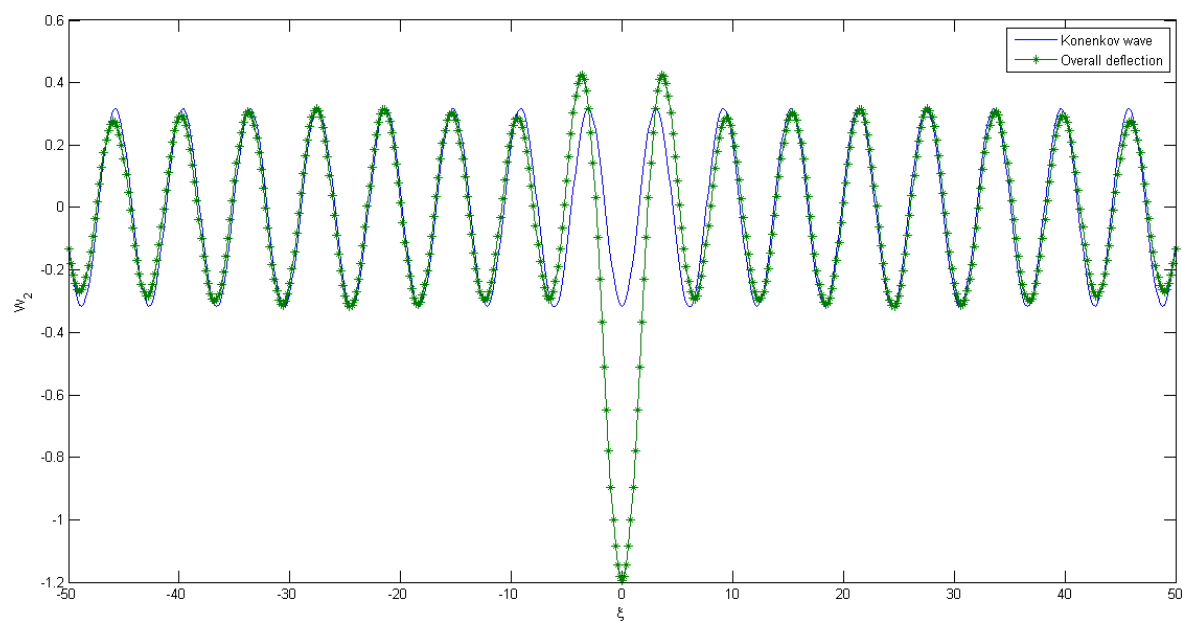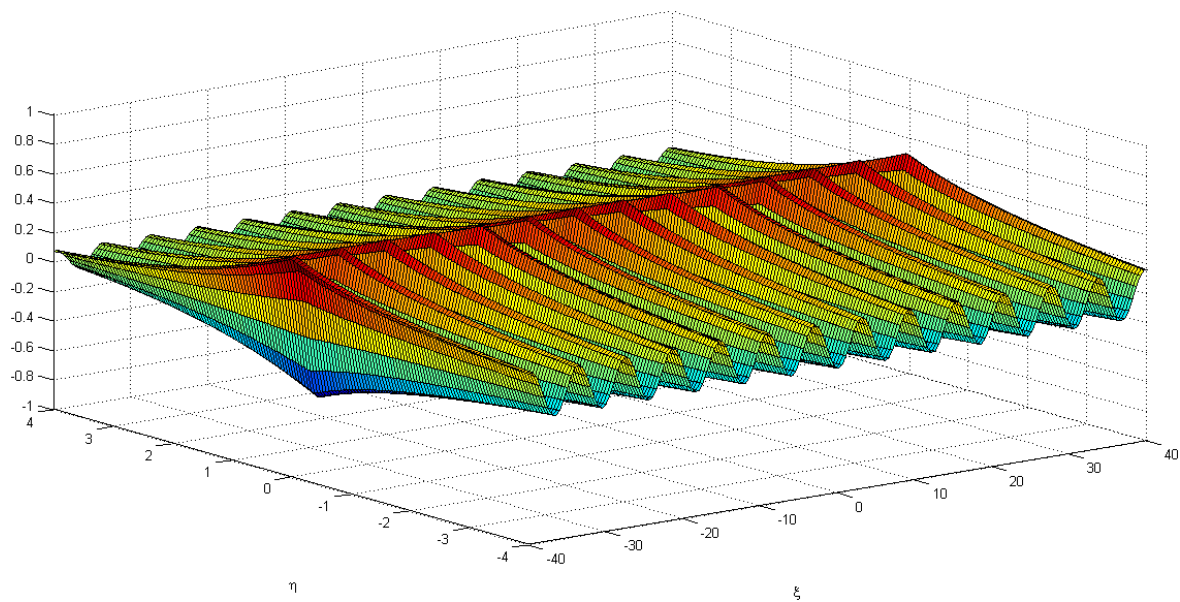
Figure 4.9: Stoneley-type flexural interfacial wave at the junction of two plates. 3D profile of the parabolic-elliptic model (4.42), (4.45)
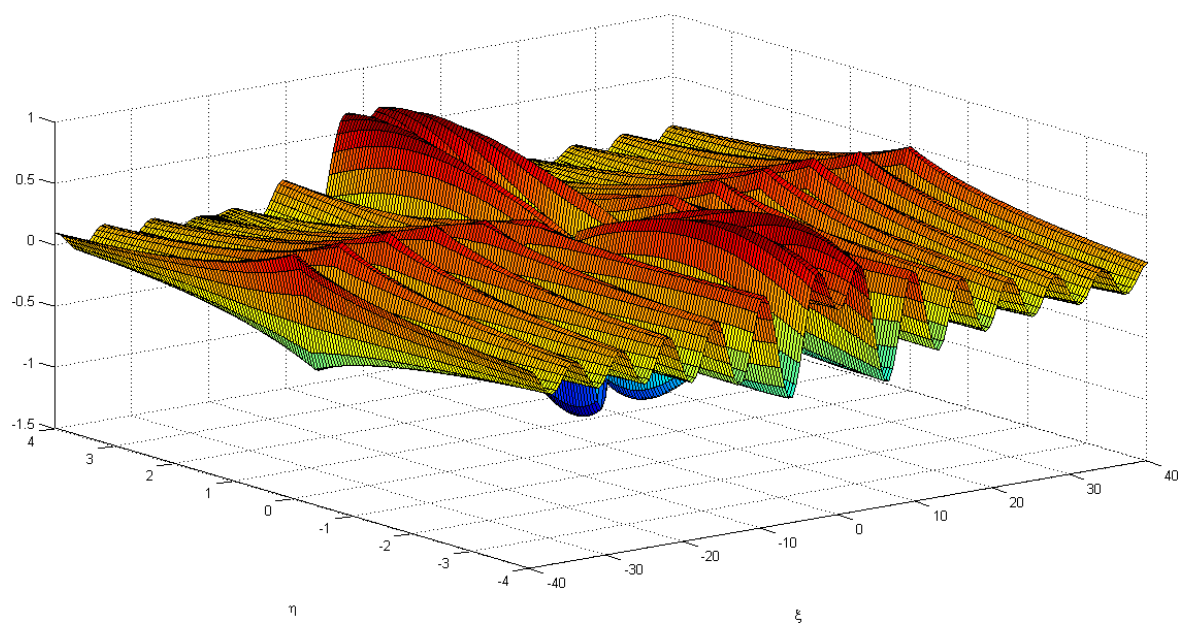
Figure 4.10: Overall deflection at the junction of two plates. 3D profile of the overall solution (4.43)

4.3   Shear force at junction of two plates

This section includes the analysis of interfacial vibrations at the junction of two isotropic semi-infinite plates induced by shear force.
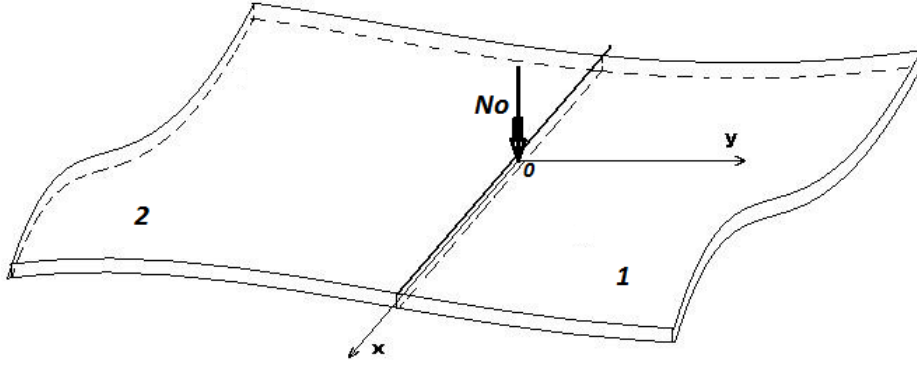
Figure 4.11: Shear force at the junction. Scheme of loading

4.3.1   Basic equations

For this type of loading, shown in Figure 4.11, the equations of motion for w_i, $i = 1, 2$ remain in form (4.1), whereas the continuity conditions at the junction $(y = 0)$ become

$$
\begin{aligned}
w_1 &= w_2, \\
\frac{\partial w_1}{\partial y} &= \frac{\partial w_2}{\partial y}, \\
D_1\left[\frac{\partial^2 w_1}{\partial y^2} + \nu_1\frac{\partial^2 w_1}{\partial x^2}\right] &= D_2\left[\frac{\partial^2 w_2}{\partial y^2} + \nu_2\frac{\partial^2 w_2}{\partial x^2}\right], \\
D_1\left[\frac{\partial^3 w_1}{\partial y^3} + (2-\nu_1)\frac{\partial^3 w_1}{\partial x^2 \partial y}\right] &= D_2\left[\frac{\partial^3 w_2}{\partial y^3} + (2-\nu_2)\frac{\partial^3 w_2}{\partial x^2 \partial y}\right] - N_0(x,t),
\end{aligned}
\tag{4.46}
$$

where $N_0(x,t)$ is the applied shear force.

On using (4.3) and applying integral transforms to equation (4.1) we get (4.4). In doing so to the continuity conditions (4.46) their transformed analogue becomes

$$
\begin{aligned}
\hat{W}_1 &= \hat{W}_2, \\
\frac{d\hat{W}_1}{d\eta} &= \frac{d\hat{W}_2}{d\eta}, \\
\frac{d^2\hat{W}_1}{d\eta^2} - \nu_1 p^2 \hat{W}_1 &= \frac{\hat{D}_2}{\hat{D}_1}\left[\frac{d^2\hat{W}_2}{d\eta^2} - \nu_2 p^2 \hat{W}_2\right], \\
\frac{d^3\hat{W}_1}{d\eta^3} - (2-\nu_1)p^2\frac{d\hat{W}_1}{d\eta} &= \frac{\hat{D}_2}{\hat{D}_1}\left[\frac{d^3\hat{W}_2}{d\eta^2} - (2-\nu_2)p^2\frac{d\hat{W}_2}{d\eta}\right] + \frac{\hat{N}_0}{\hat{D}_1},
\end{aligned}
\tag{4.47}
$$

where $\hat{N}_0(s,p)$ is the transformed dimensionless shear force.

4.3.2 Solution of problem

We take (4.8)-(4.9) as the solution of the problem (4.4)-(4.47). Its substitution into the boundary conditions (4.18) permits the system of linear equations for the unknown constants A_1, B_1, A_2 and B_2 to be obtained. In matrix form it can be written as follows

$$
\begin{bmatrix} A_1 & B_1 & A_2 & B_2 \end{bmatrix}
$$

$$
\times \begin{bmatrix}
1 & \alpha_1 & \alpha_1^2 - \nu_1 p^2 & \left(\alpha_1^2 - (2 - \nu_1)p^2\right)\alpha_1 \\
1 & \beta_1 & \beta_1^2 - \nu_1 p^2 & \left(\beta_1^2 - (2 - \nu_1)p^2\right)\beta_1 \\
-1 & -\alpha_2 & -\dfrac{\hat{D}_2}{\hat{D}_1}\left(\alpha_2^2 - \nu_2 p^2\right) & -\dfrac{\hat{D}_2}{\hat{D}_1}\left(\alpha_2^2 - (2 - \nu_2)p^2\right)\alpha_2 \\
-1 & -\beta_2 & -\dfrac{\hat{D}_2}{\hat{D}_1}\left(\beta_2^2 - \nu_2 p^2\right) & -\dfrac{\hat{D}_2}{\hat{D}_1}\left(\beta_2^2 - (2 - \nu_2)p^2\right)\beta_2
\end{bmatrix} \tag{4.48}
$$

$$
= \begin{bmatrix} 0 & 0 & 0 & \dfrac{\hat{N}_0}{\hat{D}_1} \end{bmatrix}.
$$

For the sake of brevity we do not provide here the full solution derivation and present the final result for the transformed rotation angle $\hat{V}_i = \dfrac{d\hat{W}_i}{d\eta}$, $i = 1, 2$ (see Section 2.1.3 for more details and explanations) as

$$
\begin{aligned}
\hat{V}_1(\eta) &= \frac{\hat{N}_0}{\hat{D}_1^2(-is\lambda_1^2)} \frac{c^2}{c^4 - c_k^4} \frac{\Delta_1(c)e^{-\frac{\sqrt{-is\lambda_1}}{c}\alpha_1(c)|\eta|} + \Delta_2(c)e^{-\frac{\sqrt{-is\lambda_1}}{c}\beta_1(c)|\eta|}}{\Delta'(c_k^4)}, \\
\hat{V}_2(\eta) &= \frac{\hat{N}_0}{\hat{D}_1^2(-is\lambda_1^2)} \frac{c^2}{c^4 - c_k^4} \frac{\Delta_3(c)e^{-\frac{\sqrt{-is\lambda_1}}{c}\alpha_2(c)|\eta|} + \Delta_4(c)e^{-\frac{\sqrt{-is\lambda_1}}{c}\beta_2(c)|\eta|}}{\Delta'(c_k^4)},
\end{aligned} \tag{4.49}
$$

where c_k is the solution of equation (4.13), the parameters $\alpha_i(c)$, $\beta_i(c)$, $i = 1, 2$ are from (4.21),

$$\begin{aligned}
\Delta_1(c) =& -\alpha_1 \left[\beta^2 \left((\beta_1 - \alpha_2)((1 - \nu_2) + bc^2) + (\beta_1 - \beta_2)((1 - \nu_2) - bc^2)\right)\right.\\
&\left.+ (\alpha_2 - \beta_2)((1 - \nu_1) + c^2)\right],\\
\Delta_2(c) =& \beta_1 \left[\beta^2 \left((\alpha_1 - \alpha_2)((1 - \nu_2) + bc^2) + (\beta_2 - \alpha_1)((1 - \nu_2) - bc^2)\right)\right.\\
&\left.+ (\alpha_2 - \beta_2)((1 - \nu_1) - c^2)\right],\\
\Delta_3(c) =& \alpha_2 \left[\beta^2(\alpha_1 - \beta_1)((1 - \nu_2) + bc^2) + (\beta_2 - \alpha_1)((1 - \nu_1) + c^2)\right.\\
&\left.+ (\beta_1 - \beta_2)((1 - \nu_1) - c^2)\right],\\
\Delta_4(c) =& \beta_2 \left[\beta^2(\beta_1 - \alpha_1)((1 - \nu_2) - bc^2) + (\alpha_1 - \alpha_2)((1 - \nu_1) + c^2)\right.\\
&\left.+ (\alpha_2 - \beta_1)((1 - \nu_1) - c^2)\right],
\end{aligned}$$

(4.50)

and $\Delta'(c_k^4)$ is from (4.23).

4.3.3 Derivation of model

As it was mentioned in all previous chapters, analysis of the interfacial wave contribution into the overall rotation angle is connected with the derivation of the dual parabolic-elliptic model of the Stoneley-type flexural interfacial wave. It consists of the parabolic equations at the plates junction and the elliptic equations for the plates rotation angles over the interior domain. The models again can be constructed separately for the considered plates.

First, at the junction ($\eta = 0$) we obtain the following expressions in terms of the transform parameter p (see section 2.1.3 for more details)

$$\hat{V}_{e,i}(p) = -\frac{\hat{N}_0}{\hat{D}_1} \frac{p^2}{p^4 - p_k^4} Q_{e,i}^{(2)}, \quad i = 1, 2, \tag{4.51}$$

where $\hat{V}_{e,i}$ are the transformed rotation angles of plates 1 and 2 at the junction from the Stoneley-type flexural interfacial wave and

$$\begin{aligned}
Q_{e,1}^{(2)} &= \frac{\Delta_1(c_k) + \Delta_2(c_k)}{\Delta'(c_k^4)},\\
Q_{e,2}^{(2)} &= \frac{\Delta_3(c_k) + \Delta_4(c_k)}{\Delta'(c_k^4)}.
\end{aligned} \tag{4.52}$$

It is easy to check that $Q_{e,1}^{(2)} = Q_{e,2}^{(2)}$, therefore $\hat{V}_{e,1}(p) = \hat{V}_{e,2}(p)$.

In the original variables, parabolic equations for the plates rotation angles at the junction become

$$c_k^4 \frac{\partial^2 v_{e,i}}{\partial x^4} + \frac{2\rho h}{D_1}\frac{\partial^2 v_{e,i}}{\partial t^2} = \frac{1}{D_1}Q_{e,i}^{(2)}\frac{\partial^2 N_0}{\partial x^2} \tag{4.53}$$

The elliptic equations for the deflections of plates 1 and 2 respectively over the interior domain (related to the Stoneley-type flexural interfacial wave) are presented below

$$\frac{\partial^4 v_{in,i}}{\partial y^4} + 2\frac{\partial^4 v_{in,i}}{\partial x^2 \partial y^2} + (1 - \gamma c_k^4)\frac{\partial^4 v_{in,i}}{\partial x^4} = 0, \tag{4.54}$$

with $v_{in,i}(x,y)$ as the rotation angle of plate i $(i = 1, 2)$ over the interior domain, caused by the Stoneley-type flexural interfacial wave, and γ from (4.29).

The boundary conditions for $v_{in,i}(x,y)$ can be presented by

$$\begin{aligned} v_{in,i}(x,0) &= v_{e,i}(x), \\ \frac{\partial^2 v_{in,i}}{\partial y^2} &= -(2 - \nu_i)\frac{\partial^2 v_{e,i}}{\partial x^2}. \end{aligned} \tag{4.55}$$

4.3.4 Comparison with exact solution

We obtained the exact solutions (4.49) in terms of integral transforms, and also derived an explicit dual parabolic-elliptic model for the Stoneley-type flexural interfacial wave (see (4.53), (4.54)-(4.55) above). The next step is to compare of the obtained solutions by applying the inverse Fourier transform and computing graphical illustrations.

We recall that the transverse shear point force N_0 (see Section 2.1.3) is assumed to be applied at the plates junction. As before, we operate with the same frequency parameters λ_1 and λ_2 (see (4.31)). Poisson's ratios are assumed to be $\nu_1 = 0.4$, $\nu_2 = 0.3$. Derivation of the formulae that we need for computations is similar to the one described in the previous Section 4.2.4. We present first the exact solution for the rotation angles $\hat{V}_j(\eta, p)$ in terms of the transform parameter p, given by

$$\begin{aligned} \hat{V}_1(\eta) &= \frac{\hat{N}_0}{D_1}\frac{p^2}{p^4 - p_k^4}\frac{\Delta_1(p)e^{-\alpha_1|\eta|} + \Delta_2(p)e^{-\beta_1|\eta|}}{\Delta}, \\ \hat{V}_2(\eta) &= \frac{\hat{N}_0}{D_1}\frac{p^2}{p^4 - p_k^4}\frac{\Delta_3(p)e^{-\alpha_2|\eta|} + \Delta_4(p)e^{-\beta_2|\eta|}}{\Delta}, \end{aligned} \tag{4.56}$$

where α_i and β_i are from (4.33), $\Delta(p)$ is given by (4.35), p_k is connected with c_k by expression (4.36) and

$$\Delta_1(c) = -\alpha_1 \left[\beta^2 \left((\beta_1 - \alpha_2)((1-\nu_2)p^2 + \lambda_2) + (\beta_1 - \beta_2)((1-\nu_2)p^2 - \lambda_2) \right) \right.$$
$$\left. + (\sqrt{p^2 - \lambda_2} - \sqrt{p^2 + \lambda_2})((1-\nu_1)p^2 + \lambda_1) \right],$$

$$\Delta_2(c) = \beta_1 \left[\beta^2 \left((\alpha_1 - \alpha_2)((1-\nu_2)p^2 + \lambda_2) + (\beta_2 - \alpha_1)((1-\nu_2)p^2 - \lambda_2) \right) \right.$$
$$\left. + (\alpha_2 - \beta_2)((1-\nu_1)p^2 - \lambda_1) \right],$$

$$\Delta_3(c) = \alpha_2 \left[\beta^2 (\alpha_1 - \beta_1)((1-\nu_2)p^2 + \lambda_2) + (\beta_2 - \alpha_1)((1-\nu_1)p^2 + \lambda_1) \right.$$
$$\left. + (\beta_1 - \beta_2)((1-\nu_1)p^2 - \lambda_1) \right],$$

$$\Delta_4(c) = \beta_2 \left[\beta^2(\beta_1 - \alpha_1)((1-\nu_2)p^2 - \lambda_2) + (\alpha_1 - \alpha_2)((1-\nu_1)p^2 + \lambda_1) \right.$$
$$\left. + (\alpha_2 - \beta_1)((1-\nu_1)p^2 - \lambda_1) \right].$$

$$(4.57)$$

The deflection related to the Stoneley-type flexural interfacial wave may be found from exact solution (4.49) by isolating the contribution of the poles $p = \pm p_k$. This contribution may be found using contour integration (see Section 1.2.3 above) as well as using the solutions of the parabolic equations (4.53) which immediately follow from the residue theory (e.g. see Section 1.2.4). We find them as

$$V_{e,j}^*(\xi,\eta) = \frac{1}{\sqrt{2\pi}} \int_{-\infty}^{\infty} \hat{V}_{e,j}(\eta,p)e^{ipx}dp = \frac{2\pi i}{\sqrt{2\pi}} Res_{z=p_k}(\hat{V}_{e,j}(\eta,z)e^{izx}),$$
$$j = 1,2,$$

$$(4.58)$$

where

$$\hat{V}_{e,j}(\eta,p) = Q_{e,j}^{(2)} \hat{N}_0 \frac{p^2}{p^4 - p_k^4}, \quad j = 1,2,$$

$$(4.59)$$

with

$$Q_{e,1}^{(2)} = \frac{\Delta_1(p_k) + \Delta_2(p_k)}{\Delta},$$
$$Q_{e,2}^{(2)} = \frac{\Delta_3(p_k) + \Delta_4(p_k)}{\Delta},$$

$$(4.60)$$

and Δ is given by (4.40). Therefore, the explicit solution for the dimensionless plate edge rotation angle $V_{e,j}^*(\xi)$ is given by

$$V_{e,j}^*(\xi) = \sqrt{2\pi} i Q_{e,j}^{(2)} \hat{N}_0 \frac{1}{2p_k} e^{ip_k\xi}, \quad j = 1,2.$$

$$(4.61)$$

To find the overall solution in the dimensionless form $V_j^*(\xi, \eta)$, $j = 1, 2$, we need to integrate the following expressions

$$V_j^*(\xi, \eta) = \frac{1}{\sqrt{2\pi}} \int_{-\infty}^{\infty} \hat{V}_j(\eta, p) e^{ip\xi} dp. \tag{4.62}$$

The method of finding it was described in Section 1.2.3. The branch points and the cut remain the same as mentioned above in Section 4.2.4.

The solution related to the Stoneley-type flexural interfacial wave over the interior domain in terms of transform parameter p can be found from the elliptic problems (4.54)-(4.55). It is

$$\hat{V}_{in,j}(\eta, p) = \frac{Q_{e,j}^{(2)} \hat{N}_0}{2c_k^2} \frac{p^2}{p^4 - p_k^4}$$
$$\times \left[-[(\nu_j - 1) - c_k^2]p^2 e^{-\alpha_j(c_k)p|\eta|} + [(\nu_j - 1) + c_k^2]p^2 e^{-\beta_j(c_k)p|\eta|} \right] \tag{4.63}$$

for $j = 1, 2$.

This function can be integrated using the residue theory (see Section 1.2.4), and the final solution for the Stoneley-type flexural interfacial wave rotation angle over the interior domain is

$$V_{in,j}^*(\xi, \eta) = \sqrt{2\pi} i \frac{Q_{e,j}^{(2)} \hat{N}_0}{c_k^2} \frac{1}{4p_k}$$
$$\times \left[-[(\nu_j - 1)p_k^2 - \lambda_j]e^{-\alpha_j(c_k)p_k|\eta|} + [(\nu_j - 1)p_k^2 + \lambda_j]e^{-\beta_j(c_k)p_k|\eta|} \right] e^{ip_k\xi}. \tag{4.64}$$

As above, all numerical data is created for the following material parameters $\alpha = \sqrt{\dfrac{\rho_2}{\rho_1}} = 0.4382$, $\beta = \sqrt{\dfrac{\hat{D}_2}{\hat{D}_1}} = 0.5477$ and $c_k = 0.9714$. Frequency parameter $\lambda_1 = 1$ and $\hat{N}_0 = \sqrt{2\pi}$. Here the small radius r of the contour arcs is taken as (2.36).

Numerical results for the current problem are presented below in Figures 4.12-4.13. The general conclusion is that the effect of junction on the magnitude of the Stoneley component is analogous to that for the excitation by a point-bending moment.
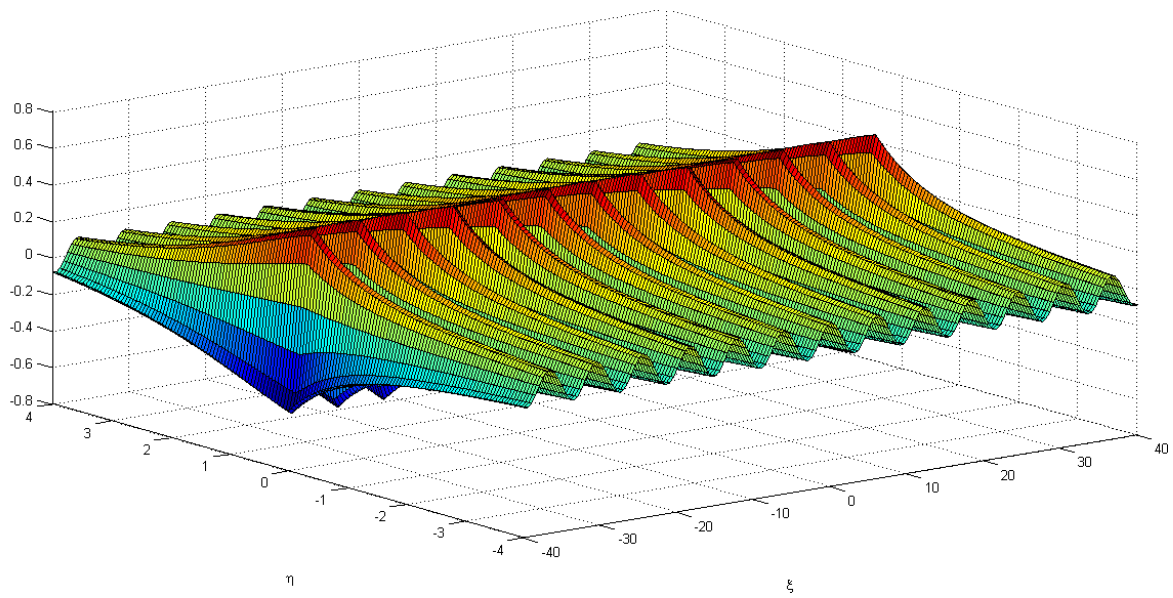
Figure 4.12: Stoneley-type flexural interfacial wave at the junction of two plates. 3D profile of the parabolic-elliptic model (4.61), (4.64)
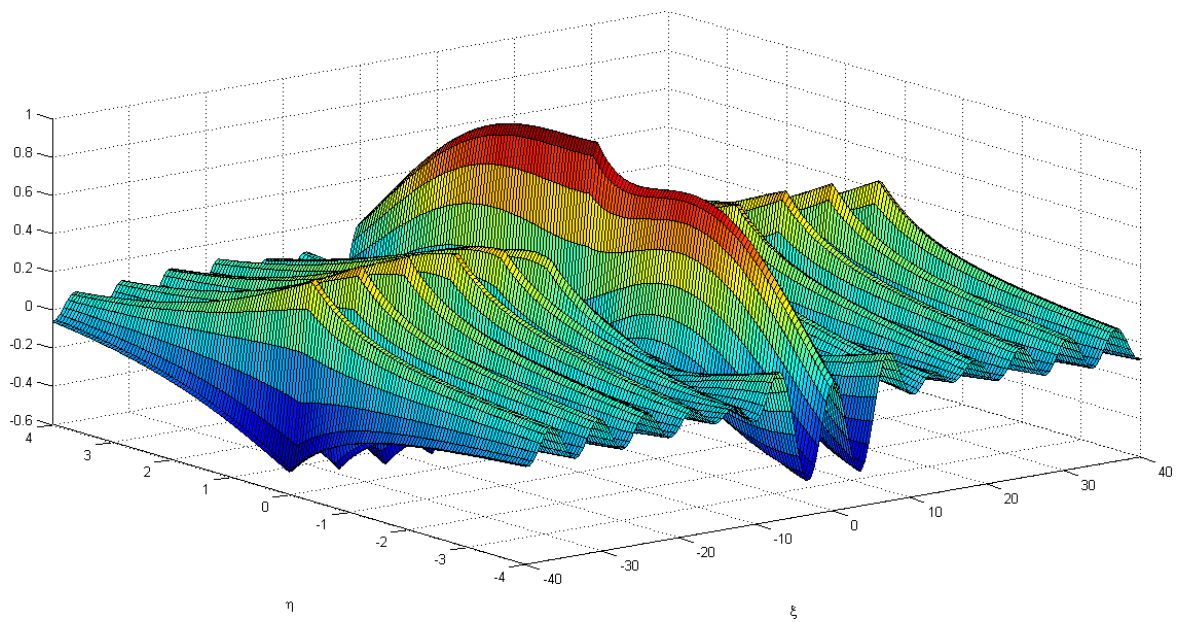

Figure 4.13: Overall rotation angle at the junction of two plates. 3D profile of the exact solution (4.62)

Chapter 5

Conclusion

In this thesis we studied the Konenkov edge and interfacial waves in plates of various shapes and made of different materials: the classical Konenkov flexural edge wave in an isotropic semi-infinite plate (Chapter 2, Section 2.1), the edge wave in a thin elastic isotropic circular plate (Chapter 2, Section 2.2), also, the existence of this wave studied in orthotropic semi-infinite plates (see Chapter 3), and, finally, the Stoneley-type flexural interfacial wave at the junction of two isotropic semi-infinite plates (Chapter 4). The main goal of the thesis involved derivation of the explicit approximate models, revealing a dual parabolic-elliptic nature of flexural edge and interfacial waves, which were derived for the aforementioned cases. The obtained explicit models extract the contribution of the flexural wave into the full dynamic response. The wave propagating in the isotropic semi-infinite plate can be depicted explicitly by the following models: (2.25), (2.27)-(2.29) for the case of a bending moment applied at the edge, and (2.61)-(2.64) for the applied shear force. If the plate under consideration is made of an orthotropic material, the model is formulated by the following equations (3.20)-(3.22) (for the bending moment loading) and (3.37) and (3.40)-(3.41) (for the shear force loading). The principal difference between these models for isotropic and orthotropic plates lies in the fact that in case of orthotropy we can vary the parameters and therefore vary the edge wave contribution into the overall deflection or rotation of the plate. This is illustrated by Figures 3.4-3.21 of Chapter 3. Analogously, a dual parabolic-elliptic model of the Stoneley-type flexural interfacial wave was derived in Chapter 4. It appears to be a natural generalisation of the case of edge waves. For the bending moment applied at the junction, this model has the following form (4.27)-(4.30) whereas for the shear force it is (4.53), (4.54)-(4.55). The

basic feature of the aforementioned model is the complexity of the transcendental equation of the wave speed and therefore the absence of its exact solution.

It is worth mentioning that unlike the dual hyperbolic-elliptic models of the Rayleigh wave, the derived parabolic-elliptic models of edge and interfacial waves govern the dispersion phenomena (absent in the surface Rayleigh-type waves). The unknown functions within the above models depend on the loading type. In particular, if we deal with loading in the form of a bending moment, the related model operates with the plate deflection in contrast to the case of the loading in the form of shear force when the model deals with the rotation angle.

It is also worth mentioning that the developed method of model derivation allows various generalisations. In particular, it can be extended to layered plates, electro-elastic materials, ets. The dual parabolic-elliptic nature of the dispersive edge and interfacial waves might also be expected for the latter.

Bibliography

M. Abramowitz and I.A. Stegun, editors. *Handbook of mathematical functions.* Dover, 1965. 45

J.D. Achenbach. *Wave propagation in elastic solids*, volume 16. North-Holland Publishing Co, 1973. 1

D.M. Barnett, J. Lothe, S.D. Gavazza, and M.J.P. Musgrave. Considerations of the existence of interfacial (Stoneley) waves in bonded anisotropic elastic half-spaces. *Proceedings of the Royal Society of London, A*, 402:153–166, 1985. 2

J. Cerv. Dispersion of elastic waves and Rayleigh-type waves in a thin disc. *Acta Technika C*, 1:89–99, 1988. 1

P. Chadwick. Interfacial and surface waves in pre-strained isotropic elastic media. *Zeitschrift fur Angewandte Mathematik und Physik (ZAMP)*, 46, 1995. 2

P. Chadwick and P. Borejko. Existence and uniqueness of Stoneley waves. *Geophysical Journal International*, 118(2):279–284, 1994. 2

P. Chadwick and G.D. Smith. Foundations of the theory of surface waves in anisotropic elastic materials. *Advances in Theoretical and Applied Mechanics*, 17:303–376, 1977. 2

T.H. Courtney. *Mechanical Behavior of Materials.* McGraw-Hill, New York, 1990. 12

H.-H. Dai, J. Kaplunov, and D.A. Prikazchikov. A long-wave model for the surface elastic wave in a coated half-space. *Proceedings of the Royal Society of London, A*, 466:3097–3116, 2010. 4

M. Destrade and Y.B. Fu. A wave near the edge of a circular disk. *The Open Acoustics Journal*, 1:15–18, 2008. 3, 5, 45

M.A. Dowaikh and R.W. Ogden. On suface waves and deformation in a pre-stressed incompressible elastic solid. *IMA Journal of Applied Mathematics (Institute of Mathematics and Its Applications)*, 44(3):261–284, 1990. 2

M.A. Dowaikh and R.W. Ogden. Interfacial waves and deformation in pre-stressed elastic media. *Proceedings: Mathematical and Physical Sciences*, 433(1888):313–328, 1991. 2

K.O. Friedrichs. Asymptotic phenomena in mathematical physics. *Bulletin of the American Mathematical Society*, 61(6):485–504, 1955. 14

Y.B. Fu. Existence and uniqueness of edge waves in a generally anisotropic elastic plate. *The Quarterly Journal of Mechanics and Applied Mathematics*, 56:605–616, 2003. 3

Y.B. Fu and D.W. Brookes. Edge waves in asymmetrically laminated plates. *Journal of the Mechanics and Physics of Solids*, 54:1–21, 2006. 3

Y.B. Fu and J. Kaplunov. Analysis of localised edge vibrations of cylindrical shells using the stroh formalism. *Mathematics and Mechanics of Solids*, 2011. URL http://mms.sagepub.com/content/early/2011/06/30/1081286511412442.abstract. 3

V.G. Gogoladse. Rayleigh waves on the interface between a compressible fluid medium and a solid elastic half-space. *Trudy Seismologicheskogo Instituta Academii Nauk SSSR*, 127:27–32, 1948. 2

A.L. Goldenveizer. *Theory of elastic thin shells.* Oxford: Pergammon Press, 1961. 3

G.R. Gulgazaryan, L.G. Gulgazaryan, and R.D. Saakyan. The vibrations of a thin elastic orthotropic cylindrical shell with free and hinged edges. *Journal of Applied Mathematics and Mechanics*, 72:312–322, 2008. 3

P. Henrici. *Applied and Computational Complex Analysis, Vol. 1: Power Series, Integration, Conformal Mapping, Location of Zeros.* Wiley, New York, 1988. 8, 9

A.Y. Ishlinskii. On a limiting process in the theory of the stability of elastic rectangular plates. *Dokladi Akademii Nauk SSSR*, 95(3):477–479, 1954. 2

J. Kaplunov, L. Kossovich, and A. Zakharov. An explicit asymptotic model for the Bleustein-Gulyaev wave. *Comptes Rendus Mecanique*, 332:487–492, 2004a. 4

J. Kaplunov, D.A. Prikazchikov, and G.A. Rogerson. On three dimensional edge waves in semi-infinite isotropic plates subject to mixed face boundary conditions. *Journal of the Acoustical Society of America*, 118(5):2975–2983, 2005. 3

J. Kaplunov, A. Zakharov, and D. Prikazchikov. Explicit models for elastic and piezoelastic surface waves. *IMA Journal of Applied Mathematics*, 71:768–782, 2006. 4, 25, 28

J. Kaplunov, E. Nolde, and D. Prikazchikov. A revisit to the moving load problem using an asymptotic model for the Rayleigh wave. *Wave motion*, 47(7):440–451, 2010. 4

J.D. Kaplunov and M.V. Wilde. Edge and interfacial vibrations in elastic shells of revolution. *Zeitschrift fur Angewandte Mathematik und Physik (ZAMP)*, 51:530–549, 2000. 3

J.D. Kaplunov and M.V. Wilde. Free interfacial vibrations in cylindrical shells. *Journal of the Acoustical Society of America*, 111:2692–2704, 2002. 3

J.D. Kaplunov, L.Yu. Kossovich, and M.V. Wilde. Free localized vibrations of a semi-infinite cylindrical shell. *Journal of the Acoustical Society of America*, 107(3):1383–1393, 2000. 3

J.D. Kaplunov, D.A. Prikazchikov, and G.A. Rogerson. Edge vibration of a pre-stressed semi-infinite strip with traction-free edge and mixed face boundary conditions. *Zeitschrift fur Angewandte Mathematik und Physik (ZAMP)*, 55(4):701– 719, 2004b. 4

Yu.D. Kaplunov and L.Yu. Kossovich. Asymptotic model of Rayleigh waves in the far-field zone in an elastic half-plane. *Doklady Physics*, 49(4):234–236, 2004. Translated from Doklady Akademii Nauk, Vol.395, No.4,2004,pp.482-484. 4

G. Kirchhoff. Uber das gleichewicht und die bewegung einer elastischen scheibe. *Journal fur die reine und angewandte Mathematik (Crelle's Journal)*, 40:51, 1850. 14

Yu.K. Konenkov. A Rayleigh-type flexural wave. *Soviet Physics - Acoustics*, 6:122–123, 1960. 2, 5, 21, 45

A.A. Krushynska. Flexural edge waves in semi-infinite elastic plates. *Journal of Sound and Vibration*, 330:1964–1976, 2011. 3

P.E. Lagasse and A.A. Oliner. Acoustic flexural mode on a ridge of semi-infinite height. *Electronics Letters*, 12(1):11–13, 1976. 3

J.B. Lawrie and J.D. Kaplunov. Edge waves and resonance on elastic structures: An overview. *Journal of Mathematics and Mechanics of Solids*, 2011. URL http://mms.sagepub.com/content/early/2011/07/09/1081286511412281.abstract. 2, 3

P. Lu, H.B. Chen, and C. Lu. Further studies on edge waves in anisotropic elastic plates. *International Journal of Solids and Structures*, 44:2192–2208, 2007. 3

P.G. Malischevsky. Comment to "a new formula for the velocity of Rayleigh waves" by D. Nkemzi [Wave Motion 26(1997) 199-205]. *Wave Motion*, 31(1):93–96, 2000. 1

J.J. McCoy and R.D. Mindlin. Extensional waves along the edge of an elastic plate. *Journal of Applied Mechanics*, 30(1):75–78, 1963. 1

A. Mielke and Y.B. Fu. Uniqueness of the surface-wave speed: A proof that is independent of the Stroh formalism. *Journal of Mathematics and Mechanics of Solids*, 9(1):5–15, 2004. 2

D. Nkemzi. A new formula for the velocity of Rayleigh waves. *Wave Motion*, 26(2):199–205, 1997. 1

A.N. Norris. Flexural edge waves. *Journal of Sound and Vibration*, 171:571–573, 1994. 3

A.N. Norris and I.D. Abrahams. On the existence of flexural edge waves on submerged elastic plates. *Proceedings of the Royal Society of London, A*, 456(1559-1582), 2000. 3

A.N. Norris and Z. Wang. Bending wave diffraction from strips and cracks on thin plates. *The Quarterly Journal of Mechanics and Applied Mathematics*, 47:607–627, 1994. 3

A.N. Norris, V.V. Krylov, and I.D. Abrahams. Flexural edge waves and comments on A new bending wave solution for the classical plate equation [J.Acoust. Soc. Am.104,2220-2222(1998)]. *Journal of the Acoustical Society of America*, 107(3):1781–1784, 2000. 2

R.W. Ogden and P.C. Vinh. On Rayleigh waves in incompressible orthotropic elastic solids. *Journal of the Acoustical Society of America*, 115(2):530–533, 2004. 2

J. Oliver, F. Press, and M. Ewing. Two-dimensional model seismology. *Geophysics*, 19(2): 202–219, 1954. 1

C.V. Pham and R.W. Ogden. Formulas for the Rayleigh wave speed in orthotropic elastic solids. *Archives of Mechanics*, 56(3):247–265, 2004. 2

G.T. Piliposian, M.V. Belubekyan, and K.B. Ghazaryan. Localized bending waves in a transersely isotropic plate. *Journal of Sound and Vibration*, 329:3596–3605, 2010. 3

D.A. Prikazchikov, G.A. Rogerson, and K.J. Sandiford. On localised vibrations on incompressible pre-stressed transversely isotropic elastic solids. *Journal of Sound and Vibration*, 301(3-5):701–717, 2007. 4

M. Rahman and J.R. Barber. Exact expression for the roots of the secular equation for Rayleigh waves. *Journal of Applied Mechanics, Transactions ASME*, 62(1):250–252, 1995. 1

M. Rahman and T. Michelitsch. A note on the formula for the Rayleigh wave speed. *Wave Motion*, 43(3):272–276, 2006. 1

Lord Rayleigh. On waves propagated along the plane surface of an elastic solid. *Proceedings of the London Mathematical Society*, 17(253):4–11, 1885. 1, 25

G.A. Rogerson and A.V. Krynkin. Resonance phenomena at the interface of two perfectly bonded, prestressed elastic strips. *Journal of Mechanics of Materials and Structures*, 2(5): 983996, 2007. 4

J.G. Scholte. The range of existence of Rayleigh and Stoneley waves. *Geophysical Journal International*, 5(s5):120–126, 1947. 2

R. Sinclair and R.W.B. Stephens. Velocity dispersion of waves propagating along the edge of a plate. *Acustica*, 24(3):160–165, 1971. 1

B.K. Sinha. Some remarks on propagation characteristics of ridge for acoustic waves at low frequencies. *Journal of the Acoustical Society of America*, 56:16–18, 1974. 2

R. Stoneley. Elastic waves at the surface of separation of two solids. *Proceedings of the Royal Society of London A*, 106(732):416–428, 1924. 2

I. Thompson and I.D. Abrahams. Diffraction of flexural waves by cracks in orthotropic thin elastic plates. I Formal solution. *Proceedings of the Royal Society of London, A*, 461: 3413–3436, 2005. 3

I. Thompson and I.D. Abrahams. Diffraction of flexural waves by cracks in orthotropic thin elastic plates. II Far field analysis. *Proceedings of the Royal Society of London, A*, 463: 1615–1638, 2007. 3

I. Thompson, I.D. Abrahams, and A.N. Norris. On the existence of flexural edge waves on thin orthotropic plates. *Journal of the Acoustical Society of America*, 112:1756–1765, 2002. 3

R.N. Thurston and J. McKenna. Flexural acoustic waves along the edge of a plate. *IEEE Transactions on Sonics and Ultrasonics*, 21:296–297, 1974. 2

S. Timoshenko and S. Woinowsky-Krieger. *Theory of Plates and Shells*. A McGraw-Hill Classic Textbook Reissue. McGraw-Hill Book Company, 1987. 2, 11

P.C. Vinh and R.W. Ogden. On the Rayleigh wave speed in otrhotropic elastic solids. *Meccanica*, 40(2):147–161, 2005. 2

M.V. Wilde, J.D. Kaplunov, and L.Yu Kossovich. *Edge and interfacial resonance phenomena in elastic bodies*. FIZMATLIT, 2010. ISBN 978-5-9221-1280-2. In Russian. 4

D.D. Zakharov. Konenkov's waves in anisotropic layered plates. *Acoustical Physics*, 48: 171–175, 2002. 3

D.D. Zakharov. Analysis of the acoustical edge flexural mode in a plate using refined asymptotics. *Journal of the Acoustical Society of America*, 116(2):872–878, 2004. 3

D.D. Zakharov and W. Becker. Rayleigh type bending waves in anisotropic media. *Journal of Sound and Vibration*, 261:805–818, 2003. 3

V. Zernov and J. Kaplunov. Three-dimensional edge-waves in plates. *Proceedings of the Royal Society of London, A*, 464:301–318, 2008. 3

A.S. Zilbergleit and A.B. Suslova. Contact flexural waves in thin plates. *Soviet Physics - Acoustics*, 29:108–111, 1983. 3